DEEP STRUCTURE OF THE HIMALAYA AND TIBET FROM GRAVITY AND SEISMOLOGICAL DATA

by

Hélène Lyon-Caen

Thèse de 3ème cycle, Université Paris VII (1980)

Submitted to the Department of Earth, Atmospheric
and Planetary Sciences
in Partial Fulfillment of the
Requirements of the Degree of

DOCTOR OF PHILOSOPHY

at the

MASSACHUSETTS INSTITUTE OF TECHNOLOGY

December 1985

Signature of Author _____
Department of Earth, Atmospheric and Planetary Sciences

Certified by _____
Peter Molnar
Thesis Supervisor

Accepted by _____
Chairman, Department Committee on Graduate Students

DEEP STRUCTURE OF THE HIMALAYA AND TIBET FROM GRAVITY AND SEISMOLOGICAL DATA

by

Hélène Lyon-Caen

Submitted to the Department of Earth, Atmospheric and Planetary Sciences
on December 2, 1985 in partial fullfilment of the requirements
for the Degree of Doctor of Philosophy

Abstract

Most mountain ranges are flanked by foredeep basins, and in general neither the ranges nor the basins are in local isostatic equilibrium. The basins are overcompensated whereas the ranges themselves are usually undercompensated. I describe a method of analysing gravity anomalies over mountain ranges assuming that the topography is supported by the elastic strength of the continental lithosphere which is flexed down by the weight of both the overthrust mountain and the sediments in the adjacent foredeep. Using Bouguer gravity data from one profile across the Himalaya and Ganga Basin, I present a detailed study of the effects of each of the parameters (flexural rigidity, extent to which the elastic plate underlies the range, density contrasts between the crust and mantle and between the sediments and crust) on the configuration of the elastic plate and the gravity anomalies. Deviations from local isostatic equilibrium on five profiles across the Himalaya and the Ganga Basin can be understood if the strong Indian plate underthrusts the Lesser Himalaya. However the load of the High Himalaya is too large to be supported solely by the elastic stress in the Indian plate if the flexural rigidity of the plate is constant and if no other external forces act on the plate. The increase of the gradient in Bouguer gravity anomalies from about 1 mGal/km over the Ganga Basin and the Lesser Himalaya to about 2 mGal/km over the High Himalaya implies that the Moho dips more steeply (10°-15°) beneath the High Himalaya than beneath the Lesser Himalaya (2°-3°). This steepening is interpreted to be due to a weakening of the plate. Even with a weak plate beneath the High Himalaya, the weight of the mountains depresses the plate too much unless an external force system helps support the weight of the High Himalaya. Both the reduced flexural rigidity and the bending moment and force applied to the plate can be understood if part or all of the Indian crust has been detached from India's mantle lithosphere. The magnitudes of the bending moment and force are compatible with their source being gravity acting on part of the stripped mantle lithosphere.

The tectonic implications of these results are studied by means of a series of idealized balanced cross sections, from the collision of India with Eurasia to present, that reproduce several important features of the geology of the Himalaya and predict an amount of eroded material comparable to that in the Ganga Basin and the Bay of Bengal. They also predict rapid uplift only in the High Himalaya and at the foot of the Lesser Himalaya. The cross sectional shape of the Ganga Basin is controlled by the deflection of the Indian plate.

Thus, if the Ganga Basin is a steady state feature, the age of the basal sediments in a given locality should be proportional to the distance of that locality from the southern edge of the basin. If the rate of convergence of India and the Himalaya were constant, that rate should equal the distance divided by the corresponding age. A rate of 10 to 15 mm/a for the last 15 to 20 Ma is found, which is consistent with a large part of the 50 mm/a rate of convergence between India and Eurasia being absorbed by the eastward extrusion of parts of Tibet. Profiles of Bouguer gravity anomalies show only a small peak or plateau over the southern edge of the Lesser Himalaya, implying that the boundary between the light sediments of the Ganga Basin and the heavier crustal rocks of the Lesser Himalaya is not sharp and that there exists some light material beneath the range. We infer that some sediment deposited in the Ganga Basin has been underthrust beneath the Lesser Himalaya, but the quantity is small; most of this sediment probably is scraped off the Indian plate to make the foothills of the range.

Gravity anomalies across the western part of the Tarim Basin and the Kunlun mountain belt show also that this area also is not in local isostatic equilibrium. These data can be explained if a strong plate underlying the Tarim Basin extends southwestward beneath the belt at least 80 km and supports part of the topography of northwest Tibet. This corroborates an earlier inference that late Tertiary crustal shortening has occured in this area by southward underthrusting of the Tarim Basin beneath the Kunlun, and it places a lower bound on the amount of underthrusting.

Travel times and waveforms of SH waves recorded at distances of 10° to 30° and some SS waveforms are used to constrain the upper mantle shear wave velocities down to a depth of 400 km beneath both the Indian Shield and the Tibetan Plateau. The uppermost mantle shear velocity beneath both the Indian Shield and the Tibetan Plateau is high and close to 4.7 km/s. The Indian Shield has a fairly thick lid and the mean velocity between 40 and 250 km is between 4.58 and 4.68 km/s. In contrast, S wave travel times and waveforms, as well as a few SS waveforms, show that the mean velocity between 70 and 250 km beneath the central and northern part of the Tibetan Plateau is slower by 4% or more than that beneath the Indian Shield and probably is between 4.4 and 4.5 km/s. No large differences below about 250 km are required. These results show that the structure of Tibet is not that of a shield and imply that the Indian plate is not underthrusting the whole of the Tibetan Plateau.

Thesis Supervisor: Peter Molnar

Title: Professor of Geophysics

Acknowledgments

I would like to thank Peter Molnar for having given me the chance to get lost in the New World and for having been, as my advisor, a constant source of stimulation and ideas. I wish to thank him also for a seemingly endless supply of enthusiasm, moral support, cheese, airplane tickets, etc... . It has been a pleasure to learn from him (not only about Geophysics) and my only regret is my inability to take full advantage of his knowledge and experience when it was time.

Steve Grand kindly introduced me to the world of upper mantle phases and provided precious help and advices. I thank Philip England, Kip Hodges, Patrick LeFort and Marcia McNutt for taking the time to read this thesis and be part of the Examination Committee.

I thank Dorothy Frank and Sara Luria for their help in typing this thesis.

Special thanks to Rob McCaffrey for being present each time I needed a friend and for many geophysical as well as non-geophysical discussions. Many other people at MIT helped me and made the not-easy days better. Among them, I particularly appreciate the friendship of Fico Pardo-Casas, Bob Nowack, John Nabelek, Kaye Shedlock, Rafael Benites, Yves Bernabé, Kiyoshi Yomogida, Anne Tréhu, Tianqing Cao, Paul Huang, Steve Roecker and Jeanne Sauber.

I also wish to thank the people who encouraged me to cross the Atlantic Ocean, and in particular Raul Madariaga. I certainly don't regret it.

Table of contents

PREFACE

> "We have met woods-dwellers before," said Rama, "but there is no one else like Agastya. North lives Lord Shiva, north are the Himalaya hills, and Mount Meru the center of the world, and Kailasa Hill of silver, and all manner of weight, and Agastya alone by living here in the south keeps Earth from tipping over. He is very powerful, and the heaviest person alive."
>
> (Ramayana, retold by W. Buck)

Whereas geological studies provide a description of the superficial structure and evolution of orogenic belts, information on their deep structure is necessary to understand the mechanisms that support them and drive their formation and evolution. Certainly no two mountain belts formed and evolved exactly the same way but on a large scale the plausible physical mechanisms responsible for their support and evolution are limited.

The Himalaya is the most spectacular example of a mountain belt built by thrusting of material on top of a continental lithosphere and because it is still active and very large, it is a good place to study large scale structures that may help constrain and understand some of the deep processes and relate them to geological observations. In the three first chapters of this thesis gravity anomalies are used to examine how the Himalaya and the Karakorum ranges are supported and to study the implications of these support mechanisms on the way they may have formed and evolved.

Gravity anomalies provide information on the mechanisms that support the topography of mountain ranges. Virtually all mountain belts that formed by

thrusting on a continental lithosphere are flanked by contemporary foredeep sedimentary basins that are overcompensated whereas the ranges themselves are usually undercompensated. Chapter I describes in detail a simple method of analysing gravity anomalies assuming that the continental lithosphere behaves as an elastic plate and is flexed down beneath mountain ranges by the weight of the topography. This model relates the geometry and gravity anomalies of the foredeep basin to the geometry and gravity anomalies of the adjacent range and to the strength of the continental lithosphere. A detailed application of this method to the study of the Himalaya and the Ganga Basin (Chapter I and II) is presented. The implications for the structure, support and evolution of this range and of the Ganga Basin are also discussed and compared to geological observations. In Chapter III the same method is used to study the Kunlun belt and its related foredeep, the Tarim Basin.

The deep structure of the Tibetan Plateau is not well known at present. This has led to controversial interpretations on the mechanism of formation of the plateau and on its present role in the continental collision of India with Eurasia. The study in Chapter IV tries to put constraints on the present structure of the Indian Shield and the Tibetan Plateau down to a depth of 400 km by analysing the travel times and waveforms of long period shear waves that cross the Shield or the Plateau. The mechanisms currently presented for the origin of the plateau are examined in light of the results of the study.

Peter Molnar built the balanced cross sections presented in Chapter II and wrote the section describing them. In Chapter II he did the work to constrain the rate of convergence of India and the Himalaya and wrote the corresponding section. He is also responsible for the work described in Appendix A of Chapter II.

CHAPTER I

CONSTRAINTS ON THE STRUCTURE OF THE HIMALAYA FROM AN ANALYSIS OF GRAVITY ANOMALIES AND A FLEXURAL MODEL OF THE LITHOSPHERE

JOURNAL OF GEOPHYSICAL RESEARCH, VOL. 88, NO. B10, PAGES 8171-8191, OCTOBER 10, 1983

CONSTRAINTS ON THE STRUCTURE OF THE HIMALAYA FROM AN ANALYSIS OF GRAVITY ANOMALIES AND A FLEXURAL MODEL OF THE LITHOSPHERE

Hélène Lyon-Caen and Peter Molnar

Department of Earth and Planetary Sciences, Massachusetts Institute of Technology

Abstract. The intracontinental subduction of India beneath the Himalaya presents several similarities to that occurring at island arcs. We study one of those similarities by analyzing gravity anomalies across the Himalaya assuming that the topography is supported by the Indian elastic plate, flexed under the weight of both the overthrust mountains and the sediments in the Ganga Basin. We first examine in detail the effects of each of the following parameters on the configuration of the elastic plate and on the gravity anomalies: the flexural rigidity, the position of the northern end of the elastic plate (the amount of underthrusting of such a plate beneath the range), and the density contrasts between the crust and mantle and between the sediments and the crust. A plate with a constant flexural rigidity of about 0.7×10^{25} N m (between 0.2 and 2.0×10^{25} N m) allows a good fit to the data from the Lesser Himalaya and the Ganga Basin. Such a plate, however, cannot underthrust the entire Himalaya. Instead, the gravity anomalies show that the Moho steepens from only about 3° beneath the Lesser Himalaya to about 15° beneath the Greater Himalaya. This implies a smaller flexural rigidity beneath the Greater Himalaya (0.1 to 1.0×10^{23} N m) than beneath the Ganga Basin and the Lesser Himalaya. Even with a thin, weak plate beneath the Greater Himalaya, the weight of the mountains depresses the plate too much unless an additional force or moment is applied to the plate. The application of a bending moment/unit length to the end of the plate of about 0.6×10^{18} N is adequate to elevate the Indian plate and to bring the calculated gravity anomalies in agreement with those observed. Both, the smaller flexural rigidity and the bending moment can be understood if we assume that part or all of the Indian crust has been detached from the lower lithosphere that underthrusts the Greater Himalaya. We study the tectonic implications of these results by means of a series of idealized balanced cross sections, from the collision to the present, that reproduce several important features of the geology of the Himalaya and predict an amount of eroded material comparable to that in the Ganga Basin and the Bay of Bengal. These cross sections include high-grade metamorphic rocks near the Main Central Thrust and a steeper dip of it there than in the Lesser Himalaya. They predict rapid uplift only in the Greater Himalaya and at the foot of the Lesser Himalaya.

Paper number 3B1070.
0148-0227/83/003B-1070$05.00

Introduction

Geologic studies of the Himalaya suggest that the range was built by slivers of the Indian continent that successively overthrust the Indian shield to the south [e.g., Gansser, 1964, 1966; LeFort, 1975; Mattauer, 1975]. Following the closure of the Tethys Ocean at the Indus-Tsangpo suture zone, the northern margin of India was underthrust beneath southern Tibet an unknown amount. Later, probably during the Oligocene, convergence between India and southern Tibet apparently ceased at the Indus-Tsangpo suture, and slip began on the Main Central Thrust, the major fault within the Himalaya [e.g., Gansser, 1964, 1966] (Figure 1). More recently, the locus of underthrusting was again transferred southward to the presently active Main Boundary Fault. Both the Main Central Thrust and the Main Boundary Fault appear to the schuppenzones with slip on many separate, subparallel faults. Much of the present seismicity seems to us to occur on the Main Boundary Fault, which dips at a shallow angle beneath the Lesser Himalaya, and at present India seems to slide under the Himalaya on this fault [e.g., Molnar et al., 1977; Seeber and Armbruster, 1981; Seeber et al., 1981].

This description of the tectonic history in terms of successive southward jumps in the active underthrust zone is, of course, an oversimplification and ignores numerous less important thrust faults within the range [e.g., Valdiya, 1981]. Nevertheless, it provides a simple framework within which other aspects of the geologic history can be fit, and it serves as a reasonable working model with which geophysical observations can be compared [e.g., Molnar et al., 1977]. Specifically, fault plane solutions of earthquakes consistently show shallow north or northeast dipping nodal planes that probably are the fault planes [e.g., Fitch, 1970; Molnar et al., 1977]. Depths of foci of these events imply that many of these events lie on the Main Boundary Fault and therefore on the top surface of the Indian shield that presently underthrusts the Lesser Himalaya [Molnar and Chen, 1982]. Drilling of the sediments in the Ganga Basin [Sastri et al., 1971; Rao, 1973] and gravity anomalies [e.g., Choudhury, 1975; Warsi and Molnar, 1977] show the existence of a deep basin south of the Himalaya, similar in shape and dimensions to deep-sea trenches at island arcs. Finally, gravity data imply that the crust gradually thickens northward beneath the Greater Himalaya [e.g., Choudhury, 1975; Kono, 1974; Warsi and Molnar, 1977]. These observations suggest that this intracontinental subduction of India beneath the Himalaya is very similar to that occurring at island arcs, where oceanic lithosphere is being subducted. The essential difference comes from the underthrusting of thick buoyant continental crust instead of thin

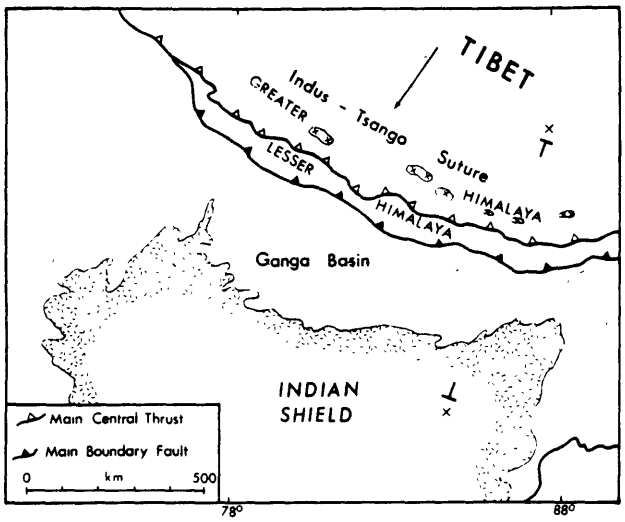

Fig. 1a. General setting of the Himalaya region. The arrow indicates the location of the cross section. XX' is the location of the gravity profile.

oceanic crust on top of cold mantle lithosphere.

In the present paper we examine one of the similarities of the Himalayan region to island arcs: that much of the topography owes its existence to the flexure of an elastic plate. Using such a simple mechanical model, we then use both the gravity anomalies over the Himalaya and the shape of the basement of the Ganga Basin to place constraints on the mechanical properties of such a plate and on the forces that deform it. Several studies of gravity anomalies in the Himalayan region have estimated the crustal thickness or have addressed whether or not isostatic equilibrium prevails [e.g., Choudhury, 1975; Kono, 1974; Marussi, 1964; Qureshy et al., 1974; Warsi and Molnar, 1977]. Although the inferred density models generally yield acceptable fits to the data, they are not constrained by assumptions of plausible mechanical behavior. Here we use the published data of Choudhury [1975], Kono [1974], and Warsi [1976] plus a few data in Greater Himalaya and Tibet [Tang et al., 1981].

We assume that the mass distribution results from the loading and flexure of an elastic continental lithosphere bent under the distributed load of Himalayan mass itself. The physical model is similar to those used for subduction of oceanic lithosphere at island arcs [e.g., Hanks, 1971; Watts and Talwani, 1974]. It differs principally by the trough (or trench) created by the flexure being filled by sediments and by the load being distributed and defined by the Himalayan topography. This is a simplistic model since elastic behavior is an idealization, but this will allow a test to be made of the simple hypothesis that the Indian (elastic) plate underthrusts the Himalaya and will provide a step toward a physical understanding of the structure and dynamics of the region. Instead of examining models with a large number of adjustable and arbitrary chosen locations of irregularly shaped bodies with different densities, we are free to vary only a few parameters, and the effects of each on the computed gravity anomalies may be studied independently. These parameters are the flexural rigidity of the

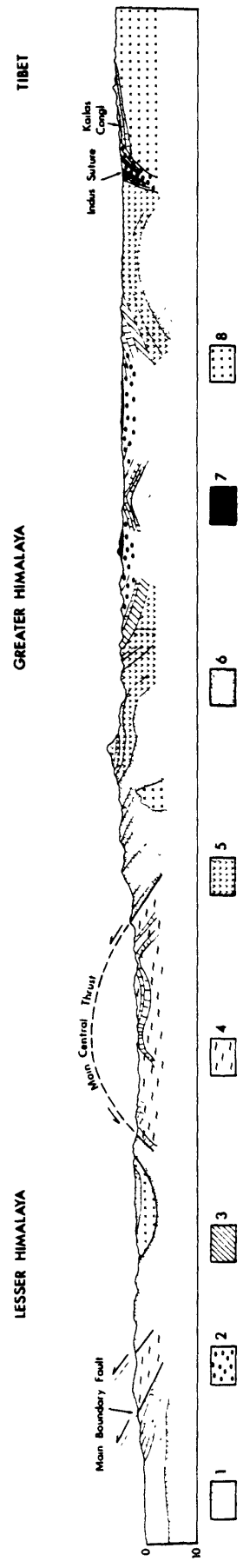

Fig. 1b. Geological cross section, simplified from Gansser [1964]. 1, Tertiary and Quaternary sedimentary rocks; 2, Mesozoic Indus flysch; 3, Paleozoic sedimentary rocks of Greater Himalaya; 4, Paleozoic sedimentary rocks of Lesser Himalaya; 5, upper Precambrian and lower Paleozoic sedimentary rocks; 6, Precambrian crystalline basement; 7, ophiolites; 8, granites. No vertical exageration.

plate (defined below), density differences between the crust and mantle and between the crust and sediments in the Ganga Basin, the position of the northern end of the elastic plate, and the bending moment and the shear force applied at the end of the plate.

The final results of this study involve a sufficient number of modifications to the simple model of an underthrust elastic plate of constant flexural rigidity that we cannot expect the reader to believe them without a systematic analysis of each. Following both a brief discussion of the methods used to determine the shape of the plate and to calculate the gravity anomalies and a presentation of the gravity data, we begin by considering a simple plate with a constant flexural rigidity beneath the Ganga Basin, and we show that such a plate cannot underthrust the entire Himalaya. We then consider a plate with a smaller flexural rigidity in a short segment beneath the Greater Himalaya than that beneath the Lesser Himalaya, the Ganga Basin, and the Indian shield in order to examine the effect of a weak northern segment of plate. We show that regardless of the flexural rigidity, the weight of the material in the Greater Himalaya depresses the Moho too much to fit the observed gravity anomalies unless a bending moment is applied to the north end of the plate. Finally, we discuss the possible physical mechanisms responsible for such a moment and the tectonic implications of the range of possible structures implied by the gravity and topographic data.

Basic Physical Model and its Mathematical Description

The Indian plate is treated as a two-dimensional thin plate. We analyze its elastic response to the loads of the Himalaya and of the sediments that fill the trough (Ganga Basin) created by the bending of the plate. The basic equation for two-dimensional bending of an elastic plate is [e.g. Hanks, 1971; Turcotte and Schubert, 1982]:

$$D\frac{d^4y(x)}{dx^4} + g\Delta\rho\, y(x) = L(x) \qquad (1)$$

where y is the deflection at the abscissa x, $\Delta\rho$ is the density contrast between the two materials above and below the plate, g is gravity, and $D = EH_e^3/12(1-\nu^2)$ is the flexural rigidity, E is the Young's modulus ($E = 1.6 \times 10^{11}$ N/m^2), H_e is the elastic thickness of the plate, and ν is Poisson's ratio ($\nu = 0.25$). L(x) is the weight/unit area of the topography at x. To obtain L(x), we average the elevation within 100 km of either side of the profile. Below, we discuss the effects of errors in the observed load. We assume that the plate overlies an inviscid fluid with a density appropriate for mantle material. Above the plate, however, there are different segments with air, sediments, and rock of crustal density. Accordingly, it is convenient to separate the plate into three domains (Figure 2). We then solve (1) in each domain and obtain the complete solution by matching boundary conditions where the segments are joined. For two dimensions and if we assume no shear stress at the base of the plate, the equation for a thick plate reduces to (1) [Parsons and Molnar, 1976]. Thus there is no problem in using the thin plate approximation for a series of short plate segments.

The first domain ($x>X_s$) includes the Indian shield where its surface is exposed. The equation to solve is (1) with $L(x) = 0$ and $\Delta\rho = \Delta\rho_1 = \rho_m$, where ρ_m is the mantle density. The second domain ($0<x<X_s$) spans the Ganga Basin. Here $L(x) = 0$ and the plate is overlain by sediments of density ρ_s; $\Delta\rho = \Delta\rho_2 = \rho_m - \rho_s$. Thus the sediment thickness is not assumed but is calculated. The third domain ($X_o<x<0$), where the load is applied, includes most of the Himalaya and possibly part of Tibet, depending on how far to the north the end of the plate, defined by X_o, is asssumed to extend. Effectively, we assume that the plate is overlain by material of crustal density, with a load equal to the mass of rock above sea level; $\Delta\rho = \Delta\rho_3 = \rho_m - \rho_c$, where ρ_c is the crustal density; $L(x) = \rho_\ell g T(x)$ is calculated from the topographic profile T(x), and ρ_ℓ is the assumed mean density for the mountains, $\rho_\ell = 2.7 \times 10^3$ kg/m^3. Note that we do not assume the thickness of the overthrust material but calculate it. Later we add a fourth domain ($X_o'<x<X_o$), with a smaller flexural rigidity D' but in which L(x) and $\Delta\rho$ are defined in the same way as in the third domain. X_o' will define the end of the elastic plate in this case.

The solution for (1) in domains 1 and 2 and for the homogeneous equation associated with (1) in domain 3 (and 4) is of the form

$$y_i(x) = e^{-\lambda_i x}[A_i \cos \lambda_i x + B_i \sin \lambda_i x] + e^{\lambda_i x}[C_i \cos \lambda_i x + D_i \sin \lambda_i x] \qquad (2)$$

with $\lambda_i = (\Delta\rho_i g/4D)^{1/4}$, i=1,4. Solving (1) in domain 3 (and 4) requires the addition of a particular solution to the previous general solutions. This has been computed numerically by taking Fourier transforms of both sides of (1). Wavelengths ranging from ∞ to 2 km are considered in the computation. A check of the method has been made by comparing solutions with those obtained analyticaly for loads of rectangular and triangular shapes. Numerical and analytical solutions differ by less than 1%. In (2), A_i, B_i, C_i, D_i with i = 1,2, 3 (and sometimes 4) are 12 (or 16) constants to be determined. Since y must be finite as x approaches $+\infty$, $C_i = D_i = 0$. The following set of boundary conditions establishes a linear system of 10 (or 14) equations which may be solved for the 10 (or 14) remaining constants. At x = 0, x = X_s, and at x = X_o, if a fourth domain is used, there must be continuity of the deflection of the plate y, of the slope of the plate dy/dx, of the bending moment $D(d^2y/dx^2)$ and of the vertical shear stress $D(d^3y/dx^3)$. At x = X_o, or at x = X_o' when there is a fourth domain, the bending moment and the vertical shear stress must be specified. In most calculations (but not the final ones) both are assumed to be zero, so that the end of the plate is free. An equilibrium of forces and moments results directly from (1) and from the specification of the boundary conditions.

We used the method described by Talwani et al. [1959] to compute the gravitational attractions of polygonal, two-dimensional bodies. We assume that the gravity anomalies of interest are caused by density contrasts between the crust and mantle and

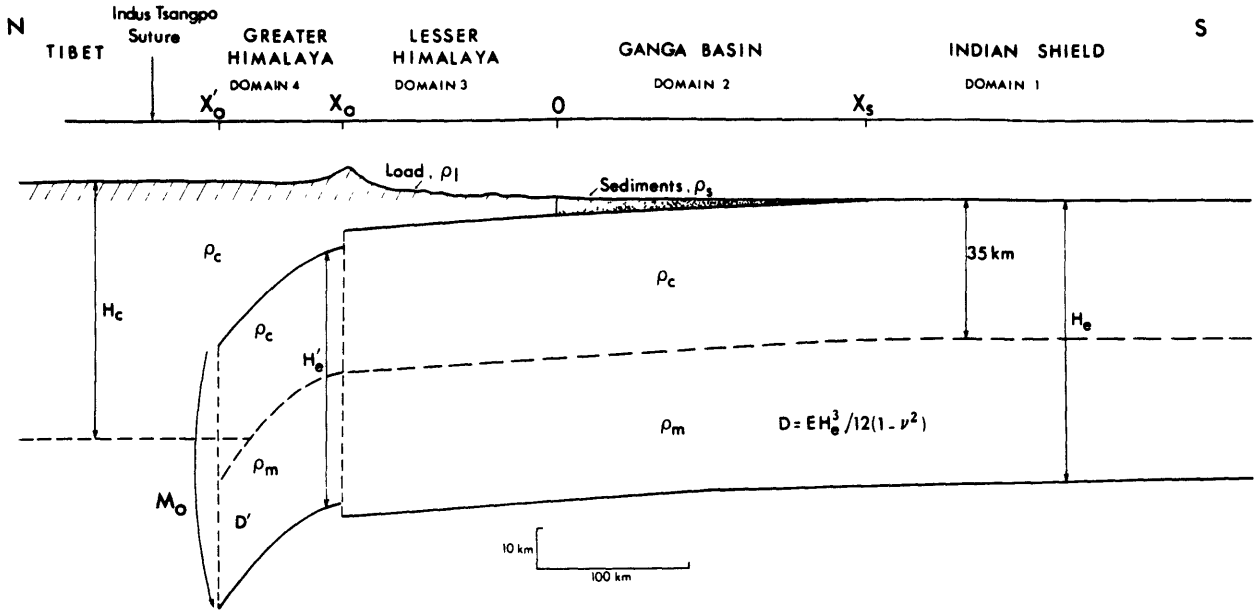

Fig. 2. Schematic cross section of the geometry used. Dashed line shows the Moho, separating crustal material of density ρ_c from mantle material of density ρ_m. The density of the mantle is assumed to be the same in the plate and below it. A segment of plate with a reduced value of the flexural rigidity $D'<D$ is shown on the northern end of the plate. This reduction is probably accomplished by reducing the effective thickness of the plate H_e to H_e'. North of X_o' (or sometimes $x = -250$ km), we assume a constant value of crustal thickness, defined by equation (3). We solve equation (1) in domain 3 (or 4) with different values of $\Delta\rho$. The load is taken to be the region above sea level, shown by hatches.

between the sediments and mantle (Figure 2). Since both the bottom of the sedimentary basin and the Moho are parallel to y(x), which we calculate, we know the shapes of these two bodies for the region $x>X_o$ (or X_o'). We also assumed that the crust of Tibet ($x<-250$ km) is in isostatic equilibrium [Amboldt, 1948; Chang and Cheng, 1973; Tang et al., 1981], so that a column of its mass weighs the same as that to the same depth beneath the Indian shield. Assuming a crustal thickness of 35 km for the Indian shield, the depth of compensation D_c is given by

$$35\rho_c + (D_c-35)\rho_m = 5\rho_\ell + D_c\rho_c \qquad (3)$$

With a mean elevation of 5 km and a mean density $\rho_\ell = 2.7 \times 10^3$ kg/m^3 of the material above sea level for Tibet, this yields a value of D_c between 60 and 70 km for $\rho_m-\rho_c$ between 0.55 and 0.4 $\times 10^3$ kg/m^3 . Although the crustal thickness H_c is difficult to resolve from surface waves data across Tibet, the more recent studies lead to estimates on crustal depth between 65 and 80 km [Chen and Molnar, 1981; Romanowicz, 1982] with a preference for $H_c = 65$ km $= 5+D_c$ from pure paths across Tibet [Romanowicz, 1982]. A different assumed crustal thickness for India leads to a different one for Tibet, but such a change introduces a negligible perturbation in the calculated gravity anomalies. The assumed shape of the junction between the end of the elastic plate and the base of the crust in Tibet, however, does affect the calculated gravity anomalies and will be discussed later in more detail. At first we simply assume a smooth transition zone of the Moho from the end of the elastic plate to the position where local isostatic compensation obtains, near the suture at about $x = -250$ km, but this is an arbitrary choice.

Gravity Data

Bouguer anomalies are taken from different sources: Warsi's [1976] 1° averages; and Choudhury's [1975] contour maps for the Indian shield, the Ganga Basin, and the Lesser Himalaya; Kono [1974] for the Lesser and part of the Greater Himalaya; Tang et al. [1981] for the Greater Himalaya and Tibet; and one datum within the Tibetan plateau from Amboldt [1948].

Warsi's and Choudhury's contours generally agree within 0.15 mm/s^2 (15 mGal), but over a part of the Ganga Basin ($100<x<130$) they disagree by about 0.30 mm/s^2. In this latter case we took the mean of the two values and assumed an uncertainty of ±0.25 mm/s^2 (±25 mGal). Elsewhere we assumed it to be ±0.15 mm/s^2 (±15 mGal). We averaged Kono's measurements in the Central Himalaya and assigned an uncertainty on the basis of the scatter; it varies from about ±0.15 to ±0.20 mm/s^2. Kono's data include terrain corrections, but Warsi's do not. From Kono's calculation the terrain correction in the Lesser Himalaya is of the order of 0.10 to 0.15 mm/s^2 . Warsi's datum for $x = -50$ has been corrected on this basis. For the Greater Himalaya and Tibet we used four measurements (Table 1) that apparently include terrain corrections [Tang et al., 1981] and one measurement of Amboldt [1948] within the plateau (34°38.5'N, 84°50.3'E). It is reassuring that Kono's and Tang et al.'s anomalies agree in the Mount Everest region and that Kono's, Warsi's, and

TABLE 1. Gravity Data From Tang et al. [1981]

Latitude °N	Longitude °E	Bouguer, mm/s^2 or 10^2 mGal
28°01.5'	86°56'	-3.04
28°33'	86°40'	-3.92
29°04.5'	86°17'	-5.23
29°28'	86°13'	-4.94

Choudhury's anomalies agree in the Lesser Himalaya.

From all of these data a profile was drawn, perpendicular to the trend of the Himalayan Mountains, in the Mount Everest area (Figure 1). We projected data measured within 60 km from the profile onto it.

Calculations of Flexure and Gravity Anomalies

Simple plate with a constant flexural rigidity. We calculated the shape of the top surface of the Indian plate and the corresponding gravity anomalies for a variety of assumed values for the flexural rigidity, density differences, and positions of the northern end of the plate. To some extent these series of calculations serve as numerical experiments to constrain the values of the parameters that are varied. The data are the gravity anomalies, the depth of the sediments in the Ganga Basin, and the width of the sediment-filled Ganga Basin. The sediment thickness is maximum at the foot of the range. There is no direct measurement of the sediment thickness where the profile crosses the basin, but the maximum thickness is probably between 4 and 5 km [Rao, 1973] and may reach 6 km farther west of the gravity profile in the Sarda depression (28°N, 80°E). The width of the basin is about 250 km. The top of the Central Indian Plateau, which may be analogous to an "outer topographic rise" at island arcs, is situated about 600 km from the foot of the range.

The calculations show that the flexural rigidity controls the dip of the plate, the width of the basin, and the position of an "outer topographic rise," whereas the thickness of the sediments at the foot of the range is controlled more by the position of the north end of the plate X_o than by the flexural rigidity (Table 2). Values of D between 0.2 and 0.7 x 10^{25} N m and of X_o between 125 and 130 km yield the closest matches to observed maximum thickness of the sediments and width of the Ganga Basin (Tables 2 and 3).

TABLE 2. Calculated Maximum Thicknesses of Sediments in the Ganga Basin Assuming That $\rho_m-\rho_c$ = 0.55 x 10^3 kg/m^3 and $\rho_c-\rho_s$ = 0.5 x 10^3 kg/m^3

	X_o, km						
D,N m	-100	-125	-130	-150	-200	-400	-1000
2. x 10^{25}	1.8	3.15	3.5	4.7	6.55	7.85	7.9
0.7 x 10^{25}	2.25	3.8	4.2	5.5	7.	7.3	7.75
0.2 x 10^{25}	2.7	4.25	4.6	5.8	6.7	6.6	7.

In kilometers.

TABLE 3. Calculated Widths (km) of the Ganga Basin Assuming $\rho_m-\rho_c$ = 0.55 x 10^3 kg/m^3 and $\rho_c-\rho_s$ = 0.5 x 10^3 kg/m^3

	X_o, km						
D,N m	-100	-125	-130	-150	-200	-400	-1000
2. x 10^{25}	390	370	370	370	350	350	360
0.7 x 10^{25}	310	290	290	290	290	290	300
0.2 x 10^{25}	230	220	220	210	200	200	220

In kilometers.

These ranges of values of X_o (Figure 3) and D (Figures 4 and 5) also yield the most satisfactory fits to the gravity data over the Ganga Basin. Note that the position of the Moho between x = X_o, the northern end of the plate, and x = -250 km is arbitrarily drawn as a straight line. Therefore the fit of the observed and calculated gravity anomalies for $x \leq X_o$ is not a criterion for accepting or rejecting any of the parameters. The effects of different assumed values of the width X_s of the Ganga Basin are negligible. Assumed values of X_s between 200 and 300 km lead to very similar profiles. The effects of other parameters are now described in detail.

Constraints on the position of the northern end of the elastic plate (Figure 3). For a position of the northern end of the plate, X_o, closer than 120 km to the Himalayan front, the load is not sufficiently large to bend the plate enough: the calculated thickness of sediments is no more than 3.5 km (Table 2) and the computed gravity anomalies are less negative by 0.50 mm/s^2 (50 mGal) than those observed.

For X_o between -150 and -200 km, the computed maximum thickness of the sediments is large (about 6.5 km) and the calculated gravity anomalies are large, with maximum residuals of the order of 1.00 mm/s^2 (100 mGal) in the Ganga Basin. Calculated gravity anomalies for profiles with X_o between -200 and -1000 km are not very different one from another and can barely be distinguished. These results obtain for a wide range of acceptable flexural rigidities (Figure 4). An increase of the assumed density of the sediments from 2.3 to 2.5 x 10^3 kg/m^3 can halve the large residuals in the Ganga Basin, but nevertheless, nearly 0.5 mm/s^2 (50 mGal) cannot be explained, and 2.5 x 10^3 kg/m^3 is an upper limit for density of sediments.

For X_o betweem -130 and -135 km, the maximum calculated depth of the sediments is between 4.2 and 5 km. As we discuss below, the fit of the gravity data can be improved by reducing $\rho_c-\rho_s$

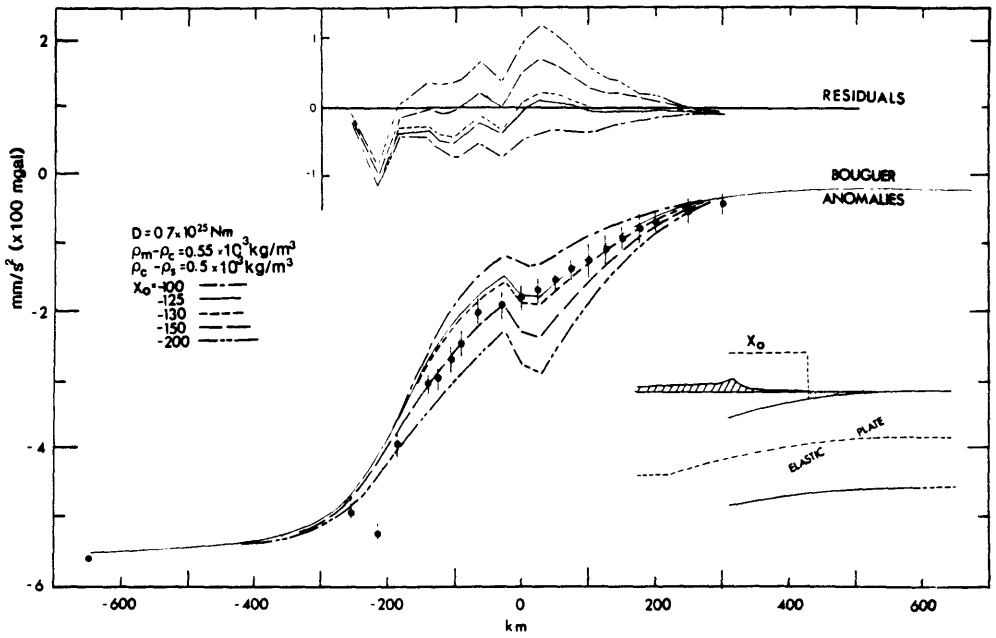

Fig. 3. Comparison of calculated and measured Bouguer anomalies for different position of the northern end of the plate (X_o). The black dots are observed Bouguer anomalies (1 mm/s^2 is 100 mGal). Error bars represent assumed uncertainties, as discussed in the text. At the top, residuals of observed minus calculated anomalies are shown. In the lower right, configuration of the plate is sketched. Notice that the fit over the Ganga Basin implies a value of X_o between -125 and -135 km. The Moho between X_o and x=-250 km is arbitrarily drawn as a straight line, so the poor fit of calculated to the observed anomalies for $x < -100$ km is not significant.

(Figure 7). Thus the most likely value of X_o is between about -125 and -135 km.

Constraints on the flexural rigidity (Figures 4 and 5). The value of the flexural rigidity affects the curvature of the plate, while manifesting itself most clearly in the width (Table 3) and less obviously in the depth of the Ganga Basin (Table 2). Values of D as small as 0.2 x 10^{25} N m yield basins that are only 200-230 km in width, and values as large as 2.0 x 10^{25} N m yield basins wider than 350 km (Table 3). These results suggest that D is between these values and close to 0.7 x 10^{25} N m.

The gravity anomalies provide a weaker

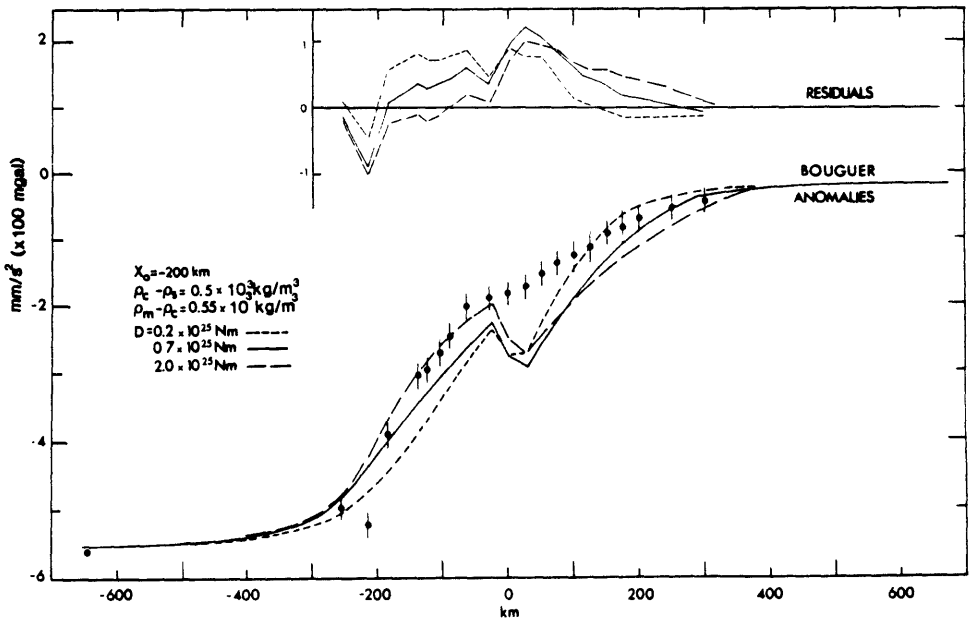

Fig. 4. Comparison of calculated and measured Bouguer anomalies for different values of the flexural rigidity (D) when X_o = -200 km. Layout as in Figure 3. Note that there is no value of D that allows an acceptable fit of calculated to observed anomalies .

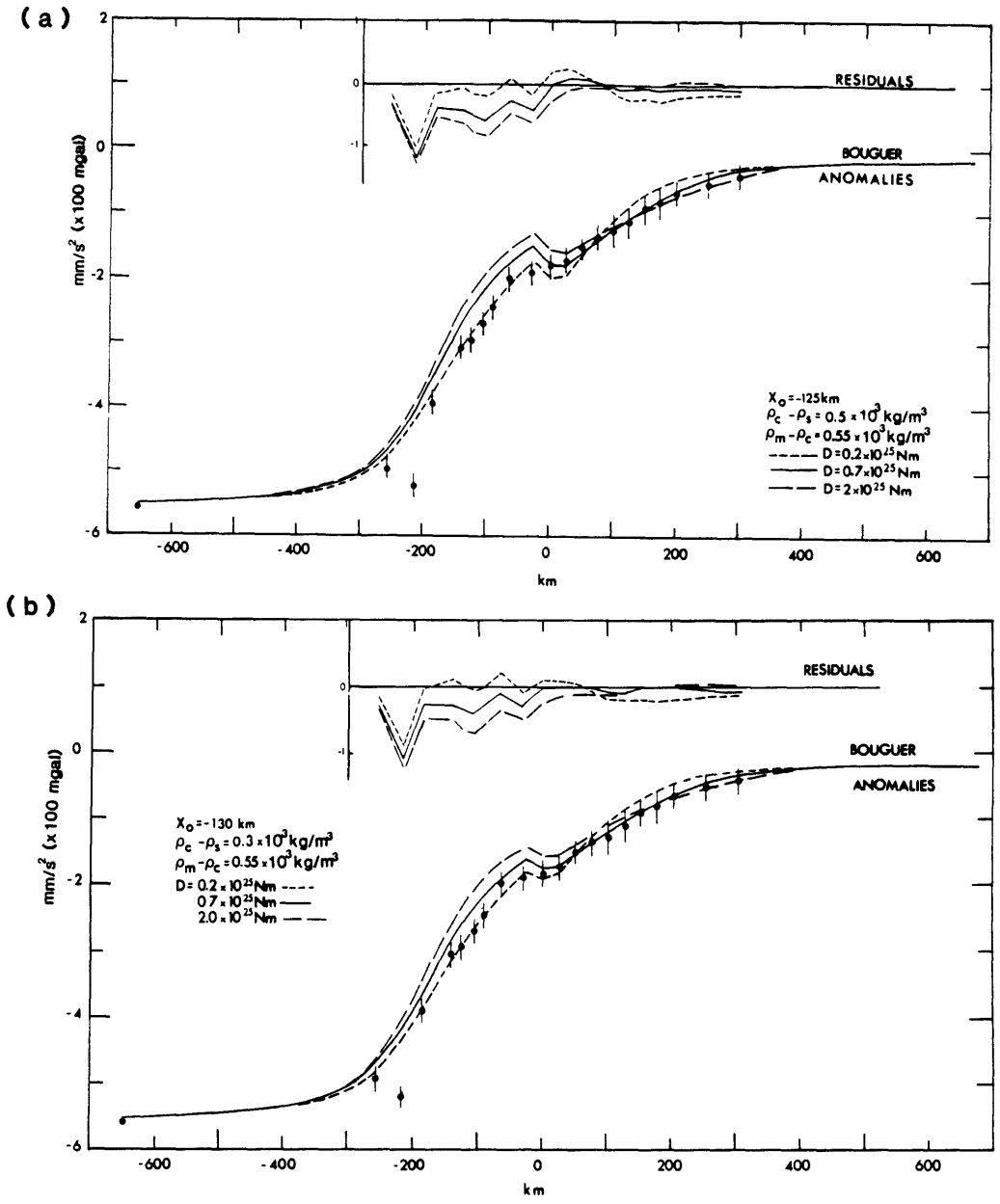

Fig. 5. Comparison of calculated and measured Bouguer anomalies for different values of the flexural rigidity (a) for X_o = -125 km and $\rho_c - \rho_s$ = 0.5 x 10^3 kg/m^3 and (b) for X_o = -130 km and $\rho_c - \rho_s$ = 0.3 x 10^3 kg/m^3. Layout as in Figure 3. Note that in both cases the best fit of calculated to observed gravity anomalies over the Ganga Basin is obtained for D = 0.7 x 10^{25} N m but that values of D of 0.2 x 10^{25} or 2.0 x 10^{25} N m may also be acceptable.

constraint on the value of the flexural rigidity than does the width of the basin. First, note that for X_o = -200 km, there is no value of D that allows a fit to the gravity anomalies (Figure 4). For X_o = -125 km, the gravity anomalies are matched better if D = 0.7 x 10^{25} N m, when $\rho_c - \rho_s$ = 0.5 x 10^3 kg/m^3, than for larger or smaller values of D (Figure 5a). But values as small as about 0.2 x 10^{25} N m or as large as about 2.0 x 10^{25} N m probably cannot be ruled out by the gravity data alone, especially if we allow the density contrast between the crust and the sediments to vary between 0.5 and 0.3 x 10^3 kg/m^3 and X_o to vary between -125 and -135 km (Figure 5b).

Effects of the density contrast between the mantle and crust (Figure 6). Results discussed above are based on calculations assuming that $\rho_m - \rho_c$ = 0.55 x 10^3 kg/m^3, which is a relatively large value. Calculations assuming that $\rho_m - \rho_c$ = 0.45 and 0.4 x 10^3 kg/m^3 confirm that lowering this density contrast effectively increases the load by increasing crustal density relative to mantle density. Thus for D = 0.7 x 10^{25} N m and X_o = -130 km, the maximum depth of the sediments increases from 4.2 ($\rho_m - \rho_c$ = 0.55 x 10^3 kg/m^3) to 4.75 km ($\rho_m - \rho_c$ = 0.45 x 10^3 kg/m^3) and 5 km ($\rho_m - \rho_c$ = 0.4 x 10^3 kg/m^3). If the relative density contrast between the mantle and sediments is

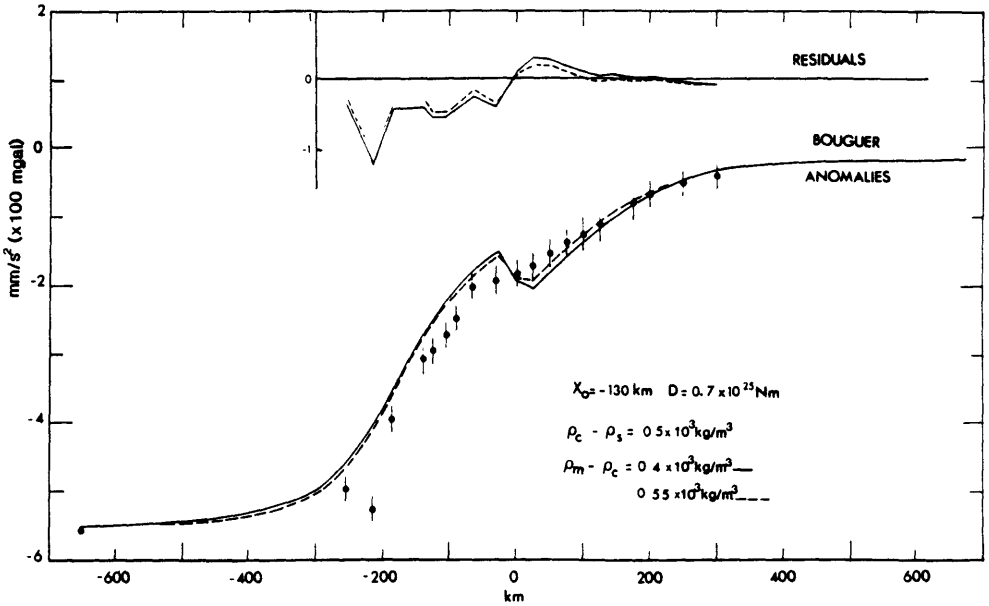

Fig. 6. Comparison of calculated and measured Bouguer anomalies for two different values of the density contrast between the mantle and the crust ($\rho_m-\rho_c$). The density contrast between the crust and the sediments is kept constant and equal to 0.5 x 10^3 kg/m^3. Layout as in Figure 3.

correspondingly reduced from 1.05 to 0.95 and 0.9 x 10^3 kg/m^3, calculated gravity anomalies in the Ganga Basin differ by a maximum of only 0.10 mm/s^2 (10 mGal) among the models with different density contrasts (Figure 6) . Thus, although the density contrast between the mantle and crust affects the shape of the plate by depressing it about 10% more when $\rho_m-\rho_c$ is 0.45 x 10^3 kg/m^3 and 20% more when 0.4 x 10^3 kg/m^3 than when it is 0.55 x 10^3 kg/m^3, it has almost no effect on the calculations of gravity anomalies. In our following calculations we will keep $\rho_m-\rho_c$ = 0.55 x 10^3 kg/m^3, but even if $\rho_m-\rho_c$ is actually closer from 0.4 than from 0.55 x 10^3 kg/m^3, this would not change our conclusions much.

Effects of the density contrast between the crust and the sediments (Figure 7). If the density contrast between the crust and the sediments is decreased from 0.5 x 10^3 kg/m^3, as assumed in most of the previous calculations, to 0.3 x 10^3 kg/m^3 and if the density contrast between mantle and crust is kept constant, the plate is depressed

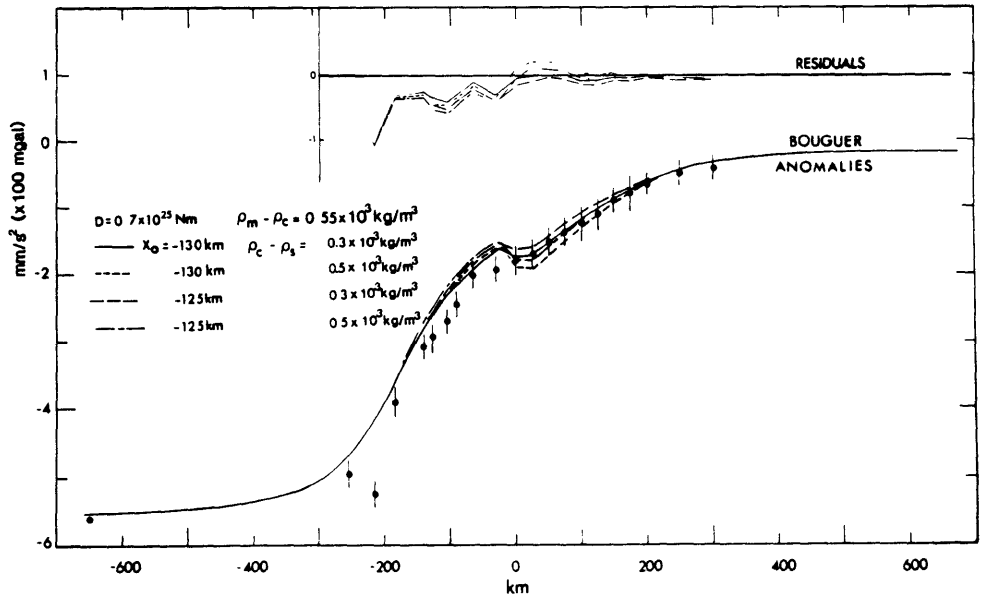

Fig. 7. Comparison of calculated and measured Bouguer anomalies for different values of the density contrast between the crust and the sediments. The density contrast between the mantle and the crust is kept constant and equal to 0.55 x 10^3 kg/m^3. Layout as in Figure 3.

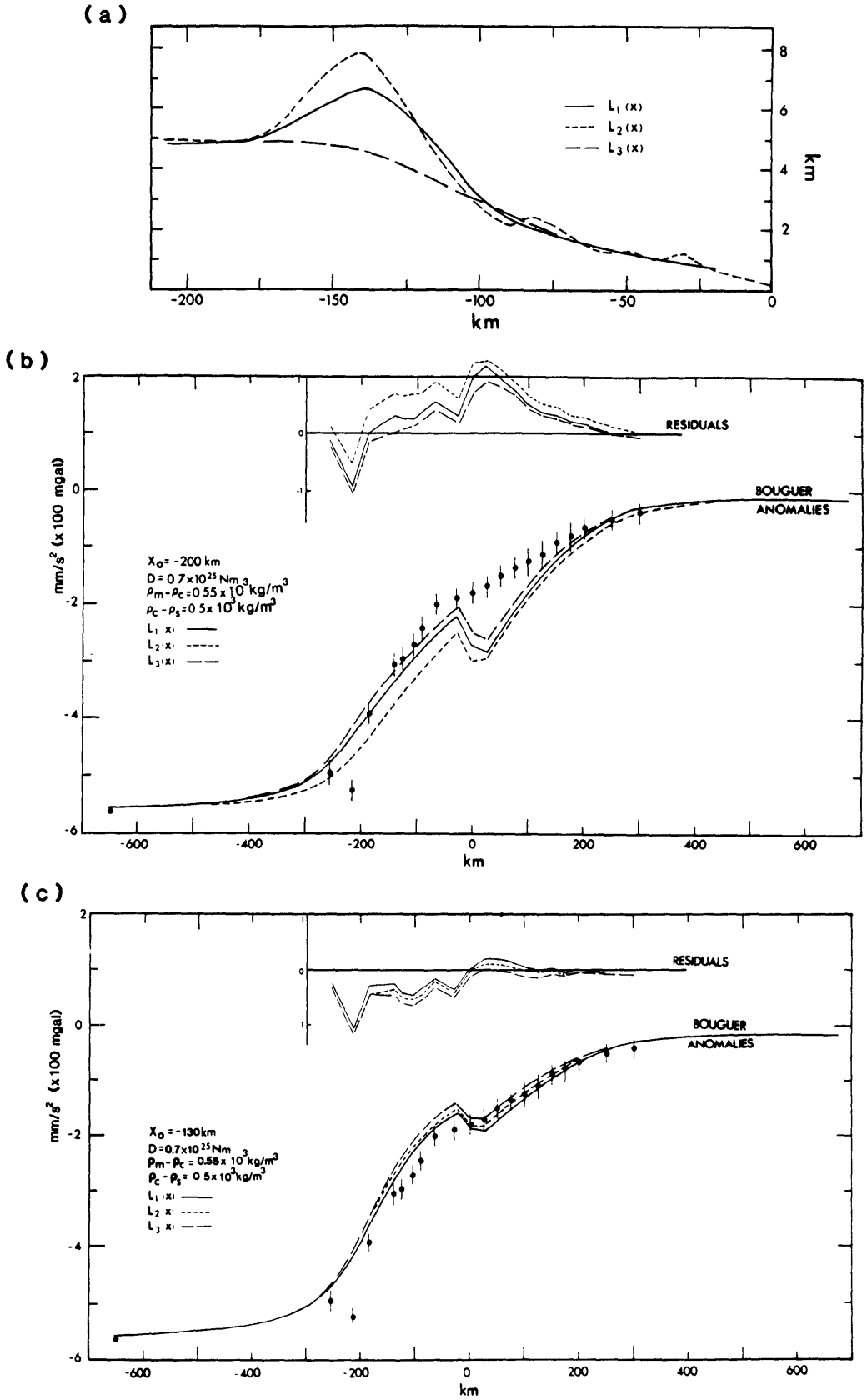

Fig. 8. Comparison of different topographic profiles and their effects. (a) $L_1(x)$ is mean elevation within 100 km and $L_2(x)$ within 20 km of either side of the the gravity profile; $L_3(x)$ is Bird's [1978] average elevation over the entire width of the range. Comparison of calculated Bouguer anomalies for the different loads for D = 0.7 x 10^{25} N m and (b) for X_o = -200 km and (c) for X_o = -130 km.

more by only about 3%. Therefore, contrary to the density contrast between the mantle and the crust, the density contrast between the crust and the sediments has almost no effect on the shape of the plate but increases the gravity anomalies in the Ganga Basin by a maximum of about 0.25 mm/s^2 (25 mGal) at its deepest point. This is the reason why we cannot differentiate between the two profiles X_o = -125 km and X_o = -130 km with D = 0.7 x 10^{25} N m (Figure 7).

Sensitivity of the model to the choice of the load (Figure 8). Previous computations were performed using a load $L_1(x)$ obtained from mean elevation along a profile 200 km wide in the region where measurements were made (Figure 8a). The mean elevation reaches a maximum of about 6500 m at the abscissa of the Mount Everest. For comparison we also made computations with a load $L_2(x)$, obtained from mean elevations along a profile 40 km wide (Figure 8a), and a load $L_3(x)$ obtained from Bird's [1978] average elevation over the entire width of the range (Figure 8a). Elevations corresponding to $L_2(x)$ are higher than for $L_1(x)$ over the Greater Himalaya, but the maximum (~8000 m) is reached at the same abscissa. At the same time, mean elevations over the Lesser Himalaya are a little smaller than for $L_1(x)$. The profile corresponding to $L_3(x)$ is lower than $L_1(x)$ and $L_2(x)$ by about 2 and 3.5 km, respectively, over the Greater Himalaya and does not have a maximum elevation near the abscissa corresponding to the Mount Everest. This profile consists of an average elevation over various parts of the range that do not necessarily share the same tectonic evolution; therefore it is probably not the appropriate load to use in this study, but it provides an extreme with which to examine the uncertainities in the parameters that results from uncertainities in the load.

The differences among computed gravity anomalies for these three profiles can reach 0.50 mm/s^2 (50 mGal) for the case where the plate is assumed to underthrust the Greater Himalaya (i.e., X_o = -200 km) (Figure 8b). For all these loads, however, a plate with a constant flexural rigidity cannot underthrust the entire mountain range (Figure 8b). Differences among calculated anomalies are smaller for plates that underthrust only a fraction of the range (i.e., X_o = -130 km) (Figure 8c), and consequently, the uncertainity in the load increases the uncertainity in X_o noted above. For instance, using Bird's [1978] profile, the data will be best fitted with X_o = -140 km instead of X_o = -130 km using $L_2(x)$ (Figure 8c) or X_o = -125 km using $L_1(x)$ (Figure 3). We present the following computations using only $L_1(x)$, but as we have shown here, using either a larger or a smaller load will only introduce small quantitative changes in our results.

Effect of a bending moment applied to the end of the plate. Below, we show that if a bending moment is applied at the end of the plate that underthrusts the entire range, the gravity anomalies cannot be fit well unless the flexural rigidity of the portion of the plate beneath the Greater Himalaya is considerably smaller than that beneath the Lesser Himalaya (Figure 13).

Summary. These calculations show clearly that a plate of constant flexural rigidity cannot underthrust even southernmost Tibet. Models that call for wholesale underthrusting of Tibet by the Indian shield [e.g., Argand, 1924; Powell and Conaghan, 1973] must do so only by allowing the Indian shield to lose a considerable amount of its strength approximately 120-140 km from the front of the Himalaya.

The calculations show that the flexural rigidity of the plate and the position of the end of the plate are constrained independently from one another. We conclude that the end of the elastic plate is between 120 and 140 km north of the Himalayan front and that a flexural rigidity of about 0.7±0.5 x 10^{25} N m, corresponding to an elastic thickness of about 80±30 km, is necessary to explain the topographic features and the gravity field of the Ganga Basin. The fit north of the Ganga Basin, however, can be improved.

The dip of the Moho beneath the Greater Himalaya. The calculated anomalies over the Greater Himalaya and Tibet may be altered by arbitrarily changing the configuration of the Moho between the end of the elastic plate, X_o, and the southern margin of Tibet where isostatic equilibrium is assumed to prevail. If the crustal thickness of Tibet is reached 200 km from the foot of the range instead of 250 km, as assumed in Figures 3 to 8, the calculated and observed anomalies agree well (Figure 9). This corresponds to a dip of the Moho of about 15° beneath the Greater Himalaya (provided that $\rho_m - \rho_c$ = 0.55 x 10^3 kg/m^3), compared with only about 3° beneath the Lesser Himalaya.

Possibility of subducted sediments beneath the Lesser Himalaya. In the Lesser Himalaya, calculated anomalies are consistently 0.25 to 0.50 mm/s^2 less negative than observed (Figures 5, 6, and 7). To eliminate this difference requires the introduction of material with low density beneath the Lesser Himalaya. The introduction of a thin wedge of material with a density ρ = 2.5 x 10^3 kg/m^3 beneath the Lesser Himalaya is adequate to eliminate this negative residual (Figure 9) and suggests that sediments were probably subducted along with the underthrust plate.

Plate with a reduced flexural rigidity beneath the Greater Himalaya. The steeper dip of the Moho beneath the Greater Himalaya suggests that the plate is flexed more and therefore that the flexural rigidity is less than beneath the Lesser Himalaya and farther south. To analyze quantitatively this change in dip, we studied the flexure of a plate consisting of two segments with different flexural rigidities (Figure 2). There are now two additional parameters that we can vary: the flexural rigidity of the northern segment D' and the position of the junction between the two segments, now defined by X_o. First, we fix the end of the elastic plate, X_o', equal to -200 km in order to mimic the structure used in Figure 8. We seek values of D' and X_o that will lead to a plate with a shape close to that used in the computation of Figure 9. We already know that X_o is between about -100 and -150 km. Although the purpose of adding another segment of plate is to fit the steepening of the Moho beneath the Greater Himalaya, the addition of this segment has a second important effect. The load of the Greater Himalaya on this additional segment must be supported by the elastic strength of the plate, and consequently, the plate is flexed down more than for the cases considered above that ignored the support of this mass. Even if D' is small so that the northern segment bends

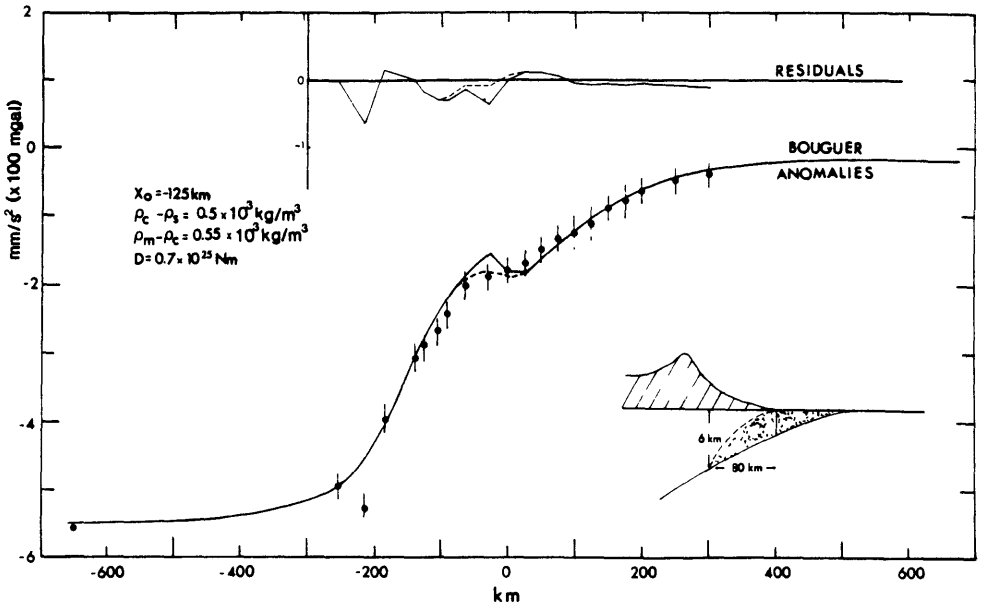

Fig. 9. Comparison of calculated and measured Bouguer anomalies. Layout as in Figure 3. Solid line shows calculated anomalies as in Figures 3-7 but with the Moho set at a depth of 60 km at x = -200 km not -250 km, as in Figures 3-8. Note the better fit of calculated to observed anomalies for x <-100 km than in Figures 3-8. Dashed curve shows the effect of including a thin wedge of light material $\rho = 2.5 \times 10^3$ kg/m^3 (sediments) beneath the Lesser Himalaya. (See inset in lower right.)

a great deal, the effect of this additional load is important. For a wide range of flexural rigidities of this segment (0.2×10^{22} to 0.4×10^{24} N m), and X_o = -130 km or -100 km, the plate is depressed about 50% more (Figure 10a) than for the case in Figure 9. The same effect is observed for other values of X_o between -100 and -150 km. The corresponding gravity profiles (Figure 10b) show that it is not possible to match the gravity anomalies by just considering a plate with a variable flexural rigidity. If X_o is -130 km, values of D' from 0.2×10^{22} to 0.4×10^{24} N m allow the entire plate to be depressed too much, leading to an overall positive residual. If X_o is only -100 km, the entire plate is less depressed than in the case where X_o is -130 km, especially if D' is small (0.5 to 0.2×10^{22} N m), but in this case the northern segment of the plate steepens too rapidly (Figure 10).

Profiles computed using other loads ($L_2(x)$ or $L_3(x)$) show the same qualitative features, but the deflection of the plate is smaller when $L_3(x)$ is used and larger when $L_2(x)$ is used. For instance for profiles computed with $L_3(x)$ and with X_o = -130 km, X_o' = -200 km, D = 0.7×10^{25} N m and D' = 0.2×10^{22} N m, the maximum depth of the basin at x = 0 km is only 5.2 km, compared with 6.5 km when $L_2(x)$ is used and 6.0 km when $L_1(x)$ is used (Figure 10).

The calculations discussed in the previous section implied that an elastic plate flexed by the load of the Lesser Himalaya could account for the gravity anomalies over that region and the Ganga Basin. The results of these calculations, however, show that if the load includes the Greater Himalaya, this additional load depresses the plate too much to allow a match of calculated and observed gravity anomalies. Either additional sources or deficits of mass are required or additional forces must operate on the plate.

Inclusion of a bending moment. Rather than appeal to additional and somewhat arbitrarily chosen excesses or deficiencies in mass, we examine the effects of other likely forces. We first investigate the effect of a bending moment applied at the end of the elastic plate. The moment both depresses the northern end of the plate and, in reaction, elevates a portion farther south. A sufficiently large moment can flex the plate up enough to overcome the subsidence created by the additional weight. An increase in the bending moment, however, causes the northern end of the plate to steepen. We found that a bending moment applied at the end of a plate with X_o' = -200 km will not allow a satisfactory fit to the data. A bending moment of the order of 0.5 to 1.1×10^{18} N m is needed to elevate the plate enough beneath the Lesser Himalaya and the Ganga Basin, but in this case the slope of the northern part becomes too large (~25°) (Figure 11). These calculations apply for values of D' between about 10^{22} and 10^{23} N m. If D' is smaller than 10^{22} N m, the contrast between the two flexural rigidities becomes too large, and the interaction between the two parts of the plate is very small. The bending moment will then bend the northern part of the plate a great deal but will have very little effect on the slope or position of the plate beneath the Lesser Himalaya. On the other hand, if D' is larger than 10^{23} N m, the difference between the two flexural rigidities is not sufficiently large to allow the steepening observed beneath the Greater Himalaya. We conclude that no bending moment applied 200 km north of the Himalayan front will allow a fit of observed and calculated gravity anomalies.

The position of the northern end of the plate, where the bending moment is applied, must be farther north. If the bending moment is applied at

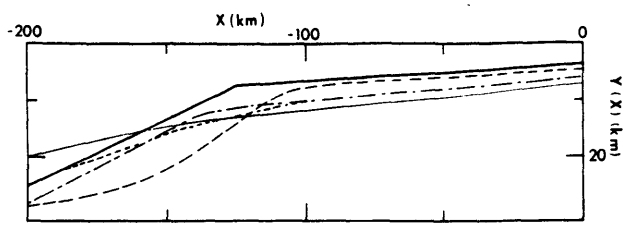

Fig. 10a. Calculated deflections of the plate for the combination of parameters shown in Figure 10b. The heavy line shows the deflection used in Figure 9.

$X_o' \leq -270$ km, it does not change the shape of the plate for x between -130 and -200 km enough, and if it is applied at $X_o' \geq -230$ km, it steepens the end of the plate ($-200 \leq x \leq -130$) too much and too quickly (Figure 12). Therefore if a bending moment is applied at the end of the elastic plate, this should be between 230 and 270 km from the Himalayan front.

If the moment is applied at the end of a plate where $X_o' = -250$ km, it is possible to find different combinations of D' and of the applied bending moment M_o that will lead to acceptable fits of calculated and observed gravity anomalies (Figure 13). If D' is 0.7×10^{23} N m and $X_o = -125$ km, M_o must be about 0.85×10^{18} N m, but if D' = 0.2×10^{23} N m, M_o need only be 0.55×10^{18} N. For the same value of D' the moment must be about 10% larger if $X_o = -150$ km than if $X_o = -130$ km. Again profiles computed with $L_2(x)$ or $L_3(x)$ show the same qualitative features as for $L_1(x)$, but $L_2(x)$ requires a larger bending moment ($\sim 0.65 \times 10^{18}$ N) and $L_3(x)$ a smaller one ($\sim 0.45 \times 10^{18}$ N) than $L_1(x)$ (0.55×10^{18} N m).

One difficulty with applying a bending moment at x = -250 km is that although the calculated shape of the plate is fairly close to that used in Figure 9 for $x \geq -200$ km, the curvature of the plate continues to increase beyond this point, and the calculated depth of the Moho reaches 115 km at x = -250 km (Figure 11)! We do not believe that the Moho necessarily does reach such a depth. It would not be required, for instance, if we assumed that the decrease in flexural rigidity of the northern segment of the plate were accomplished by detaching the crust from the rest of the Indian lithosphere. In any case, the calculated gravity profiles obtained directly from the flexed plate with a Moho reaching 115 km and those obtained by arbitrarily assuming that the depth of the Moho does not exceed 65 km for $x < -200$ km differ primarily in the range $-400 \leq x \leq -200$ km (Figure 14). The data that we have are inadequate to eliminate one or the other extreme. It is interesting, however, that the profile given by Tang et al. [1981] for a portion of Tibet about 200 km farther east shows a minimum of about 0.30 mm/s^2 (30 mGal) near the Indus-Tsangpo suture, suggesting that the crust might be deeper there than farther north or south.

We conclude that to match the gravity anomalies with an elastic plate loaded by the weight of the overthrust mountains, there must be a bending moment applied to the end of the plate.

Origin of the bending moment. If a horizontal force/unit length F acts on the end of the plate that is bent down a distance y_o, then provided that this force is much less than critical buckling strength, it produces a bending moment $M_o = Fy_o/2$ [Parsons and Molnar, 1976]. If we assume that this force is produced by a compressive stress σ, acting on a plate of thickness H and depressed an amount y_o at its end, then $\sigma = 2M_o/Hy_o$. If $y_o = 30$ km, H = 50 km, and $M_o = 0.55 \times 10^{18}$ N m, $\sigma = 730$ MPa (7.3 kbar). Since the horizontal compressive stress needed to maintain the high elevation and thick crustal root of Tibet is only 50 to 100 MPa [e.g., Frank, 1972; Tapponnier and Molnar, 1976], it does not seem possible to invoke a compressive stress as a mechanism to create the bending moment. We do not think that a large stress of 730 MPa can exist throughout the lithosphere.

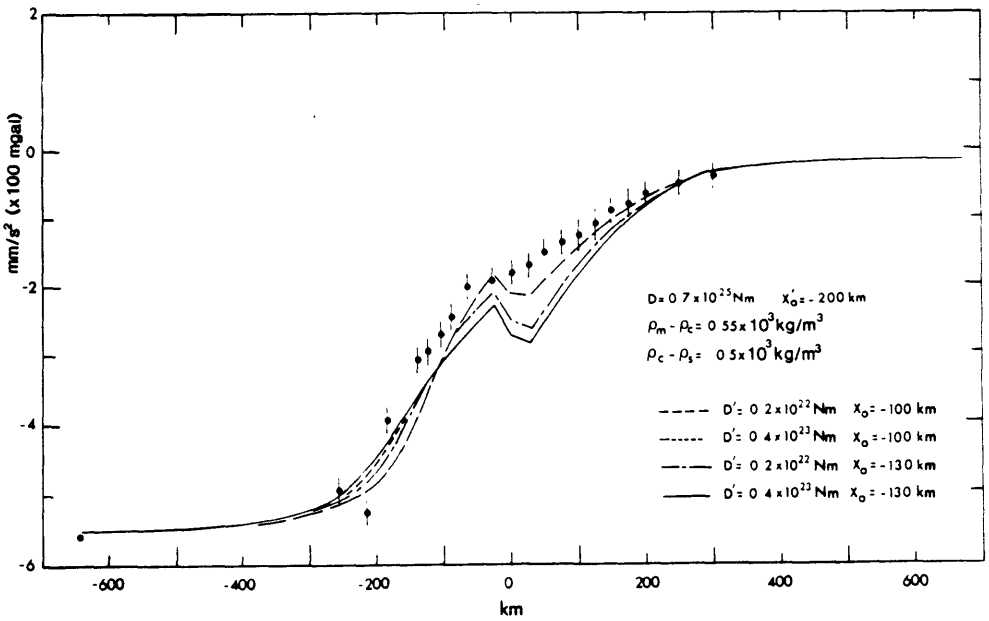

Fig. 10b. Calculated Bouguer anomalies for the deflections shown in Figure 10a. Layout as in Figure 3.

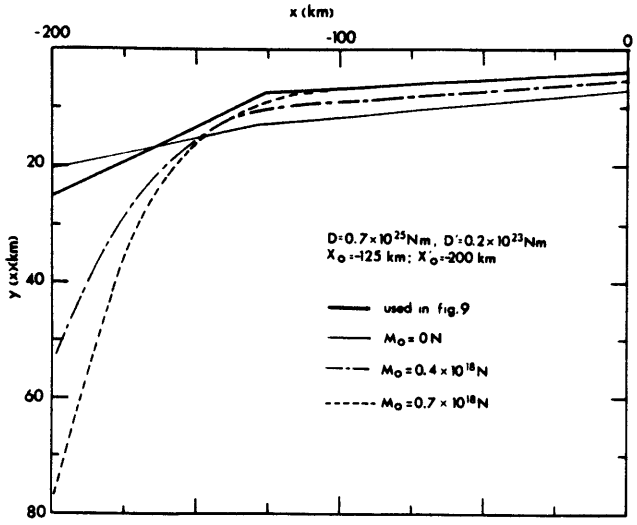

Fig. 11a. Calculated deflections of the plate for different applied bending moments, M_o, at X_o' = -200 km.

Another possible source of a large bending moment would be the torque applied to the Indian plate by gravity acting on a piece of relatively cold and dense material north of the range. If the mantle (elastic) lithosphere of India extended north of the Indus suture and were pulled down by gravity acting on it or by convective downwelling of the lower lithosphere, the force acting on this material would apply a torque to the portion of the plate beneath the Himalaya. We are not aware of evidence requiring such cold material beneath southern Tibet, but the downwelling of cold material beneath mountains is likely where crustal shortening has occurred [e.g., Fleitout and Froideveaux, 1982; Houseman et al., 1981]. If the center of gravity of this cold material is situated at a distance L from the end of the elastic plate beneath the Himalaya, the moment applied to it is $M_o = mgL$, where $m = \Delta\rho S$ is the excess of mass per unit of length. Taking $\Delta\rho$ = 50 kg/m^3, corresponding to material an average of 500°C colder than the asthenosphere, S = 10^4 km^2 and L = 120 km, we obtain a moment per unit of length of 0.55×10^{18} N m. We must not neglect the additional force/unit length acting on the plate, mg = 0.45×10^{13} N/m, caused by this excess mass. This represents 15-20% of the total force due to the weight of the mountains, and therefore its effects both on the size of the deflection of the plate and on the gravity anomalies are relatively small (Figure 14). In fact, the gravity anomaly caused by this additional mass improves the fit to the data from calculations in which the cause of the bending moment is unspecified (Figure 14). The contribution to the gravity anomalies depends on the position, depth, and amount of mass, which cannot be constrainted independently of one another but whose contributions may be chosen somewhat arbitrarily. Therefore there is no unique configuration that can explain the gravity data. There are trade-offs among the bending moment, the position and amount of excess mass, and the flexural rigidity of the northern part of the plate. Without more information it is impossible to be more precise, but insofar as a bending moment must be applied to the Indian plate, the presence of relatively dense material beneath Tibet is a plausible cause of that bending moment.

In summary, first, the flexural rigidity of the northern part of the plate beneath the Greater Himalaya must be less (0.1 to 1.0×10^{23} N m) than that of the rest of the plate (0.7×10^{25} N m) beneath the Lesser Himalaya, the Ganga Basin, and the Indian shield. Second, a bending moment/unit length acting at the end of the plate (0.5 to 1.1×10^{18} N m) is necessary to support the mass of the mountains. Third, both to generate the moment and improve the fit to the gravity data in the Greater Himalaya, we suggest that there is cold dense material beneath southern Tibet that contributes a positive gravity anomaly over it,

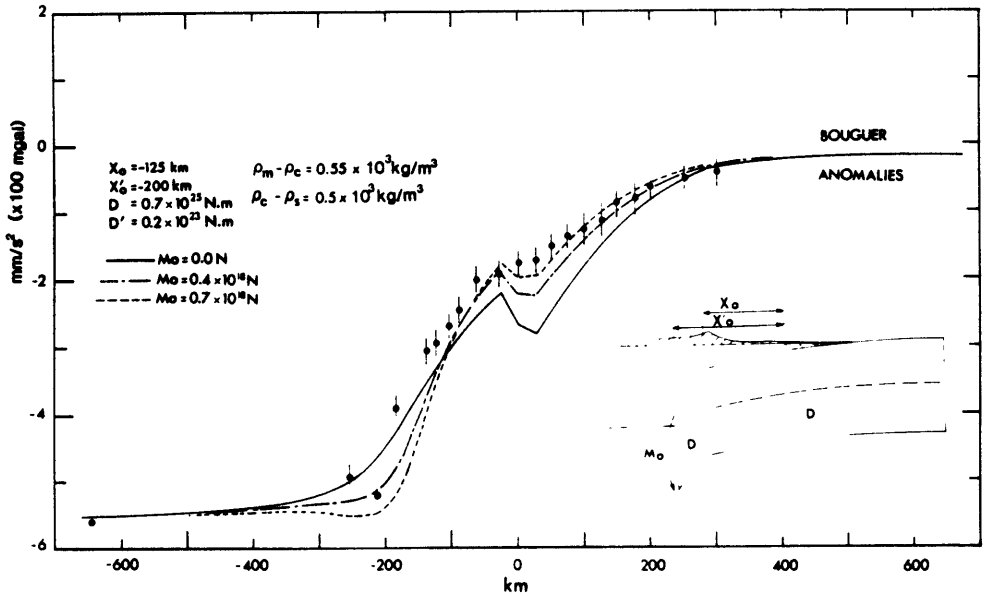

Fig. 11b. Calculated Bouguer anomalies for the deflections shown in Figure 11a. Layout as in Figure 3.

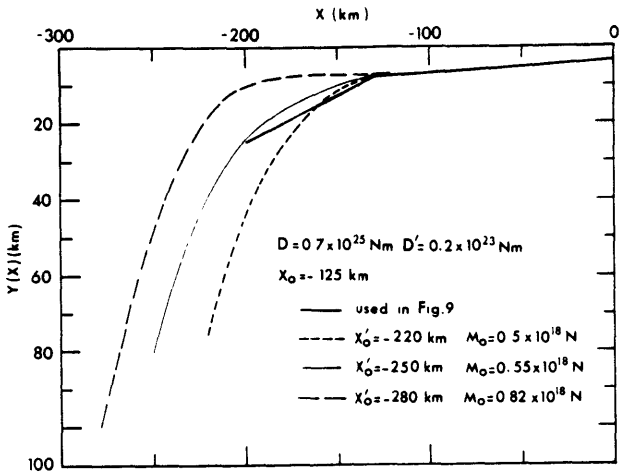

Fig. 12. Calculated deflections of the plate for different positions, X_o', where the bending moment is applied and for the combination of parameters shown.

pulls the Indian plate down slightly, but exerts a torque to the end of the plate so as to apply a bending moment.

Implications for the Tectonic Evolution of the Himalaya

Several aspects of the structures required by the gravity anomalies carry implications for the geologic evolution of the Himalaya. If the flexure of the Indian plate is an appropriate description of its present configuration, then it probably was also when slip occurred on the Main Central Thrust. Therefore it seems likely that the present structure serves as a reasonable model for that that existed while the Main Central Thrust was active.

The suggestion that sediments deposited in the Ganga Basin have been underthrust beneath the Lesser Himalaya may find analogy with the Siwaliks. The Siwaliks are clastic sedimentary rocks of Miocene age and derived from erosion of the Himalaya [e.g., Gansser, 1964]. They are overthrust and folded in a schuppenzone near the foot of the Lesser Himalaya. Older units of the Siwaliks may have been overthrust by the Main Central Thrust. The possibility that both the Siwaliks and the more recent sediments of the Ganga Basin have been overthrust by crystalline terrains of the Lesser Himalaya probably should not be overlooked in the consideration of the petroleum potential of the Himalaya.

The gravity anomalies as well as some of the fault plane solutions and focal depths of earthquakes in the Himalaya suggest that the Indian plate underthrusts the Lesser Himalaya coherently at least 100-150 km. The metamorphic terrains of the Lesser Himalaya would thus have been thrust on top of an effectively elastic plate whose flexural strength supports the mountain belt. Again, it seems likely that the same situation existed when the Main Central Thrust was the active northern boundary of the Indian plate.

We have ascribed the apparent steepening of the Moho from just a few degrees beneath the Lesser Himalaya to about 15° beneath the Greater Himalaya to a reduction in the flexural rigidity of the Indian plate at its northern extremity. If such a reduction in flexural rigidity has occurred, then two likely ways to accomplish this would be by warming, and hence weakening the plate, or by detachment of some of it. The top of the plate will warm much more rapidly than the interior or bottom [e.g., Molnar et al., 1983], and if the top weakens, it will detach from the deeper portions yet more easily than if it remained cold. Thus we think it likely that the decrease in flexural rigidity is a consequence of part or all of the crust being detached from the Indian lithosphere. Since the material below the Main Central Thrust and above the Main Boundary Fault was once part of

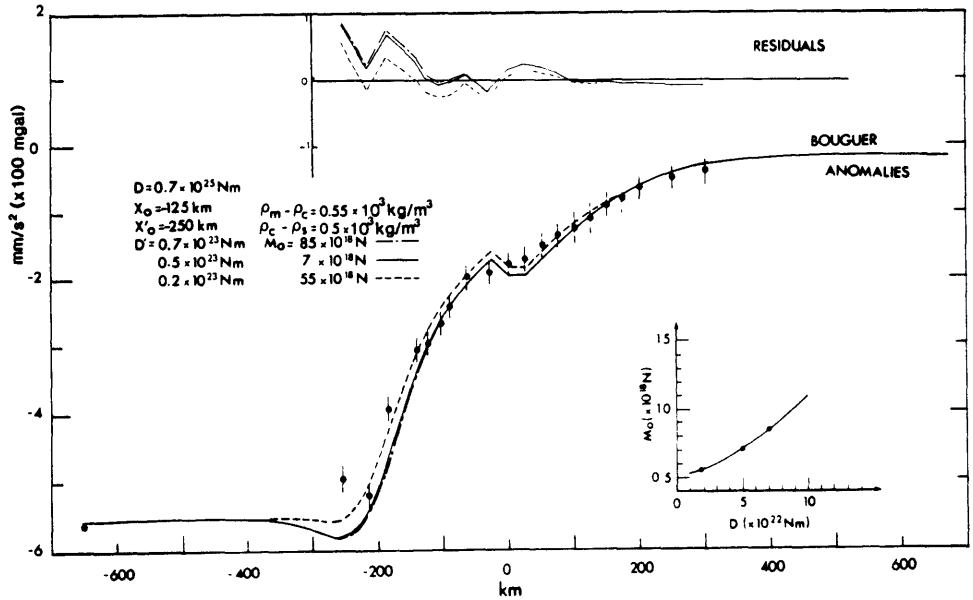

Fig. 13. Three different structures yielding similar Bouguer anomalies. Plot in lower right shows the interdependence between the bending moment and the flexural rigidity.

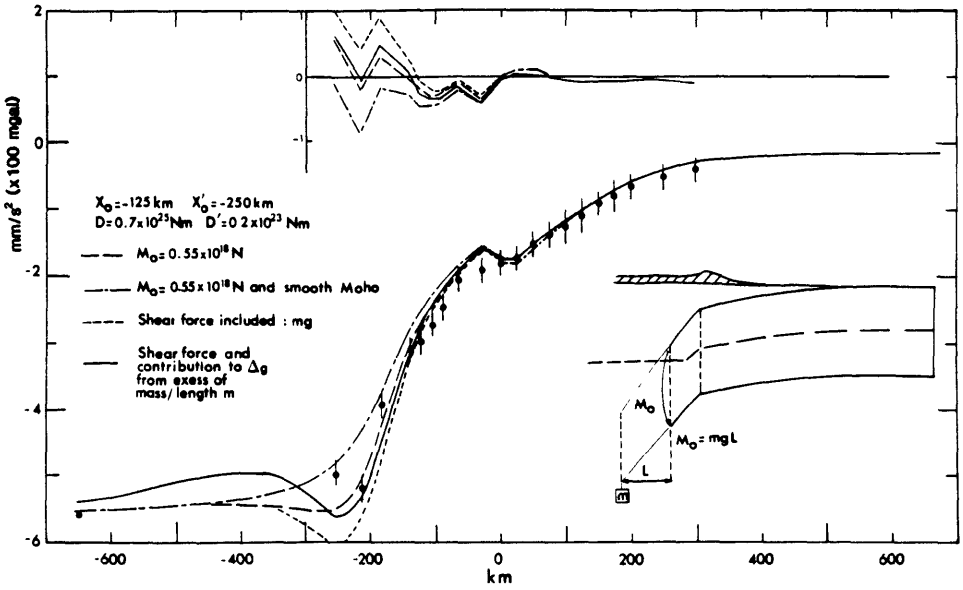

Fig. 14. Comparison of calculated and measured Bouguer anomalies for the combination of parameters shown. Different curves show effects of different forces and of the assumed shape of the Moho beneath southern Tibet on calculated anomalies. Long dashed line shows anomalies calculated directly from the computed deflection (solid line in Figure 12), in which the Moho reaches 115 km at x = -250 km. Dotted-dashed line shows anomalies calculated assuming that the depth of the Moho does not exceed 60 km. Dashed line shows anomalies calculated when the effect of the shear stress due to the excess of mass/length m that creates the bending moment is included. (See sketch in lower right.) When the contribution to the gravity of the excess of mass is also included, the fit to the data is improved (solid line). Note that this contribution depends on the choice of m, L,and the depth of the mass. Here the mass (0.5×10^{12} kg/m) is situated at a depth of 150 km and L = 120 km.

the Indian subcontinent, detachment of it must have taken place sometime in the past. Associating the steepened dip of the Moho with the thinning of the crust on the Indian lithosphere implies a throw of 100-130 km on the Main Boundary Thrust. Similarly, because the material above the Main Central Thrust was once part of the Indian subcontinent, it probably was detached from the Indian lithosphere on the Main Central Thrust earlier.

To present these inferences in an evolving scheme for the geologic history of the Himalaya, we constructed a series of idealized balanced cross sections from before the collision to the present (Figure 15). Several assumptions were used to construct these cross sections: first, we assume that prior to the collision subduction of oceanic lithosphere occurred beneath southern Tibet much as it does beneath the Andes (Figures 15a and 15b). We arbitrarily began with a crustal thickness of 65 km beneath the Kangdese granites of southern Tibet. We do not know when the crust beneath southernmost Tibet thickened, but clearly, this assumption is not critical for the cross sections shown here. Second, we assumed that continental crust was not carried to great depth in the asthenosphere, so that the cross-sectional area of the crust must be conserved. In fact, subduction of the lowermost crust is a reasonable possibility [e.g., Molnar and Gray, 1979], but its exclusion here will not affect the major features of the cross sections much. Third, we drew both the Main Central Thrust and the Main Boundary Fault initially as planar faults through the crust (Figures 15c and 15d). For the Main Central Thrust we arbitrarily detached the crust at the Moho (Figure 15c) in order to make conservation of crustal material easier. Clearly, these faults could have begun as listric faults detaching the upper crust along a subhorizontal zone in the crust. It is not our purpose, however, to examine all possibilities but only the gross implications of a few simple assumptions. Fourth, we assume that throughout the period the Indian plate is flexed in a manner analogous to that inferred from the gravity anomalies. Therefore while slip occurred on the Main Central Thrust, the Moho dipped at a shallow angle where coherent lithosphere was underthrust and more steeply farther north where crust had been detached (Figure 15d). Finally, to maintain balanced cross sections, because the position of the Moho is fixed, we stacked the overthrust material up on top of this underthrusting plate, paying no heed to the elevations that such material would reach if there were no erosion (Figures 15c, 15d, and 15e). Notice, however that at the toes of both the Main Central Thrust and the Main Boundary Fault, we have schematically allowed a small amount of underthrusting of sediments. Unlike the rest of the cross sections, however, we have not balanced this portion. To compare with a typical geologic cross section (Figure 1), we show the final cross section (Figure 15e) eroded appropriately to the level of the present topography (Figure 15f).

We show simple underthrusting of oceanic lithosphere (Figures 15a and 15b) followed by collision and underthrusting of Indian crust beneath southern Tibet (Figure 15c). After 100 km

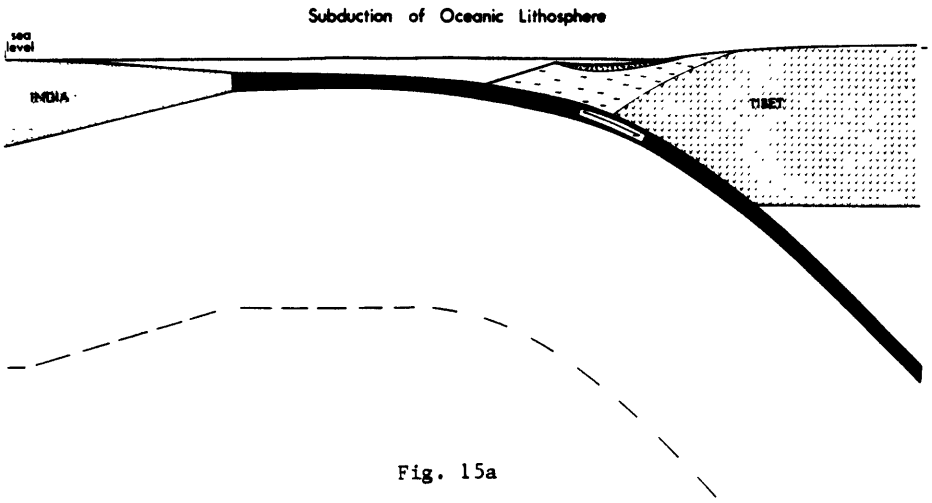

Fig. 15a

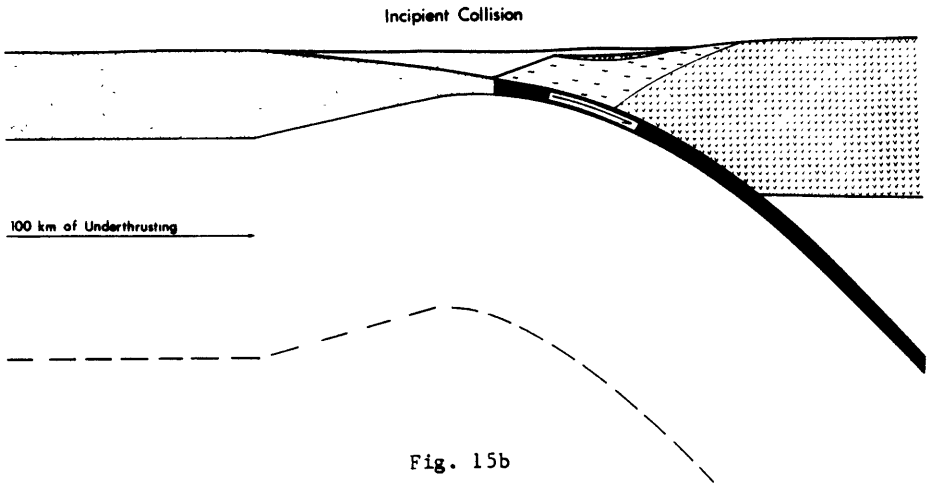

Fig. 15b

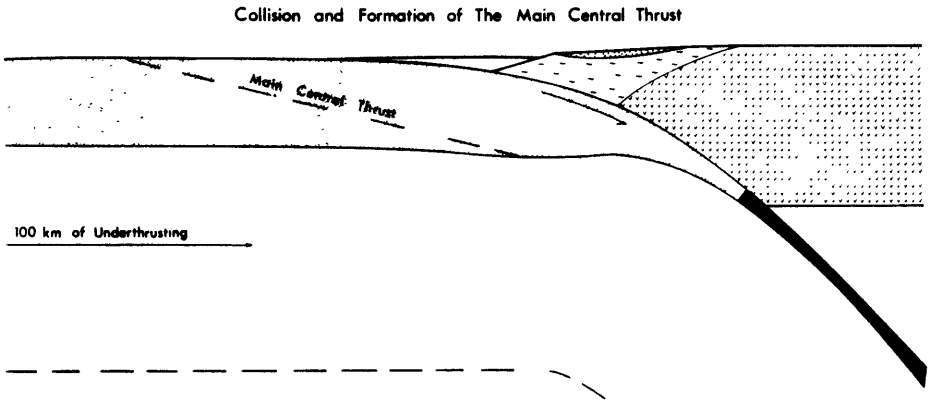

Fig. 15c

Fig. 15. Sequence of idealized cross sections from before the collision to the present. (a) Subduction of oceanic lithosphere before collision. (b) Initial contact of Indian margin with the subduction zone on the southern edge of Tibet. (c) Formation of the Main Central Thrust (MCT) after 100 km of subduction of part of the northern margin of India. (d) Formation of the Main Boundary Fault (MBF) after 125 km of underthrusting of India along the MCT. Note the marked uplift of material over the MCT. (e) Underthrusting of 125 km of India along the MBF. Note that again pronouced uplift occurs where the MBF changes dip. (f) Same as Figure 15e but with material eroded to the level of the present topography. Note that many features of the present Himalaya are present (see Figure 1): the overthrust sediments are analogous to the Siwaliks, the klippe of crystalline rocks transported bv the MCT to the south is present, the MCT dips at a gentle angle to the south but more steeply to the north, the metamorphosed sediments in the Lesser Himalaya are domed slightlv, and high-grade metamorphic rocks are present above the MCT.

Underthrusting Along The MCT And Formation of The Main Boundary Fault

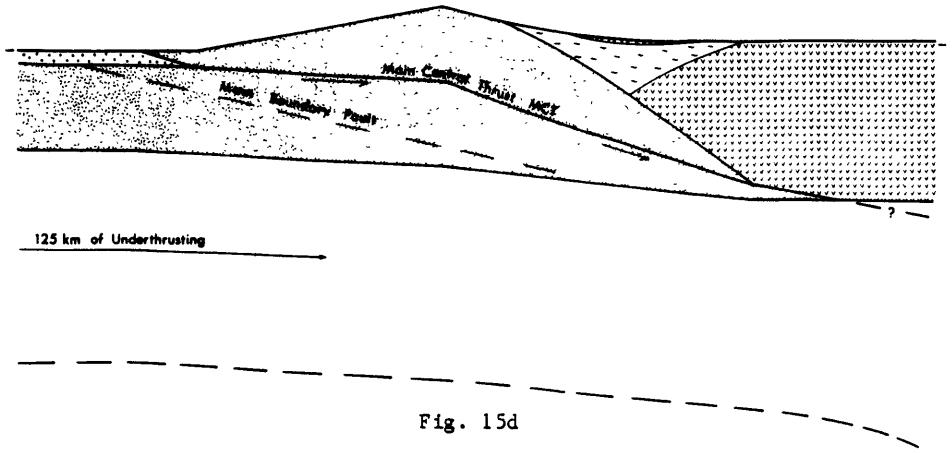

Fig. 15d

Underthrusting Along The Main Boundary Fault

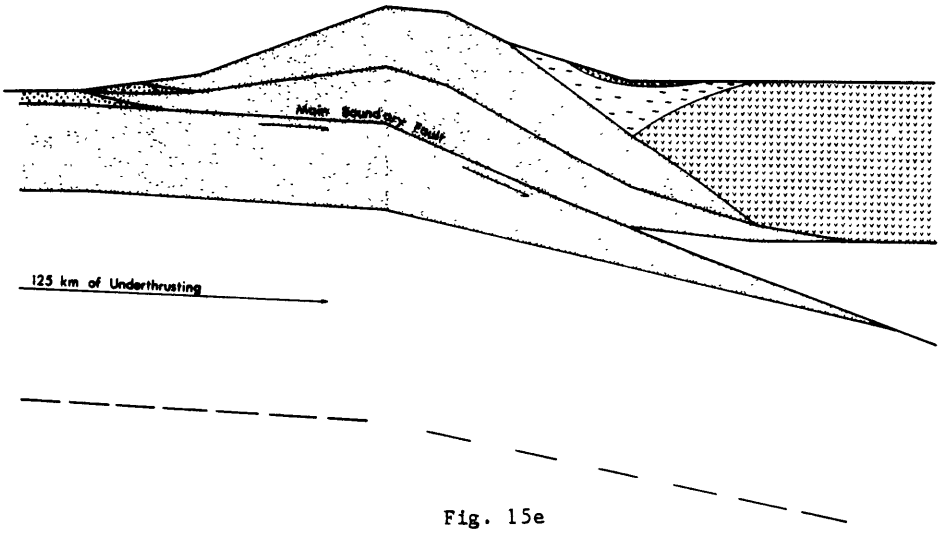

Fig. 15e

Analogy With Present Geologic Structure

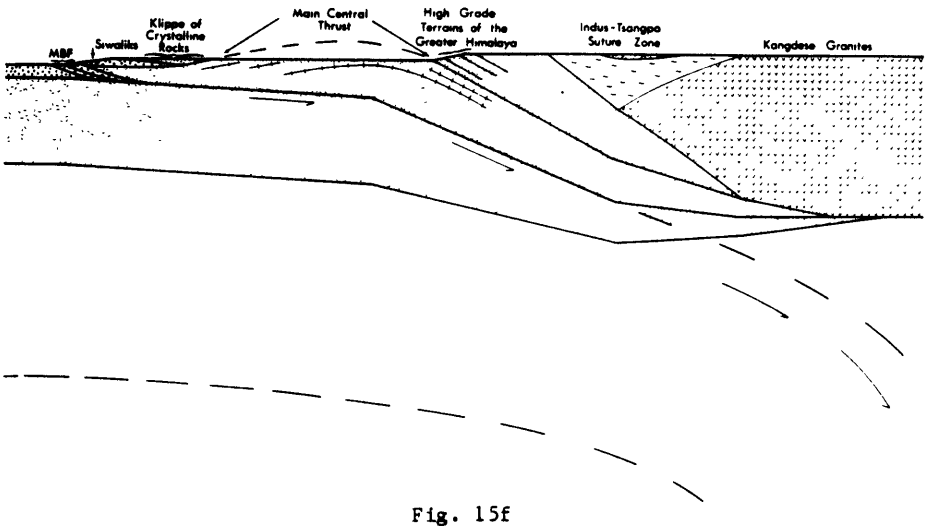

Fig. 15f

of convergence, we arbitrarily let slip begin on the Main Central Thrust (Figures 15c and 15d). By insisting that the shape of the Indian plate be similar to that inferred above from the gravity anomalies, both the slice of crust that once was the northern margin of the Indian subcontinent and part of accretionary prism are uplifted (Figure 15d) and presumably are eroded. After (an arbitrarily selected amount of) 125 km of underthrusting, we let slip begin on the Main Boundary Fault (Figures 15d and 15e). Again, requiring a shallow dipping Moho leads to a large uplift in the Central Himalaya (Figure 15e).

When we remove material that must be eroded in order to achieve a topographic profile similar to those across the Himalaya, several aspects of the hypothetical geologic structure are similar to those in the Himalaya today (Figure 15f). The klippe of crystalline rocks inferred to have been carried by the Main Central Thrust where it dips at a shallow angle southward into a gentle syncline is shown overthrust onto sediments analogous with the Siwaliks [e.g., Gansser, 1964; Heim and Gansser, 1939]. The gentle doming of metamorphosed sediments in the Midland terrain of the Lesser Himalaya [e.g., Hashimoto et al., 1973; Pecher, 1978] is present, underlying the Main Central Thrust where it dips steeply (30°) to the north. The high-grade terrain over the Main Central Thrust [e.g., Hashimoto et al., 1973; LeFort, 1975; Valdiya, 1981] is shown as material once buried about 30 km beneath the northern margin of the Indian subcontinent. If this interpretation were correct, the high metamorphic grades would not be due to heating during Tertiary orogenesis but would be simply due to transport of lower crustal material to the surface, as inferred by Bordet [1961] and Valdiya [1980]. (Such an inference is not inconsistent with the existence of the late Tertiary tourmaline granites in the Himalaya, if these granites formed below the Main Central Thrust or if the melting temperature in the crust is very low [Molnar et al., 1983].) Hence several aspects of the gross structure of the Himalaya are reproduced in Figure 15f.

Numerous palynological and paleontological studies by Chinese scientists in the Tibetan Himalaya have turned up evidence suggesting rapid uplift of this region [Guo, 1981; Li et al., 1981; Song and Liu, 1981; Xu, 1981; Zhang et al., 1981]. Such results are often generalized to include the whole of the Tibetan plateau, but it appears to us that the least equivocal data are from high altitudes on the north slope of the Greater Himalaya. Rapid uplift is also reported at the foot of the Lesser Himalaya (work of R.S. Chugh as cited by Molnar et al. [1977]). Chugh presented changes in elevation from releveling of one line from the Ganga Basin into the Lesser Himalaya in the northwestern Himalaya. The measured rate of uplift is a maximum of about 5 mm/yr at the crossing of the Main Boundary Fault and decreases both north and south. We are not aware of evidence for rapid uplift in most of the Lesser Himalaya, however.

Notice that the sequence of cross sections in Figures 15e and 15f imply that uplift of the Greater Himalaya should be large. If the dip of the top surface of the Indian plate beneath the Greater Himalaya is ϕ(=20-30°) and the rate of convergence in the Himalayas is v_x(=10 to 20 mm/yr), then the rate of uplift is $v_z = v_x \tan \phi$ (=5 to 12 mm/yr). Similarly, if the system of faults that compose the Main Boundary Fault at the foot of the Himalaya are listric [e.g., Seeber et al., 1981], then rapid uplift should occur there. The cross sections in Figures 15e and 15f, however, do not call for uplift in most of the Lesser Himalaya or of the Tibetan plateau.

Finally, we estimate the amount of material eroded from the cross section in Figure 15f to be 4.44×10^3 km^2. If this number were representative for the whole of the Himalaya, about 2000 km long, then this estimate implies that 8.88×10^6 km^3 of material have been eroded from the Himalaya. Let us compare this with some estimates of sediments nearby. If we assume a mean thickness of sediment in the Ganga Basin of 2 km, a width of 250 km, and a length of 2000 km, there are about 10^6 km^3 there. Curray and Moore [1971] estimated a volume of sediments above a well-defined horizon in the Bay of Bengal to be about 10.1×10^6 km^3. Later they assigned a Paleocene age to this horizon [Curray et al., 1982]. Therefore most of these sediments postdate the collision. The combination of the Ganga Basin and the Bengal fan contain 11.1×10^6 km^3. If we assume that the density of these sediments is 90% of the eroded crustal material, then this value should be reduced to 10×10^6 km^3, a value remarkably close to that estimated to have been eroded from the hypothetical cross section in Figures 15e and 15f, and that agreement certainly lends support to it.

Although we would have been satisfied with a greater difference between volumes of material eroded from the hypothetical cross sections and deposited in the Ganga and Bengal basins, it is worth noting some items that have been ignored. The Arabian Sea also contains sediments from the Himalaya, via the Indus River and its predecessors. The present transport of suspended material of the Indus River is about 1/5 that of the Ganga-Bramaputra [Curray and Moore, 1971] so that if this rate were representative of the entire history of the Himalaya, we might add about 2×10^6 km^2 to the value of sediments. At the same time, but choosing a length of 2000 km for the Himalaya, we have neglected about 500 km of the range now drained by the Indus River. Thus ignoring the Indus River and the region that it drains might not modify at all the agreement between hypothetical erosion and sediment volume. Finally, the slightly larger value of sediment than calculated erosion is consistent with a small amount of erosion of southern Tibet. Since we cannot estimate useful uncertainties in the amounts of sediment volume or the amounts of erosion and since the cross section in Figure 15f is only one among a large family of possibilities, these comparisons should be taken only as evidence supporting the general aspects of the cross sections and not the details.

The final cross section in Figure 15f is an oversimplification and is imperfect in many ways. It neglects numerous thrusts in the Lesser Himalaya [see Valdiya, 1981], and it does not portray the structure of Greater Himalaya and Indus-Tsangpo suture as it is shown in cross sections such as those of Bally et al. [1980]; Frank et al. [1977]; Gansser [1964, 1977]; and LeFort [1975]. We have not been concerned as much with this partly because of the variation along strike in the Himalaya and because of the clear evidence for northward reverse

or back thrusting in the Greater Himalaya. Finally, notice also that we have allowed for further detachment of deeply thrust crust by attaching the subducted crust beneath southern Tibet in Figure 15e to the base of the Moho in Figure 15f. The reader will probably note aspects of the cross sections that are artifacts of the simplistic and limited number of assumptions made. For instance, if we began in Figure 15a with a thinner crust beneath the Kangdese granites in southern Tibet, we could underthrust more Indian crust beneath these than we did in Figure 15c. This addition of material could then cause an uplift and denudation of the cover. Clearly, numerous variations are possible. Moreover, the reader should not assume that 125 km of underthrusting along the Main Central Thrust is a precise estimate or that the equality of values used here for the Main Central Thrust and Main Boundary Fault implies that slip on the Main Boundary Fault will soon stop. These cross sections are meant to be cartoons drawn quantitatively accurately in order to explore qualitatively some aspects of the geology. Nevertheless, the rather small amount of material shown underthrusting southern Tibet and the Himalaya (350 km) compared with the total penetration of India into Eurasia since their collision (2000-3000 km) is consistent with most of this penetration being absorbed north of the Himalaya [Molnar and Tapponnier, 1975].

Summary

The flexure of the Indian plate is a plausible mechanism to support the mass of the Himalaya. The flexural rigidity of the plate beneath the Ganga Basin and the Lesser Himalaya is about 0.7 (± 0.5) x 10^{25} N m. A plate of constant flexural rigidity cannot underthrust the entire Himalaya. The plate must lose a considerable amount of its strength about 130 km north of the Himalayan front, where the Main Central Thrust crops out. Moreover, a bending moment must be applied to the end of the plate in order to compensate for the large weight of the Himalayan Mountains. These features are required by the gravity anomalies, which show that the dip of the Moho increases from about 3° beneath the Ganga Basin and the Lesser Himalaya to about 15° beneath the Greater Himalaya (for $\rho_m - \rho_c$ = 0.55 x 10^3 kg/m^3).

Both the decrease in flexural rigidity at the Greater Himalaya and the bending moment can be understood if we assume that beneath the Greater Himalaya part or all of the Indian crust has been detached from the lower part of the Indian lithosphere, probably after warming and weakening of the plate during the collision process. Gravity acting on the cold sinking mantle material then is a possible cause of the bending moment. Although gravity anomalies allow this interpretation, the existence of such a cold material beneath the range is not demonstrated and is a possibility that needs further study.

Although the model studied here is simplistic in many ways, idealized balanced cross sections constrained by the above results reproduce various important aspects of the geology of the Himalaya. The estimated amount of eroded material is in good agreement with the volume of sediments that are thought to be derived from the Himalaya. The cross sections suggest that the high-grade metamorphic terrain over the Main Central Thrust is due to transport of lower crustal material to the surface and not to heating during the orogenesis. They also predict a large uplift only at the foot of the range and in the Greater Himalaya. The methods used here and the cross sections derived suggest that simple mechanical models coupled with classical techniques of structural geology can be combined to yield realistic models of the structure and dynamics of overthrust belts.

Acknowledgments. We thank B. C. Burchfiel for acquainting us with balanced cross sections and P. Bird for a thorough, constructive review. This research was supported by NSF grant EAR 8121184 and NASA grant NAG 5-41.

References

Amboldt, N., Relative schwerkraftsbestimmungen mit pendeln in Zentral Asien, 2 reports from scientific expedition to northwestern provinces of China under leadership of Dr. Sven Hedin, Publ. 30, II Geodes., Truckeri Aktiebolaget Thule, Stockholm, 1948.

Argand, E., La tectonique de l'Asie, Proc. Int. Geol. Congr. 3rd., (Pt. 5), 171-372, 1924.

Bally, A. W., C. R. Allen, R. E. Geyer, W. B. Hamilton, C. A. Hopson, P. H. Molnar, J. E. Oliver, N. D. Opdyke, G. Plafker, and F. T. Wu, Notes on the geology of Tibet and adjacent areas - Report of the American plate tectonics delegation to the People's Republic of China, U.S. Geol. Surv. Open File Rep., 80-501, 100 pp., 1980.

Bird, P., Initiation of intracontinental subduction in the Himalaya, J. Geophys. Res., 83, 4975-4987, 1978.

Bordet, P., Recherches Géologiques dans l'Himalaya du Népal, Région du Makalu, 275 pp., Centre National de la Recherche Scientifique, Paris, 1961.

Chang, C. F. and H. L. Cheng, Some tectonic features of the Mt. Jolmo Lungma area, Southern Tibet, China, Sci. Sin. Enmgl. Ed., 16, 257-265, 1973.

Chen, W. P., and P. Molnar, Constraints on the seismic wave velocity structure beneath the Tibetan Plateau and their tectonic implications, J. Geophys. Res., 86, 5937-5962, 1981.

Choudhury, S. K., Gravity and crustal thickness in the Indo-Gangetic Plains and Himalayan region, India, Geophys. J. R. Astron. Soc., 41, 441-452, 1975.

Curray, J. R. and D. G. Moore, Growth of the Bengal deep-sea fan and denudation of the Himalayas, Geol. Soc. Am. Bull., 82, 563-572, 1971.

Curray, J. R., F. J. Emmel, D. G. Moore, and R. W. Raitt, Structure, tectonics, and geological history of the northeastern Indian Ocean, in The Ocean Basins and Margins, vol. 6, The Indian Ocean, Plenum, New York, 1982.

Fitch, T. J., Earthquake mechanisms in the Himalayan, Burmese and Andamar regions and continental tectonics in Central Asia, J. Geophys. Res., 75, 2699-2709, 1970.

Fleitout, L., and C. Froidevaux, Tectonics and topography for a lithosphere containing density heterogeneities, Tectonics, 1, 21-56, 1982.

Frank, F. C., Plate tectonics, the analogy with glacier flow and isostasy, in Flow and Fracture of Rocks, Geophys. Monogr. Ser.; vol. 16, edited by H.C. Heard et al., pp. 285-292, AGU, Washington, D.C., 1972.

Frank, W., M. Thoni, and F. Purtsheller, Geology and petrography of Kulu-South Lakul area, Colloques Internationaux du CNRS, in Himalaya: Sciences de la Terre, pp. 147-172, Editions du Centre National de la Recherche Scientifique, Paris, 1977.

Gansser, A., Geology of the Himalayas, 289 pp., Interscience, New York, 1964.

Gansser, A., The Indian Ocean and the Himalayas: A geologic interpretation, Eclogae Geol. Helv., 59, 832-848, 1966.

Gansser, A., The great suture zone between Himalaya and Tibet, A preliminary account, Colloques Internationaux du CNRS, in Himalaya: Sciences de la Terre, pp. 181-192, Editions du Centre National de la Recherche Scientifique, Paris, 1977.

Guo S., On the elevation and climatic changes of the Qinghai-Xizang Plateau based on fossil angiosperms, Proceedings Symposium on Qinghai-Xizang (Tibet) Plateau (Beijing, China), in Geological and Ecological Studies of Qinghai-Xizang Plateau, vol. 1, pp. 201-206, Science Press, Beijing, 1981.

Hanks, T. C., The Kuril trench-Hokkaido rise system, large shallow earthquakes and simple models of deformation, Geophys. J. R. Astron. Soc., 23, 173-189, 1971.

Hashimoto, S., Y. Ohta, and C. Akiba (Eds.), Geology of the Nepal Himalayas, 292 pp., Saikon, Sapporo, Japan, 1973.

Heim, A. and A. Gansser, Central Himalaya, geological observations of the Swiss expedition 1936, Mem. Soc. Helv. Sci. Nat., 73, 1-245, 1939.

Houseman, G. A., D. P. McKenzie, and P. Molnar, Convective instability of a thickened boundary layer and its relevance for the thermal evolution of continental convergent belts, J. Geophys. Res., 86, 6115-6132, 1981.

Kono, M., Gravity anomalies in East Nepal and their implications to the crustal structure of the Himalayas, Geophys. J. R. Astron. Soc., 39, 283-300, 1974.

LeFort, P., Himalayas: The collided range; present knowledge of continental arc, Am. J. Sci., 275-A, 1-44, 1975.

Li J., Li B., Wang F., Zhang Q., Wen S., and Zheng B., The process of the uplift of the Qinghai-Xizang Plateau, Proceedings Symposium on Qinghai-Xizang (Tibet) Plateau (Beijing, China), Geological and Ecological Studies of Qinghai-Xizang Plateau, vol. 1, pp. 111-118, Science Press, Beijing, 1981.

Marussi, A., Italian Expeditions to the Karakorum (K^2) and Hindu Kush, Sci. Rep. II, vol. I, Geophysics of the Karakorum, 242 pp., E.J. Brill, Leiden, 1964.

Mattauer, M., Sur le mécanisme de formation de la shistosité dans l'Himalaya, Earth Planet. Sci. Lett., 28, 144-154, 1975.

Molnar, P., and W. P. Chen, Seismicity and mountain building, in Mountain Building Processes, edited by U. Briegel and K.J. Hsu, pp. 41-57, Academic, New York, 1982.

Molnar, P., and D. Gray, Subduction of continental lithosphere: Some constraints and uncertainties, Geology, 7, 58-62 1979.

Molnar, P., and P. Tapponnier, Cenozoic tectonics of Asia: Effects of a continental collision, Science, 189, 419-426, 1975.

Molnar, P., W. P. Chen, T. J. Fitch, P. Tapponnier, W. E. K. Warsi, and F. T. Wu, Structure and tectonics of the Himalayas: A brief summary of relevant geophysical observations, Colloques Internationaux du CNRS, in Himalaya: Sciences de la Terre, pp. 269-294, Editions du Centre National de la Recherche Scientifique, Paris, 1977.

Molnar, P., W. P. Chen, and E. Padovani, Calculated temperatures in overthrust terrains and possible combinations of heat sources responsible for the Tertiary granites in the Greater Himalaya, J. Geophys. Res., 88, 6415-6429, 1983.

Parsons, B., and P. Molnar, The origin of outer topographic rises associated with trenches, Geophys. J. R. Astron. Soc., 45, 707-712, 1976.

Pecher, A., Déformations et métamorphisme associés à une zone de cisaillement. Exemple du grand chevauchement central Himalayen (M.C.T.), transversale des Annapurnas et du Manaslu, Népal, thèse d'état, 354 pp., Univ. Sci. et Médicale de Grenoble, France, 1978.

Powell, C. H., and P. J. Conaghan, Plate tectonics and the Himalayas, Earth Planet. Sci. Lett., 20, 1-20, 1973.

Qureshy, H. N., S. Venkatachalah, and C. Susrahmanyam, Vertical tectonics in the Middle Himalayas: An appraisal from recent gravity data, Geol. Soc. Am. Bull., 85, 921-926, 1974.

Rao, M. B. R., The subsurface geology of the Indo-gangetic plains, J. Geol. Soc. India, 14, 217-242, 1973.

Romanowicz, B., Constraints on the structure of the Tibet Plateau from pure path phase velocities of Love and Rayleigh waves, J. Geophys. Res., 87, 6865-6883, 1982.

Sastri, V. V., L. L. Bhandari, A. T. R. Rasu, and A. K. Datta, Tectonic framework and subsurface stratigraphy of the Ganga Basin, J. Geol. Soc. India, 12, 222-223, 1971.

Seeber, L., and J. G. Armbruster, Great detachment earthquakes along the Himalayan arc and long-term forecasting, in Earthquake Prediction, An International Review, Maurice Ewing Ser., vol. 4, edited by D.W. Simpso and P.G. Richards, pp. 259-277, AGU, Washington, D.C., 1981.

Seeber, L., J. G. Armbruster, and R. C. Quittmeyer, Seismicity and continental subduction in the Himalayan arc, in Zagros, Hindu Kush, Himalaya-Geodynamic Evolution, Geodyn. Ser., vol. 3, edited by H.K. Gupta and F.M. Delany, pp. 215-242, AGU, Washington, D.C., 1981.

Song Z., and Liu G., Tertiary palynological assemblages from Xizang with references to their paleogeographical significance, Proceedings Symposium on Qinghai-Xizang (Tibet) Plateau (Beijing, China), in Geological and Ecological Studies of Qinghai-Xizang Plateau, vol. 1, pp. 207-214, Science Press, Beijing, 1981.

Talwani, M., J. L. Worzel, and M. Landisman, Rapid gravity computation of two dimensional bodies with application to Mendocino submarine fracture zone, J. Geophys. Res., 64, 95-137, 1959.

Tang B., Liu Y., Zhang L., Zhou W. and Wang Q.,

Isostatic gravity anomalies in the central portion of the Himalayas, Proceedings Symposium on Qinghai-Xizang (Tibet) Plateau (Beijing, China), in Geological and Ecological Studies of Qinghai-Xizang Plateau, vol. 1, pp. 683-690, Science Press, Beijing, 1981.

Tapponnier, P., and P. Molnar, Slip-line field theory and large scale continental tectonics, Nature, 264, 319-324, 1976.

Turcotte, D., and G. Schubert, Geodynamics, John Wiley, 450 pp., New York, 1982.

Valdiya, K. S., The two intracrustal Boundary thrusts of the Himalaya, Tectonophysics, 66, 323-348, 1980.

Valdiya, K. S., Tectonics of the central sector of the Himalaya, in Zagros, Hindu Kush, Himalaya-Geodynamic Evolution, Geodyn. Ser. vol. 3, edited by H.K. Gupta and F.M. Delany, pp. 87-110, AGU, Washington, D.C., 1981.

Warsi, W. E. K., Plate tectonics and the Himalaya orogeny, a modelling study based on gravity data, M.S. thesis, Mass. Inst. of Techn., Cambridge, 1976.

Warsi, W. E. K., and P. Molnar, Gravity anomalies and plate tectonics in the Himalaya, Colloques Internationaux du CNRS, in Himalaya: Sciences de la Terre, pp. 463-478, Editions du Centre National de la Recherche Scientifique, Paris, 1977.

Watts, A. B., and M. Talwani, Gravity anomalies seaward of deep trenches and their tectonic implications, Geophys. J. R. Astr. Soc., 36, 57-90, 1974.

Xu R., Vegetational changes in the past and the uplift of Qinghai-Xizang Plateau, Proceedings Symposium on Qinghai-Xizang (Tibet) Plateau (Beijing, China), in Geological and Ecological Studies of Qinghai-Xizang Plateau, vol. 1, pp. 139-144, Science Press, Beijing, 1981.

Zhang Q., Li B., Yang Y., Yi Z., and Wang F., Basic characteristics of neotectonic movement of Qinghai-Xizang Plateau, Proceedings Symposium on Qinghai-Xizang (Tibet) Plateau (Beijing, China), in Geological and Ecological Studies of Qinghai-Xizang Plateau, vol. 1, pp. 103-110, Science Press, Beijing, 1981.

H. Lyon-Caen and P. Molnar, Department of Earth and Planetary Sciences, Massachusetts Institute of Technology, Cambridge, MA 02139.

(Received June 23, 1982;
revised June 13, 1983;
accepted June 16, 1983.)

CHAPTER II

GRAVITY ANOMALIES, FLEXURE OF THE INDIAN PLATE, AND THE STRUCTURE, SUPPORT AND EVOLUTION OF THE HIMALAYA AND GANGA BASIN

Hélène Lyon-Caen and Peter Molnar

Department of Earth, Atmospheric, and Planetary Sciences,

Massachussetts Institute of Technology, Cambridge

INTRODUCTION

Gravity anomalies over both the Himalaya and the Alps show large deviations from local isostatic equilibrium. Both ranges are associated with a local excess of mass, but adjacent to both are foredeep basins characterized by a deficit of mass. This undercompensation of the mountain ranges and overcompensation of the neigh-boring foredeeps can be understood if the continental lithosphere is flexed down by the load of the mountains and if its strength supports part of the mass of the mountain range [Gunn, 1943; Karner and Watts, 1983; Lyon-Caen and Molnar, 1983]. The deflection of the plate creates a foredeep basin in front of the load such that the depth and shape of the basin are directly related both to the strength of the plate and to the amount of load acting on it.

Various studies have assumed that, to a first approximation, the response of the lithosphere to such external loads can be treated as elastic and that of the asthenosphere as an inviscid fluid, at least for loads younger than about 100 Ma [e.g., Gunn, 1943; Hanks, 1971; Walcott, 1970; Watts and Talwani, 1974]. Both Karner and Watts [1983] and we [Lyon-Caen and Molnar, 1983] have used such a simple model to analyze gravity anomalies across the Himalaya, and in doing so we have tried to gain some insight into how the range is supported. Although the gravity field along at least one profile across the Ganga Basin and the Lesser Himalaya can be explained in the context of an elastic plate over an inviscid fluid, we found the load of the High Himalaya, at least in the Mount Everest region, to be too large to be supported solely by the strength of the Indian plate without additional forces applied to it [Lyon-Caen and Molnar, 1983]. A few gravity data in the area of Mount Everest

and farther north suggest that the Moho steepens just south of the Mount Everest and reaches a depth of ap proximately 70 km at a position about 50 km south of the Indus-Tsangpo suture zone. New gravity data in this area [Van de Meulebrouck et al., 1983; Van de Meulebrouck, 1984] corroborate these inferences. We interpreted this steepening to be due to the weakening of the plate beneath the High Himalaya, probably at least in part, by detachment of the Indian crust during the collision process. We then found that the High Himalaya can be supported by the Indian plate if an external force or a moment is applied to the end of the plate, and we suggest that the source of this external force could be gravity acting on the cold mantle part of the Indian lithosphere detached from the crust [Lyon-Caen and Molnar, 1983].

The present paper describes a similar analysis of 4 gravity profiles across the western part of the Himalaya, in India, and across the Ganga Basin (Figure 1). These data are qualitatively consistent with the conclusions described above, but among them the profiles show differences in the various parameters controlling the shape of the flexed Indian plate. These data also allow a more detailed study of the structure of the Ganga Basin and Lesser Himalaya than was possible in our previous study, because the structure of these areas in western India is quite well known from deep wells, seismic reflection profiles, and detailed geological mapping. After a brief review of the methods used to analyze the data, we show that the deviation from local isostatic equilibrium is large along all five profiles across the Himalaya. We then present an analysis of each profile separately, comparing inferences about the structure of the Ganga Basin and the Himalaya with geological observations when they are available. Finally, we discuss these inferences in light of the tectonic evolution of this region, and we use this inferred

evolution of the Ganga Basin to place a constraint on the rate of convergence between India and the Himalaya.

DATA AND ANALYSIS

Gravity Anomalies

We obtained from the Defense Mapping Agency (DMA) a listing of gravity measurements made in the Ganga Basin. These measurements include simple Bouguer gravity anomalies, without terrain corrections, referenced to the 1971 Geodetic Reference System. Terrain corrections over the Ganga Basin are, indeed, small (a few milligals or less) and can be neglected here [e.g., Kono, 1974]. Bouguer anomalies over the Himalaya were taken from plots given by Das et al. [1979], who carefully made terrain corrections, some of which reach 100 mGals, but who reduced their measurements using the 1930 Reference System. Since the difference between the anomalies computed with the two reference systems is less than 1 mGal at the latitude of 30° [Woollard, 1979], however, we ignored this difference and simply connected the data presented by Das et al. [1979] with those from the DMA to obtain complete profiles across the Ganga Basin and the Himalaya.

A possibly important error in the Bouguer anomalies over the Himalaya could have been introduced by the way that we retrieved Das et al.'s [1979] data, because the profiles published by them show only relative variations of gravity. We obtained the absolute scale on their profiles by assigning to the southern end point of each profile the value given by the DMA for the closest point that we could find (Figure 1). Except for profile 5 the two points were within 2 or 3 km of one another. Verma and Subrahamanyam [1984], however, published plots of measurements for two of the profiles used here (profiles 3 and 5) with an absolute scale. Comparing the values of gravity given by Verma and Subrahamanyam [1984] for the end points with those from the DMA makes us

confident that the errors involved in this process are less than 5 mGals at the northern edge of the Ganga Basin. For a given point, along each profile, however, the uncertainties probably increase proportionally to its distance from the edge of the Basin and may reach 25 mGals at the northern edge of each profile. In particular, the value of the Bouguer anomaly around Leh, at the northern end of profile 5, could have an error of 30 mGals attached to it, in part because the values given by Verma and Subrahamanyam [1984] and by Das et al. [1979] apparently disagree by about 25 mGals. Verma and Subrahamanyam [1984] do not specify that they included terrain corrections. This may be the source of the discrepancy, but their value is close to the one reported by Marussi [1964], who did make terrain corrections. Thus we do not know why the various values presented by different authors differ from one another, but we assume that the uncertain ties in measurements over the Himalaya are no larger than 5 mGals near the Ganga Basin but could reach 25 mGals at the northern ends of the profiles. We also reconsider the profile used in our previous study (profile 1 in Figure 1). At the time of that study we did not have the listing of data from the DMA, and instead we constructed a profile mostly from contours shown on published gravity maps for which variations in individual measurements had been smoothed. Although the scatter among measurements within a few tens of kilometers of one another along this profile is about 25 mGals, it turns out that there seems to be a resolv able relative gravity high about 20 km north of the edge of Ganga Basin. This high did not appear on the smoothed profile that we used, and the value that we used falls near the middle of these scattered values. We interpreted the absence of a gravity high as evidence that a substantial amount of low-density material (sediments) had been underthrust beneath the range. The additional data that we have now seem to indicate that only about half of the amount of sediment

that we suggested before may have been subducted. Each of the four new profiles presented here also shows a plateau or a relative high from the edge of the basin to about 50 km north of it. In examining each profile, we will try to relate this feature in the gravity field to geological observations and to use it to place a constraint on the amount of underthrusting of sediment beneath the Lesser Himalaya.

Deviations From Local Isostatic Equilibrium

The Himalaya, at least in the areas south of Mount Everest [Kono, 1974] and near the Pakistan border [Marussi, 1964], is known to be largely undercompensated. We show here that the Lesser and High Himalaya are undercompensated on each profile in Figure 1, and therefore probably along the entire arc, and that this excess of mass is coupled with a deficit of mass beneath the Indo-Gangetic Plains.

Instead of computing standard isostatic anomalies, we computed the Bouguer anomaly that would result if the mean topography along each profile were locally compensated. For this purpose we obtained the mean elevation along each profile by averaging the elevations on the Aéronautical Navigation Charts (ONC charts) in a zone extending 100 km on each side of the profile (Figure 2a). We then computed the Bouguer anomalies assuming that compensation occurs locally solely by the thickening of the crust, which is assumed to have a normal thickness of 38 km under the Indian Shield [Kaila, 1982]. This value of 38 km, however, is not critical, and were values of 30 or 45 km used, the computed anomalies would differ by only a few mGals. The observed gravity data clearly show that large systematic deviations from local isostatic equilibrium are present (Figure 2b). The Ganga Basin is overcompensated, whereas the Himalaya are undercompensated by as much as 100 mGals. This coupling of mass deficiency over the basin and mass excess over

the mountains can be understood if isostasy occurs regionally with the strong Indian lithosphere being flexed down at the Himalayan front and extending beneath the range a certain amount. This would imply that the structure and the evolution of the Ganga Basin are essentially controlled by the flexure of the Indian plate.

Flexural models

We analyze each of the profiles 2, 3, 4, and 5 using the method described in detail in Lyon-Caen and Molnar [1983] for profile 1. We treat the Indian lithosphere as an effectively elastic plate with a flexural rigidity D and that extends a certain distance X_o beneath the Himalaya (Figure 3). At first, we consider cases in which the plate has a constant flexural rigidity and the weight of the mountains is the only external force acting on the plate. In this first part of the analysis, only that part of the range with $x \leq X_o$ is used as a load acting on the plate. We calculate the deflection of the plate, and hence of the Moho, due to this distributed load, assuming that the trough created in front of the range is filled by sediments of lower density than crustal rock. To define the position of the Moho elsewhere, we assume that both the Tibetan Plateau [Amboldt, 1948] and the Indian Shield to the south of the Ganga Basin are in isostatic equilibrium. We then assume that the profile of the Moho is a straight line from X_o to an arbitrarily chosen place beneath southern Tibet north of which isostatic equilibrium obtains. In doing so no specific mechanism is provided for the support of the Himalaya between X_o and this place in southern Tibet. We consider this in a second step of the analysis described below.

We compute the resulting gravity anomalies assuming that they are due only to the density contrasts among crust, mantle, and sediments. The mean density of the sediments is chosen to be 2.4 g/cm^3, as suggested by measurements

reported by Raiverman et al. [1983]. We used densities of 2.8 g/cm^3 and 3.35 g/cm^3 for the crust and mantle, respectively, and of 2.7 g/cm^3 for the load. In any case, Lyon-Caen and Molnar [1983] showed that density contrasts are not important parameters as far as the calculation of gravity anomalies is concerned. The least important difference is that between 2.7 g/cm^3 assumed for the load and 2.67 g/cm^3 for the Bouguer correction. A Bouguer correction of 2.67 g/cm^3 is the standard used by the DMA and in nearly all other studies, but for calculations of deflections we refrain from assigning a value with three significant figures to a density whose uncertainty affects the second significant figure. Had we used 2.67 g/cm^3 for the density of the load, the computed deflections would differ by less than 1%, an amount different from those calculated here comparable with the width of the lines in Figures 4-7.

For the gravity anomalies over the Ganga Basin and the Lesser Himalaya, the two essential parameters are the flexural rigidity D and the length that the elastic plate extends beneath the range, X_o. The wavelength of the anomaly over the Ganga Basin is mainly controlled by the value of D. Its amplitude depends on both the amount of the Himalayan mass that is supported, which is parameterized by X_o, and on D. Inferences of these two parameters can thus be made separately, using primarily the shape and amplitude of the gravity anomaly profile over the Ganga Basin.

In trying to account for the observed gravity profiles, we first infer values of X_o and D, and then we try to deduce additional information about the structure beneath the Greater Himalaya. The four gravity profiles studied here show that the plate cannot extend more than 100 to 150 km beneath the Himalaya if its flexural rigidity remains constant and if no other forces act on it; the load of the entire High Himalaya is not supported solely by the strength of the flexed Indian plate, buoyed up by an inert asthenosphere

beneath it. An additional force must contribute to the support of this mass. Moreover, as for profile 1, an increase in the gravity gradient beneath the High Himalaya implies that the Moho must steepen beneath this part of the range. We interpret this to be due to the weakening of the plate, and we analyze this situation by considering that a northern segment of plate, between $x=X_0$ and $x=X_0'$ (Figure 3) has a smaller flexural rigidity, D' than its remaining part. In all cases, however, we found that the inclusion of a weaker, northern edge of the plate alone, is not enough to explain the gravity anomalies as for profile 1 [Lyon-Caen and Molnar, 1983]; an external force system is necessary both to bend the plate down sharply beneath the High Himalaya and at the same time to support the heavy load of this part of the range. For each profile we found combinations of values for D' and for bending moments M_0 and vertical shear forces F_0 per unit length applied to the end of the plate that allow computed gravity anomalies to match those observed. These three parameters (D', M_0, and F_0), however, are coupled and cannot be determined uniquely [Lyon-Caen and Molnar, 1983]. Estimates of M_0 and F_0 increase with increasing values of D', but in general D' cannot be varied by more than a factor of 10 and M_0 and F_0 by a factor of 2. We give values for M_0, F_0, and D' here simply to provide estimates for the orders of magnitude of the required external forces. These values not only are uncertain by factors of 2 to 10, but also the physical reality of the simple model may make the values of the parameters only qualitatively important. The need for specifying them, however, attests to presence of dynamic mechanisms for supporting the load of the mountains.

ANALYSIS OF INDIVIDUAL PROFILES

Profile 2: (Nepal Border) (Figure 4)

Bouguer anomalies over the southern part of the Ganga Basin are nearly

constant and equal to -50 mGal. Over the northern part of the Ganga Basin values become increasingly negative at about 0.75 mGal/km. Then the gradient steepens to 2.5 mGal/km over the High Himalaya. For a simple plate with a constant flexural rigidity extending a distance X_o beneath the range, the gradient over the northern part of the Ganga Basin constrains the flexural rigidity to be at least 3 x 10^{24} Nm (Figure 4a); a better fit is obtained for D = 7 x 10^{24} Nm. The values of gravity at the foot of the range constrain X_o to be 130 km 10 km (Figure 4b). Larger values of X_o, corresponding to heavier loads on the plate, yield poor fits. Thus an additional force must support this mass.

The computed Bouguer anomalies at the southern edge of the profile ($x \simeq -200$ to -400 km) differ by about 25 mGals from the observed anomalies. We think that these more negative values of observed than computed anomalies may not be related to the flexure of the lithosphere. Instead they seem to be part of a regional low that extends farther south of the profile and can be seen on the Bouguer gravity map of India (Figure 1). The source of this low may be in the Indian crust and may reflect ancient sedimentary basins on the underlying Indian Shield or may be related to deeper density anomalies. Thus we do not try to fit these low values.

In order to compute the curves shown on Figures 4a and b, the Moho north of X_o was assumed to dip at 17°, from its calculated depth of 45 km at X_o to 63 km at x = 190 km. The Moho dips at an angle of about 2° beneath most of the Lesser Himalaya and thus steepens markedly beneath the Higher Himalaya. We inferred the place where this steepening occurs (x = 130 km) from the fit of the data only over the Ganga Basin, but notice that the increase of the gravity gradient occurs close to this point, near x = 110 km (Figure 4). The steepening of the Moho of course, need not be abrupt, as assumed in

calculations here, but could take place over a few tens of kilometers.

As before, we explain the steepening of the Moho by assuming that the plate is weaker, and therefore its effective rigidity is smaller, beneath the Higher Himalaya than farther south [Lyon-Caen and Molnar, 1983]. Nevertheless, simply incorporating a segment of plate with a reduced flexural rigidity is not sufficient to provide a mechanism for both supporting the range and fitting these data. The additional load of the mountains that overlies the plate between x=130 and x=190 km would deflect the plate too much beneath the Indo-Gangetic plains. A bending moment per unit of length of 4 x 10^{17} N and a vertical force per unit of length of 2.4 x 10^{12} N/m applied to the edge of the plate at x = 190, however, are adequate to flex the plate up beneath the Ganga Basin sufficiently for the computed anomalies to match those observed (Figure 4c). The parameters used in the analysis of this profile (Table 1) are nearly identical to those used for profile 1 across the Mount Everest area [Lyon-Caen and Molnar, 1983].

The misfit between observed and computed gravity anomalies in the vicinity of x = 0 can be explained if we assume that sediments with a mean thickness of about 1 km over a length of 40 km have been underthrust with the Indian plate beneath the Lesser Himalaya (Figure 4c and 4d). Figure 4d shows the configuration of the wedge of sediment between 0 km < x < 40 km that yields the gravity profile shown by the dashed line in Figure 4c. This figure also compares the calculated position of the top of the Indian plate with, first, the depths of the pre-Tertiary basement obtained from three deep wells situated more than 130 km to the south of the Himalayan front and, second, the interface between the Lower Siwalik and the Subathu formations in the northern part of the basin inferred by Raiverman et al. [1983]. The Siwalik formation, of Miocene and Pliocence age, consists mainly of material eroded from the

Himalaya and transported to the south. In contrast, the Eocene Subathu formation is older and was deposited in a shallow marine environment probably before the collision of India with Asia. Thus the depth of the interface between these two formations presumably represents the subsidence of the Ganga Basin since the collision. The agreement between the configuration of the basin calculated here and that inferred by Raiverman and his colleagues in the Oil and National Gas Commission of India give us confidence that the flexural model is applicable, even if the gravity anomalies are fit poorly over part of the profile.

The fault plane solutions of earthquakes that occur in western Nepal and near the area traversed by profile 2 between about 90 km < x < 130 km show thrust faulting with slip vectors plunging at 25° ± 10° [Baranowski et al., 1984; Ni and Barazangi, 1984]. Depths of foci are about 13 km ± 3 km below sea level [Baranowski et al., 1984]. These earthquakes may represent slip along the top part of the Indian plate where it dips more steeply than beneath the Lesser Himalaya [Baranowski et al., 1984; Ni and Barazangi, 1984]. The depth of the top of the plate, inferred here from gravity anomalies, is shallow (only about 8 km), but if the density contrast between the mantle and the crust were 0.45 g/cm^3 instead of 0.55 g/cm^3, as we assumed in this calculation, then the top of the steeply dipping part of the plate would be at a depth of 11 km and would be at a depth consistent with the earthquakes representing slip along the underthrust Indian plate. In any case, the earthquakes seem to be too deep to represent deformation of the overriding plate [Seeber et al., 1981], at least insofar as it is correct to assume that the Indian plate is flexed down by the weight of the Himalaya. Thus, both the inferred structure and the fault plane solutions and depths of the earthquakes are consistent with the earthquakes occurring on or very near the top surface

of the Indian plate, but neither are well enough constrained to prove that this is the case.

Profile 3 (Rishikesh) (Figure 5)

Although the topographic profile, and hence the load, is almost the same as that along profile 2, the gravity gradient of about 1 mGal/km near the northern edge of the Ganga Basin is larger than that for profile 2, and the gradient over the High Himalaya of about 2 mGal/km is less than that of profile 2. For an Indian plate with a constant flexural rigidity, the values of the parameters that best fit the observations along profile 3 are a flexural rigidity between 0.5 and 3×10^{24} Nm (Figure 5a) and a value of X_o of 100 ± 30 km (Figure 5b). The smaller value of the flexural rigidity than that obtained from profile 2 is required by the larger gravity gradient over this part of the basin than farther east.

To explain the steeper gravity gradient over the High Himalaya than over the Lesser Himalaya, the calculated dip of the Moho must increase from about 2.5° beneath the Lesser Himalaya to about 9° beneath the Higher Himalaya, with the depth of 63 km reached at x = 230 km. Note that the observed gravity gradient changes from about 1.3 to 2 mGal/km near x=100 km, approximately where an equivalent elastic plate of constant flexural rigidity might end. The change in curvature of the Moho can be matched if the flexural rigidity of the plate underlying the High Himalaya is about 3×10^{22} Nm and if a bending moment per unit of length of 4×10^{17} N and a vertical force of 4×10^{12} N/m are applied to the end of the plate at X = 230 km (Figure 5c).

A rectangular wedge of sediments between x = 0 and x = 20 km allows a slight improvement to the fit of the data near the front of the range (Figure 5c). These data may not require underthrust sediments, however, but rather may be unrepresentative of those along a typical profile because of

variations in gravity along the front of the range. The area near Rishikesh, where most of the data between x = 0 and 20 km were obtained, lies in a reentrant of the Himalayan front, where the strike of the front is not perpendicular to the profile. Because of this possible three-dimensional effect, we are not confident of the existence of the sedimentary wedge used in Figure 5c.

The calculated maximum depth of the basin is 3.5 km. There are no direct measurements of the depth of the basin in this area, but the Mohand deep well, lo cated 65 km to the west of this profile (see Figure 10 below), reached the basement at a depth of about 4 km below sea level. Approximately 400 m of the Subathu and Dharamsala (Oligocene-early Miocene) formations overlie the basement (see also Figure A1) [Sastri, 1979]. Much of this material was probably deposited before the Indian plate was flexed down. If projected onto this profile, the well would be located near x=0, and thus the calculated maximum depth of the basin due to flexure differs at most by only a couple of hundred meters from that reached in the deep well.

Profile 4 (Simla) (Figure 6)

The observed gravity gradient along this profile over the Ganga Basin is only 0.5 mGal/km, and X_o need only be 70 ± 20 km for the plate to be flexed down sufficiently (Figure 6b). Consequently the flexural rigidity is very poorly constrained but probably lies between 1 x 10^{24} and 7 x 10^{24} Nm (Figure 6a). The observed gradient increases from about 1 mGal/km over the Lesser Himalaya to 1.9 mGal/km for x > 60 km. The values of gravity over the Higher Himalaya can be matched by including a segment of plate with a flexural rigidity of 3 x 10^{22} Nm between x=60 and 240 km and by applying a bending moment of 3.5 x 10^{17} N and a vertical force of 3.4 x 10^{12} N/m to the end of the plate (X_o' = 240 km) where the Moho reaches a depth of 63 km (Figure 6c).

Once again the inclusion of small wedge of sediments beneath the Lesser Himalaya (Figures 6c and 6d) improves the fit of the data near the front of the Lesser Himalaya. The calculated maximum depth of the basin is 3 km, compared to about 3.2 km inferred by Raiverman et al. [1983]. According to Raiverman et al. [1983], sediments from the Dharamsala formation are absent, and the basement is found directly below the Lower Siwalik group (Figure 6d).

Profile 5 Mandi-Leh (Figure 7)

The mean elevation, and therefore load along this profile, between x=0 and x=100 km is almost twice as large as those of profiles 2, 3, and 4 (Figure 2a), and the gravity gradient over the Ganga Basin is large, about 1.5 mGal/km. The flexural rigidity appears to be between 0.2 and 1 x 10^{24} Nm (Figure 7a), and X_o is between 80 and 120 km (Figure 7b). Thus the large gravity gradient over the basin is a consequence of both the heavy load acting on the plate and the relatively small value of the flexural rigidity. The curves shown in Figure 7 are computed assuming a structure north of the edge of the plate, similar to the one deduced from the gravity data over the southern Tarim Basin and western Tibet [Lyon-Caen and Molnar, 1984]. The thickness of the crust is assumed to be 43 km beneath the northern part of the Tarim Basin and reaches about 50 km at its southern edge. It is 65 km beneath most of the Karakorum belt. Again, by introducing a plate with a reduced flexural rigidity (D'=5x10^{23} Nm) between x=100 and 200 km and by applying a bending moment of 3.6x10^{17} N and a vertical force of 3.4x10^{22} N/m, the mass of both the Lesser and the High Himalaya can be supported and a match of observed and computed anomalies is obtained (Figure 7c).

Figure 7d shows the calculated deflection of the plate in the basin along with depths to the basement and to the bottoms of the Lower Siwalik and

Dharamsala formations obtained from deep wells. The calculated deflection passes through the middle of the Dharamsala formation in the Janauri deep well. This may, however, be a consequence of an unusually large thickness of the Dharamsala formation there, probably because of a doubling of the layer by thrust faulting (see the cross section near the Janauri well on Figure A2).

The underthrusting of a small amount of sediments beneath the Himalaya could improve the fit of calculated to observed anomalies, but it is not really required. This profile, like profile 3, lies in a reentrant of the Lesser Himalaya, and thus there is a three-dimensional effect that prevents us from giving a meaningful interpretation to subtleties of this part of the profile.

The computed gravity profile, however, does not predict the relatively small negative value of the anomaly at Leh. Although there is a wide range of values measured in this region, they all are at least 50 mGals less negative than what they would be if the area was in a state of local isostatic equilibrium (see Figure 2b also). A similar, but apparently less pronounced, relative high is present in profile 1 where it extends into southern Tibet. This high may reflect the presence of relative cold material of the mantle lithosphere of India that has been detached from the crust. This cold material might be supported dynamically by convective downwelling, and at the same time it might serve as an external force that applies a bending moment to the plate [Lyon-Caen and Molnar, 1983]. Neither the gravity anomalies nor the analysis given here prove the existence of such cold material there, but the occurrence of earthquakes at depths of at least 90 km in the mantle beneath the Karakorum belt and southern Tibet [Chen and Roecker, 1980; Chen et al., 1981; Molnar and Chen, 1983] is an indication of unusually strong, and thus

probably colder, material than is usually present in this depth range.

DISCUSSION

The simple model that treats the Indian plate as an elastic plate over an inviscid fluid can be used to explain both the gravity field and the shape of the basement of the Ganga Basin quite well in the sense that few parameters are used and that sensible values for the flexural rigidities and for the external system of forces are obtained. Apart from the flexural rigidity that appears to vary by a factor of 10 or so along the arc, the other parameters involved in the calculations are quite stable from one profile to another despite variations in the topographic profiles and therefore in the applied loads.

Deep Structure

Although the Indian plate appears to be very strong (its equivalent elastic thickness is between 40 and 100 km), we found that the load of the entire Himalaya is too large to be supported by the elastic stresses in the Indian plate alone. When no additional forces are applied to the plate, the calculated deflection of the plate is too large, and the calculated Bouguer gravity anomalies are 100 mGals more negative than observed. Therefore, some additional force must contribute to the support of the Himalaya. The opposite situation apparently occurs in the Appenines and the Carpathians where the total load of the mountains creates a foredeep that is only half as deep as what is observed [Royden and Karner, 1984]. Thus clearly the simple model of a flexed elastic plate, by itself, is not adequate to account for how mountain ranges are supported or for the depths of neighboring foredeeps. A downward force applied to the end of India's equivalent elastic plate will help to bend the plate down steeply beneath the High Himalaya where it is presumed to be weak, while a bending moment can flex it up under the Lesser

Himalaya where it is stronger. Thus the application of a bending moment can help the Indian plate to support the load of mountains.

The continuous underthrusting of India beneath the Himalaya probably prevents the portion of the Indian plate beneath the High Himalaya from becoming too weak or from being mechanically decoupled from the stronger part of the plate. One, but not the only, efficient and likely mechanism for weakening the plate is by detaching the crust, or at least part of it, from mantle portion the of the Indian lithosphere, as the mantle part slides beneath the Himalaya [Lyon-Caen and Molnar, 1983]. The mantle lithosphere with part or all of its crust removed could be negatively buoyant, and the gravitational force on it could then be transmitted to the rest of the plate. The magnitudes of the forces and moments used in the calculations are compatible with this interpretation.

We can represent the cold mantle part of the Indian lithosphere as a mass ano maly with a density contrast with the surrounding mantle $\Delta\rho$, with a constant thickness h, and with a down dip extent 2L. Then $F_o = 2\ L\ \Delta\rho\ h\ g$, $M_o = 2\ L^2\ \Delta\rho\ h\ g$, and $L = M_o/F_o$. The calculations used here are consistent with $L \simeq 100$ km for profiles 3, 4, 5, and $L \simeq 150$ km for profiles 1 and 2. Given the non uniqueness of the values of M_o and F_o, this difference is not required. Taking $\Delta\rho = 0.05$ g/cm^3 and L = 100 km, the values of M_o and F_o in Table 1 yield estimates of h that vary from about 25 to 40 km. Smaller values of $\Delta\rho$ yield larger values of h. Thus, for instance, a segment of mantle lithosphere extending 200 km beneath Tibet and 100 km thick, stripped of overlying crust, and more dense than the surrounding asthenosphere by 0.015-0.02 g/cm^3 would be adequate to account for the forces and bending moments needed. For a coefficient of thermal expansion of 3×10^{-5}°C^{-1}, these would correspond to a mean temperature difference of 150°-200°C, between the

mantle lithosphere and asthenosphere, which certainly is reasonable. Thus we consider plausible the entire scenario that includes detachment of crust from mantle lithosphere, underthrusting the mantle lithosphere beneath Tibet, and then the gravitational force acting on this material to cause a bending moment that flexes the Indian plate up. This scenario is, however, not required by the data and is merely one special case in a family of dynamic processes for applying a force to the Indian plate and for supporting the range.

Variations in the Apparent Flexural Rigidity

We infer significant variations of the flexural rigidity of the Indian plate along the arc. The flexural rigidity for the westernmost part (profiles 3, 4, and 5) seems to be from 3 to more than 10 times smaller than that determined for profile 2 in the central part or profile 1 in the eastern part of the range. The trend is not systematic, and the flexural rigidity obtained for profile 4, although poorly constrained, seems to be about 3 times larger than that of the two surounding profiles. In fact, profiles 2 and 3 are separated by only 200 km and over this distance the flexural rigidity apparently changes by a factor of 5 to 10. The differences in gravity anomalies requiring such differences in flexural rigidities are also apparent in the profiles shown by Karner and Watts [1983].

These large variations in flexural rigidity along the Himalaya are very difficult to reconcile with a model in which the flexural rigidity of the continental lithosphere depends only on its thermal structure at the time of loading [e.g., Karner et al, 1983]. These variations would imply very large lateral variations in the geotherm of the Indian plate, since a change by a factor of 5 in the flexural rigidity corresponds to a change of more then a factor of about 1.5 in the equivalent elastic thickness. If the elastic thickness were a measure of the depth to a particular isotherm, then these

different flexural rigidities would imply differences in geothermal gradients of approximately the same factor of 1.5. Part of the observed variation in the apparent flexural rigidity could be due to small scale convection in the mantle that draws the the cold boundary layer at the bottom of the plate down into the asthenosphere in some places and injects heat in others. This process, if it occurs, should introduce lateral variations in the geothermal gradient, but differences as large as a factor of 1.5 over distances as short as 200 km probably are too large to explain in this way.

Differences in the creep strengths of the crust and mantle may also affect the inferred flexural rigidity. Suppose that the crust, when hot enough, is much weaker than the neighboring mantle at nearly the same temperatures. A weak lower crust is suggested by depths of foci of earthquakes and by laboratory experiments, but neither are sufficient to prove this, to say nothing of quantifying it [e.g. Chen and Molnar, 1983]. Thus it is possible that when the temperature of the lower crust exceeds some value, the lower crust might deform rapidly by ductile deformation at relatively low stress. Were this to happen, the upper and middle crust might become partially decoupled from the upper most mantle by rapid creep in the lower crust. The lithosphere might then flex as two parallel thin plates instead of as one thicker one, as would be the case when the temperature of the lower crust is too low for significant ductile creep to occur there. Thus one can imagine that for sufficiently cold geotherms, the flexural rigidity would be large. For somewhat warmer geotherms, it would be somewhat smaller, but when temperature in the lower crust became sufficiently high for ductile creep to be rapid there, the flexural rigidity might drop precipitously with a small increase in the geothermal gradient.

In any case, more work is needed to understand how the apparent flexural

rigidity depends on rheological laws and rates of deformation, and we are puzzled by the variations along the Himalaya in the gravity profiles, the shape of the basement of the Ganga Basin, and in the flexural rigidities inferred from these.

Underthrusting and Deformation of the Siwalik Sediments

Both the computed and the measured depths of the basement beneath the Indo-Gangetic plains are 3 to 4 km. The absence of an increase in measured Bouguer gravity anomalies of 25-30 mGals from the plains to the Lesser Himalaya suggests that the boundary between the sedimentary fill in the Ganga Basin and the more dense rock of Lesser Himalaya is not sharp and not vertical. Instead, it appears that, for profiles 1, 2 and 4 at least, some relatively light sediment of the Ganga Basin has been underthrust beneath the Lesser Himalaya. The amount of light material beneath the Himalaya, however, does not appear to be very large; layers only 1 or 2 km in thickness extending 40 km or so under the range seem to be adequate to explain the observed gravity profiles. Thus probably large amounts of the sediment in the Ganga Basin have not been underthrust beneath the range.

Seeber et al. [1981] suggested that as the Indian shield slides beneath the Lesser Himalaya, the overlying sedimentary cover is scraped off the shield by a slip on a series of northward dipping, listric thrust faults. Near the Himalayan front, most exposures of the Siwalik group show steep dips and evidence of crustal shortening. In some areas, even tens of kilometers from the front, gentle folds in the Siwalik group break the otherwise feature less surface of the Indo-Gangetic plains. Published cross sections [e.g. Karunakaran and Ranga Rao, 1979; Mathur and Evans, 1964; Raiverman et al., 1983] often show basement involvement, but most such sections are not balanced. In order to examine whether or not geologic structures seen at the

surface and stratigraphic divisions recognized in deep wells required that thrust faults penetrate the basement, we constructed balanced cross sections across two relatively simple anticlines south of the Himalayan front. The details are given in Appendix A. We simply note here that the information used to construct both cross sections seems to rule out any basement involvement. Instead they indicate that the Siwalik group detaches from the basement on listric faults much as Seeber et al. [1981] suggested. Thus we infer that the absence of large amounts of light material beneath the Lesser Himalaya is more consistent with detachment of these sediments and with crustal shortening by folding and faulting of them, than with subduction of the majority of this material.

Constraints on the Rate of the Convergence of India and the Himalaya

The Siwalik sequence of sediments, which are derived from erosion of the Himalaya, presumably record the existence and some aspects of the history of the Ganga Basin. Insofar as the Himalaya result from the underthrusting of the Indian plate beneath the range, a flexural basin should be a steady state feature that has lain in front of the Himalaya while such underthrusting has occurred. Its width should depend on the flexural rigidity of the Indian plate. We expect, and therefore assume, that the present width of the Ganga Basin of 200-250 km is approximately the width of the basin that has existed since depostion of the Siwalik sediments began and perhaps for a longer period.

In an idealized evolution, a part of the shield would be emergent, as much of it is now in Central India, until it approached within 200-250 km of the range. Then relatively fine sediments from the distal edge of the Indo-Gangetic plains would be deposited onto the shield. As the shield moved north with respect to the Himalaya and flexed down, it would become buried in

increasingly thicker sediments. Presumably, these sediments would be coarser, the closer that they were deposited to the mountain front. Thus, facies boundaries would be time-transgressive (Figure 8). Older, fine grained material would underlie younger, coarser material. The age of the oldest sediments deposited on the shield would increase northward from the edge of the Indo-Gangetic plains to the foot of the Himalaya, and a plot of the age of the basal sediment as a function of the distance from the southern edge of the Indo-Gangetic plains should define a monotonically increasing curve (Figure 8). If the basin were a steady state feature and the rate of convergence were constant then this curve should be a straight line with a slope inversely proportional to the convergence rate (Figure 8).

Thus we might expect measured ages of the Tertiary sedimentary cover to provide a constraint on the rate of convergence. Stratigraphic columns from northwest India (Figures 9 and 10), indeed, suggest both a northward, time transgressive coarsening of material and southward younging of the basal sediment [Karunakaran and Ranga Rao, 1979; Mathur and Evans, 1964; Sahni and Mathur, 1964]. Before examining data in detail, however, let us consider some simple cases. Assume that the basin is in steady state with a width of 200 km. If the convergence rate were 10 mm/a, the age of the oldest observable molasse deposited on the Indian Shield would be 20 Ma. Older sediments would have been detached from the basement or underthrusted beneath the range. If the rate were 20 mm/a, that maximum age would be 10 Ma. If molasse older than 20 Ma were to overlie the shield beneath the basin, then either the average convergence rate between India and the Himalaya would be less than 10 mm/a or the Indo-Gangetic plains would have been wider than 200 km when this material was deposited.

Stratigraphy of the Ganga Basin

The Oil and Natural Gas Commission of India has drilled a number of deep wells into the sediments of the Indo-Gangetic plains, and stratigraphic columns inferred from these wells provide data relevant for deducing the convergence rate between India and the Himalaya (Figures 9 and 10). The principal sources of error in deducing a rate are uncertainties in ages of the various formations, lack of numerous drill holes that reach basement, and difficulties defining the southern edge of the Ganga Basin.

Traditionally, the Siwalik sediments are subdivided into Upper, Middle, and Lower Siwalik. Virtually the entire sequence was deposited subaerially, and the provenance appears to be nearly entirely the Himalaya to the north of the Ganga Basin. Beneath the Siwalik sequence is the Dharamsala (or Murree) formation often treated as being quite distinct from the overlying Siwalik series, but we consider their origins probably to be similar. Paleocurrent directions suggest a northerly source for the Dharamsala formation [Raiverman, 1968].

The Subathu formation, which lies beneath the Dharamsala formation, however, is characterized by layers of nummulitic limestone among layers of shale, clay and fine sandstone. Therefore, this formation is very different from the overlying material. Whereas the Subathu formation was deposited in a shallow sea, the Dharamsala apparently was deposited subaerially or in fresh water [Karunakaran and Ranga Rao, 1979]. The Subathu formation overlies the pre-Tertiary basement of the Indo-Gangetic plains and is exposed in isolated patches in the Himalaya. It apparently was deposited before the collision of India with southern Tibet.

Ages of Cenozoic sediments

The precise ages of most of the Tertiary sequence are difficult to determine because of the lack of fossils, and when dated in one locality,

correlations with other areas are risky because of the likely time-transgressive nature of the facies boundaries. The nummulitic foraminifora require an Eocene age for the Subathu formation [e.g., Karunakaran and Ranga Rao, 1979]. The Dharamsala (or Murree) formation is usually assigned an Oligocene or early Miocene age, but it could be as old as the latest Eocene [e.g., Aditya et al., 1979; Karunakaran and Ranga Rao, 1979]. The Lower, Middle, and Upper Siwalik sequences are often assigned Middle Miocene, Late Miocene, and Plio-Pleistoce ne ages, respectively [e.g., Aditya et al, 1979; Karunakaran and Ranga Rao, 1979]. Studies of magneto-stratigraphy and fission track ages of bentonite layers, largely from Pakistan, corroborate these inferences and refine the ages for these formations in that region [e.g., Barry et al., 1982; N. Johnson et al., 1982; G.D. Johnson et al., 1982, 1983; Opdyke et al., 1979; Tauxe and Opdyke, 1982]. Nevertheless, given the lack of tight constraints for the ages of the particular formations at the bottoms of the various drill holes, we take the following ages (and allowable ranges of ages) for the bases of the following formations: Upper Siwalik, 5 Ma (between 3 and 7 Ma), Middle Siwalik, 11 Ma (between 9 and 12 Ma), Lower Siwalik, 15 Ma (between 12 and 18 Ma) and Dharamsala, 30 Ma (between 20 and 40 Ma). These ranges not only span the various ages proposed for the various sequences in particular areas but also allow for differences from place to place, given the expected time-transgressive nature of the group.

Using these ranges of ages and the stratigraphy reported from drill holes that reached basement in the Indo-Gangetic plains, we can construct a plot like that in Figure 8. In general, the reported thicknesses of Middle and Lower Siwalik sequences are similar from drill holes that are within 100 km of one another [Figure 9; Karunakaran and Ranga Rao, 1979; Sastri, 1979; Sastri

et al., 1971]. Therefore, when the oldest sediments in a particular well were from either of these formations, we used the thickness from nearby wells penetrating older sequences as a reference. Then to obtain the age at the basement, we used these full thicknesses to interpolate between the ranges of ages of the top and bottom assuming the same constant rate of sedimentation for the Middle or Lower Siwalik sequence in both wells. For wells bottoming in the Dharamsala formation, we allowed wide ranges of ages for the basal sediment.

Finally, to obtain an estimate of the distance of the particular well site to the edge of the Indo-Gangetic plains, we drew a smooth curve through or near the edge of outcrops of the major Pre-Cambrian massifs of the Central Indian Highlands (Figure 10). The northwest part of the region is buried by recent sediments, and we drew the presumed former margin of the plains over the axis of a shallow basement high (Figure 10). Clearly, the edge of the Indo-Gangetic plains is not well defined, and we arbitrarily assigned an uncertainty of 30 km to each distance measured. From these ranges of distances to the edge of the Indo-Gangetic plains and ages of the oldest Tertiary sediments over the basement, we constructed a plot (Figure 11) like that in Figure 8.

Inferred convergence rates

Three widely spaced drill holes reached the Dharamsala formation before entering basement. In two wells, the thickness of the Dharamsala formation is thin: Raxaul, 65 m [Sastri et al., 1971] and Mohand, 246 m [Sastri, 1979]. In the third, Janauri, the Dharamsala formation is much thicker (Figure 9), which apparently is partly due to repetition in an overthrust section (see Appendix A). Nevertheless, half of the section of Dharamsala sediments is 1000 m, and we allowed a wider range of possible ages for its base than for

those in the other two holes.

Notice that even if we underestimated the distance for Janauri to the edge of the Indo-Gangetic plains by 100 km, the occurrence of the Dharamsala formation over the pre-Tertiary basement limits the amount of convergence between India and the Himalaya during the last 15-25 Ma to about 200 km. Best fitting average convergence rates are near 10 mm/a and probably less than 15 mm/a. Even if Dharamsala formation were deposited before the Indian plate was flexed down, and the oldest sediment deposited in the Ganga Basin were the Lower Siwalik group, the rate would still be less than 20 mm/a. We conclude that the rate cannot be as high as 20 mm/a unless one of the basic assumptions used to construct Figure 11 is in error.

In five other wells, the oldest sediments overlying pre-Tertiary basement are either Middle or Lower Siwalik sequences. For the two wells in the northwest part of the Indo-Gangetic plains [Zira and Adampur, Figure 10], we used the thicknesses of Middle and Upper Siwalik sediments in the nearby Janauri deep well as reference thicknesses to assign ages to the oldest sediment. The distances vs. ages imply a rate of convergence of about 10 mm/a. Note, however, that an underestimate of 50 km in the distance to the edge of the Indo-Gangetic plains, an error that cannot be ruled out, would allow average convergence rates of 15-20 mm/a. At the same time, the rates obtained from the differences in basal ages and differences in distances among Zira, Adampur and Janauri, for which the uncertainty in the distance scale is only tens of meters (!), favor rates nearer 10 mm/a than 20 mm/a.

The other three deep holes, Kasganj, Ujhani, and Tilhar, lie in the central part of the Indo-Gangetic Plains (Figure 10). The oldest Tertiary sediment in each is from the Middle Siwalik formation (250 m in Kasganj, 330 m Ujhani, and 1090 m in Tilhar [Sastri, 1979; Sastri et al., 1971]). Although these

localities are closer to Mohand than Raxaul, we use the thickness of 1500-1700 m for the Middle Siwalik in Raxaul for the reference thickness [Sastri, 19879; Sastri et al., 1979]. The Mohand deep well penetrates a thrust fault within or near the Middle Siwalik group [Appendix A; Raiverman et al., 1983; Rao et al., 1974], and there fore estimating the thickness of the Middle Siwalik formation in this well is problematic (see Appendix A). The basal ages and estimated distances of these three holes from the edge of the basin suggest rates of convergence of 15-20 mm/a (Figure 11). Note, however, that if the distance to the edge of the Indo-Gangetic plains were overestimated by 50 km, the inferred rate would be about 10 mm/a. Such an overestimate is quite possible given the exposures of the Aravali-Delhi massif near Delhi, some 50 km northeast of the line used for the edge of the Indo-Gangetic plains here (Figure 10).

Taken as a whole, the observations of distance vs. basal age show considerable scatter (Figure 11). Nevertheless, given the possible systematic overestimates of distance for Kasganj, Ujhani, and Tilhar and similarly possible underestimates for Zira, Adampur and Janauri, the data are consistent with an average rates of con vergence between India and the Himalaya for the last 15-20 Ma of 10-15 mm/a. Average rates as high as 20 mm/a seem to be ruled out unless one of the basic assumptions used to construct Figure 11 is in error.

The rate of convergence between India and Eurasia ranges from about 40 mm/a at the western end of the Himalaya to 65 mm/a at the eastern end [Minster and Jordan, 1978]. Much of the convergence is known to be absorbed north of the Himalaya, both by crustal shortening and thickening and by translation of material eastward and out of India's northward path toward Eurasia [e.g., Molnar and Deng, 1984; Molnar and Tapponnier, 1975; Tapponnier and Molnar,

1977]. How the roughly 50 mm/a of convergence is partitioned between underthrusting of India beneath the Himalaya and northward motion of the Himalaya and southernmost Tibet with respect to Eurasia is not well con strained. The results presented here, however, suggest that 10-15 mm/a are absorbed by underthrusting at the Himalaya. The rate of crustal shortening in the Tien Shan appears to be only 10 ± 5 mm/a [Molnar and Deng, 1984; Molnar and Tapponnier, 1975]. Thus half or more of the present convergence rate seems to occur by squeezing parts of Tibet and the areas north and east of it eastward [see also Tapponnier et al., 1982].

Note that if India were to have underthrust the whole of Tibet (~1000 km) in the last 50 ma, its average rate would have been higher than 15 mm/a (50 Ma x 15 mm/a = 750 km) and therefore its rate before 10 to 20 Ma would have to have been higher than since that time.

CONCLUSIONS

Gravity anomalies over the Himalaya and Ganga Basin show large deviations from isostatic equilibrium, which can be explained if a strong plate underthrusts the Himalaya. The weight of the mountains is supported in part by the strength of the plate, and the plate distributes the load by flexing down in front of the range to form a basin [e.g., Karner and Watts, 1983; Lyon-Caen and Molnar, 1983]. The Ganga Basin, which apparently formed by such a flexure, in turn is filled by sediment, the Siwalik group, derived largely by erosion of the Himalaya.

We analyzed the gravity anomalies in terms of the simple model of an elastic plate overlying an inviscid fluid, and we use gravity anomalies as well as profiles of the basement depth to constrain the flexural rigidity of the plate. Profiles of the basement inferred from gravity anomalies, via a flexural model, and those measured in deep wells or by seismic reflection

agree within a few hundred meters, but both show variations along the Himalayan front. In terms of an elastic plate, these variations in gravity and basement shape imply a variation in the flexural rigidity of an order of magnitude along the Himalaya. The distance to which an elastic plate of constant flexural rigidity could reach beneath the Himalaya varies along the arc from about 70 to 130 km. Thus only a part of the weight of the range is needed to flex the Indian plate down, and a plate of constant flexural rigidity could not extend all the way beneath the Himalaya and Tibet unless forces other than the weight of the mountains and the buoyant response of the underlying asthenosphere act on it.

If the Ganga Basin is a consequence of the flexure of the Indian plate and if it is a steady state feature, then the age of the basal sediments should increase from very young ages at the southern edge of the basin to the older ages at the foot of the Lesser Himalaya where the basin is deepest. If convergence between India and the Himalaya has been steady, then a plot of the distance of a particular locality to the edge of the basin divided by the age of the basal sediment derived from the Himalaya should be equal to the rate. Results from deep wells drilled by the Oil and Natural Gas Commisssion of India indicate rates of 10-15 mm/a and almost surely less than 20 mm/a for the last 10 to 20 Ma.

The fit of computed and observed gravity anomalies over the southern edge of the Lesser Himalaya can be improved if some light material underlies the mountains [Lyon-Caen and Molnar, 1983]. We presume this to be sediment deposited in the Ganga Basin on the Indian plate and underthrust with it beneath the Lesser Himalaya. Not a lot of sediment need be underthrust; a layer 1-2 km in thickness extending 40 km beneath the range is sufficient to account for a slight gravity high or plateau over the Lesser Himalaya. Since

the basin contains 3-4 km of Siwalik sediment, we conclude that most of it is scraped off the downgoing Indian plate by the overriding thrust sheets of the Lesser Himalaya [Seeber et al., 1981].

The gravity anomalies indicate that the Moho dips at a gentle angle of only a couple of degrees beneath the Lesser Himalaya but must steepen to 10°-15° beneath the Greater Himalaya [Kono, 1974; Lyon-Caen and Molnar, 1983; Warsi and Molnar, 1977]. We infer that this steepening occurs because the part of the Indian plate that has underthrust beneath the Greater Himalaya is much weaker and more flexible than that beneath the Lesser Himalaya or Ganga Basin.

To analyze this further we treat the Indian plate as consisting of two segments: one beneath the Ganga Basin and the Lesser Himalaya and a weaker one beneath the Greater Himalaya. Such a configuration alone, however, cannot support the Himalaya and allow a fit to the gravity anomalies. A plate strong enough to support the range is flexed down too much beneath the Ganga Basin and would create a much wider basin than exists. We conclude that an additional force system is needed to support the range. In a previous study [Lyon-Caen and Molnar, 1983], we examined in more detail than here the trade-offs among the flexural ridigity of the segment of plate beneath the Greater Himalaya and bending moments and forces applied to the end of the plate. Here we show that values for the moments and forces for each profile could be essentially the same for each profile. We then argue that the weakened plate, the bending moment, and the additional force could all arise if the Indian lithosphere, stripped of most or all of its crust, plunged into the asthenosphere and if this mantle lithosphere remained a few hundred degrees cooler than the asthenosphere. Then gravity acting on this segment of plate could generate the necessary bending moment. This explanation, however,

is not unique and other dynamic mechanisms could contribute to the support of the Himalaya. Regardless, some dynamic mechanism seems to be required to support the range.

APPENDIX A: BALANCED CROSS SECTIONS ACROSS TWO STRUCTURES IN THE SUB-HIMALAYA

In order to place some constraints on amounts of shortening in the Siwalik sequence, we constructed balanced cross sections for two anticlines for which subsurface information is available. These results attest to several kilometers of crustal shortening across rather gentle anticlines that lie some tens of kilometers from the front of the Himalaya. The tighter folds and steeper dips of the Siwalik group closer to the Himalaya imply tens to several tens of km of crustal shortening within this group. This style of deformation corroborates Seeber et al.'s [1981] inference that the Siwalik sediments detach from the underlying basement along a series of listric thrust faults.

Mohand Anticline

South of the Himalayan front between the Yamuna and Ganga rivers (Figure 10) the Upper and Middle Siwalik formations emerge from the post-Siwalik cover and form a broad gentle anticline, which manifests itself topographically as the Siwalik Hills [e.g., Raiverman et al., 1983; Rao et al., 1974]. In the central and western part of the Siwalik Hills, the anticline is overturned and verges south ward (Figure A1). Dips on the northern flank range from a maximum of 30° to about 20° (or rarely 15°) where recent, unconsolidated sediments bury the uppermost unit involved in the folding [Rao et al., 1974]. The crest of the anticline lies south of the topographic axis, and the beds on the south flank dip steeply south (~50°).

Two drill holes corroborate the inference that a thrust fault dips northward beneath this portion of the Siwalik hills [Raiverman et al., 1983;

Rao et al., 1974]. One shallow hole penetrated recent gravels below the Middle Siwalik formation on the south edge of the Siwalik Hills. The other, deeper hole was drilled south of the topographic axis of the Siwalik Hills, but north of the crest of the anticline (Figure A1). This hole penetrated the Middle and Lower Siwalik formations before intersecting the thrust fault and passing through another section of Middle and Lower Siwalik sediments and a thin layer of the Dharamsala formation. The Pre-Tertiary basement was reached at a depth of 4416 m below the surface [Sastri, 1979] or nearly 4000 m below sea level.

To construct a cross section, we use the reported results from the Mohand deep well and a profile of average dips of the various formations observed at the surface from Raiverman et al. [1983]. Raiverman et al [1983] used a slightly different stratigraphic column than is common for the Tertiary sedimentary sequence of the sub-Himalaya and Indo-Gangetic plains. They divided the column into nine units according to both grain size and distributions of heavy minerals. They consider their units 2 and 3 to include part of the Subathu formation and all of the Dharamsala formation. Unit 4 is essentially the same as the Lower Siwalik. The Middle Siwalik includes all of unit 5 and approximately the lower third of unit 6. The rest of unit 6 and units 7 and 8 together constitute the Upper Siwalik sequence.

To build a balanced cross section we assumed that the pre-Tertiary basement dips gently northeast beneath the Ganga Basin. We further assumed that thrust faults in the Tertiary formations do not cut the basement but instead detach the overriding formations from it. For the Mohand thrust we conclude that the sole of the detaching thrust fault is in the Dharamsala formation. The sole cannot be much above this depth because the thick ness of unit 4 (Lower Siwalik) is the same above and below the thrust fault. The absence of the

Dharamsala formation above the thrust fault suggests that detachment occurred above it. For units 4, 5, and 6, we used the thicknesses inferred by Raiverman et al. [1983] from the Mohand deep well and from the surface exposures north of it. The top and bottom of unit 6 crop out, and the nearly uniform dip of the formation leaves little room for controversy over its average thickness. The bottom of unit 5 is seen only in the Mohand deep well, but with the top exposed at the surface, a reliable estimate of the thickness can be obtained. The Mohand deep well penetrates approximately 800 m of unit 4 beneath the thrust fault, and we take this value for its thickness. Ap proximately the same thickness overlies the fault. This drill hole did not penetrate unit 6 at all. For the thickness of all three units 4, 5, and 6 to be essentially the same on both sides of the faults, we, like Raiverman et al. [1983], are forced to assume that drag folding on the thrust fault has warped unit 5 up (see Figure A1).

In earlier cross sections [e.g., Rao et al., 1974], which were published at a smaller scale than Raiverman et al.'s, the Siwalik sequence was subdivided into the classical Lower, Middle and Upper divisions. On these cross sections the thicknesses of Middle and Upper Siwalik sub groups are nearly the same. Rao et al.'s cross section, however, shows the Mohand deep well penetrating only the Middle Siwalik portion of Raiverman et al.'s unit 6. We have used Raiverman et al.'s stratigraphy with the drag fold in unit 5, because their cross section was published at a much larger scale than Rao et al.'s. Were we to use Rao et al.'s, we would obtain essentially the same cross section, but without the drag fold in unit 5.

The vertical separation of the boundary between the Lower and Middle Siwalik (units 4 and 5) is nearly 3 km. This value, therefore, is a lower bound for the slip on the fault. The 30° dip of the beds near the well

suggests that the dip of the fault must be at least 30° there. The gradual decrease northward to 20° where unit 8 crops out (Figure A1) suggests that the fault surface is listric and makes it very unlikely that the fault enters the basement in this region. The shape of the fault is then deduced by keeping the thickness of units 4, 5 and 6 constant, and a slip of 7.5 is obtained. This is probably close to an upper bound for the slip. Detachment could not have occurred at a much shallower depth, be cause the thickness of unit 4 is the same same above and below the fault. Detachment could have occurred within or at the base of the Dharamsala formation (units 2 and 3). If it did, however, then the fault would have to be steeper than is shown. If variations in thickness of the various units were 300 m, then the vertical separation could be in error by this much, and the estimated throw could be in error by 0.5-1 km. If the dip of the fault were 25° or 35° instead of 30° used here, then the slip could be in error by about 1 km. Thus we consider the slip to be between about 6 and 9 km.

Janauri Anticline

We have used much the same logic to construct a balanced cross section across the Janauri anticline. We used stratigraphic thicknesses reported for three drill holes: the Janauri deep well on the north slope of the anticline, the Hoshiarpur well about 6-7 km southwest of the edge of the anticline, and the Adampur deep well some 30 km southwest of the southwest edge (Figures 9 and 10). The first and third wells reached the basement, and all three penetrated comparable thicknesses of Middle Siwalik sediments (~1000-1400 m [Karunakaran and Ranga Rao, 1979; Sastri, 1979]). The top of the Upper Siwalik sequence is eroded from the Janauri anticline, but the gentle northward dip on the north flank and the mapped boundary between the Upper Siwlaik and Post-Siwalik formations indicate a thickness comparable to that

observed in the Adampur and Hoshiarpur wells (1400-1600 m) (see Figure A2).

We have drawn the Middle and Upper Siwalik formations each with constant thickness, despite differences of 100-200 m in the drill holes. We also treat the thickness of the Lower Siwalik formation as constant (Figure A2). (The Hoshiarpur well did not penetrate the base of the Lower Siwalik sequence.) We assume that the pre-Tertiary basement slopes gently to the northeast and that Dharamsala sediments increase in thickness in that direction. This formation pinches out southwest of the Janauri well and is not exposed is the Adampur well, but it is particularly thick in the Janauri well.

To make the cross section, we took the dips at the surface on the north flank of the anticline and projected the various contacts downwards assuming constant thickness of the various units (Figure A2). We conclude that the thickness of the Dharamsala sequence in the Janauri well is roughly double that deposited on the basement, and that the deep well penetrated a northeast dipping thrust fault. If this is not so, then there must be very large lateral variations (>1000 m) in the thickness of the Dharamsala sequence over short distances (~10 km).

The Janauri anticline is a very gentle feature (Figure A2). On the northeast side, Upper Siwalik sediments generally dip 10° to 20° to the northeast, and the dip decreases smoothly towards the south west [Mathur and Evans, 1964]. The crest of the anticline is broad with the Upper Siwalik sediments only gently warped. One the south edge of the anticline, dips become very steep (~80°) and even locally overturned [Mathur and Evans, 1964]. Thus the anticline is asymmetric, but the steep southwest side is a very local feature (Figure A2). The very steep dips are probably due to drag on the thrust fault where it approaches the surface at the southern edge of the anticline. In drawing a balanced cross section, we have not tried to match

these steep dips. The various units encountered in deep well are approximately 1000 m shallower in the Janauri well than in the Hoshiarpur or Adampur wells. Projecting the interfaces between units up dip to the south leads to approximately 1600 m of vertical separation. This value cannot be much larger; if larger vertical separation were to exist, then Middle Siwalik sediments would be exposed in the anticline. For instance, if detachment occurs within the Dharamsala formation, but if 8 km of thrust slip occurred on the fault shown, then even lower Siwalik sediments would be exposed in the anticline. Thus at least 1.6 km of slip must have occurred (if the fault were vertical), but regardless of the dip, the total slip probably does not exceed 5 km.

The dip of the fault is probably steeper than 20°, the maximum dip in the upper Siwalik sequence on the north flank. If the dip of the fault were only 20°, then the fault plane would project to the surface south of the south edge of the anticline. The fault surface could be listric between the Janauri deep well and the southern edge of the anticline, but if it is markedly listric, then the observed broad, gentle anticlinal cross section would not be matched. Therefore 20° is probably a lower bound for the average dip of the fault. We find that a dip of about 25° with a throw of 4 km allows a balanced cross section consistent with the measured dips at the surface and with the measured sections in the drill holes. If dip of the fault were as steep as 30° or 35°, then the throw could be less, but would still exceed 3 km. For steeper dips, however, the anticline would be much sharper, as it would be for a listric fault, and the broad, flat shape would not exist without introducing complexities at shallow depths. Allowing for lateral variations of 200-300 m in thicknesses of various units, ignored in drawing Figure A2, the uncertainty in the throw is probably 1 km. Hence we infer that the Janauri anticline

formed by 4 ± 1 km of slip on a fault dipping north at 25° ± 5° and detaching the overlying sediments within the Dharamsala formation.

Acknowledgments. We thank S. K. Biswas and L. L. Bhandari for allowing us to attend a conference on Petroliferous Basins in India, at the Oil and Natural Gas Commission of India, where we were able to talk with S. Aditya, D. Das, G. Mehra, V. Raiverman, and A. Ranga Rao. We thank S. Kumar, A. C. Nanda, D. P. Rao, V. C. Thakur, and K. S. Valdiya for showing us aspects of the geology of the Siwalik sedimentary sequence and its structure in the field and for rewarding discussions. We also thank V. K. Gaur and R. McCaffrey for helping us to straighten out problems with different gravity formulae and M. McNutt and M. Steckler for critical reviews of the manuscript. A research development grant from the Smithsonian Institution allowed us to visit India and to familiarize ourselves with unpublished or obscurely published material. This research was supported by NASA grant NAG5-141 and NSF grant EAR81-21184.

REFERENCES

Aditya, S., A. T. R. Raju, and S. N. Shukla, Assessment of Hydrocarbon prospects of the sub-Himalayan, Punjab and Ganga basin, India, Himalayan Geology Seminar, Section III, Oil and Natural Gas Prospects, Geol. Surv. India Misc. Publ., 41, 127-140, 1979.

Amboldt, N., Relative Schwerkrafts bestimmungen mit pendeln in Zentral Asien, Reports from Scientific Expedition to Northwestern Provinces of China under leadership of Dr. Sven Hedin, Publ. 30, II Geodes., 112 pp., 1948.

Baranowksi J., J. Armbruster, L. Seeber, and P. Molnar, Focal depths and fault plane solution of earthquakes and active tectonics of the Himalaya, J. Geophys. Res., 89, 6918-6928, 1984.

Barry, J. C., E. H. Lindsay, and L. L. Jacobs, A biostratigraphic zonation of the middle and upper Siwaliks of the Potwar Plateau of Northern Pakistan, Paolaeogeogr. Palaeoclimatol. Palaeoecol., 37, 95-130, 1982.

Chen, W.-P., and P. Molnar, Focal depths of intracontinental and intraplate earthquakes and their implications for the thermal and mechanical properties of the lithosphere, J. Geophys. Res., 88, 4183-4214, 1983.

Chen, W. P., and S. W. Roecker, Regional variation of the focal mechanism of intermediate depth earthquakes and seismicity in the Karakorum-East Hindu Kush area (abstract), Eos Trans. AGU, 61, 1031, 1980.

Chen, W.-P., J. L. Nabelek, T. J. Fitch, and P. Molnar, An intermediate depth earthquake beneath Tibet: Source characteristics of the event of September 14, 1976, J. Geophys. Res., 86, 5937-5962, 1981.

Das, D., G. Mehra, K. G. C. Rao, A. L. Roy, and M. S. Narayana, Bouguer, free-air and magnetic anomalies over northwestern Himalayas, Himalayan Geology Seminar, Section III, Oil and Natural Gas Resources, Geol. Surv. India, Misc. Publ., 41, 141-148, 1979.

Gunn, R., A quantitative evaluation of the influence of the lithosphere on the anomalies of gravity, J. Franklin Inst., 236, 47-65, 1943.

Hanks, T. C., The Kurile trench-Hokkaido rise system: Large shallow earthquakes and simple models of deformation, Geophys. J. R. Aston. Soc., 23, 173-189, 1971.

Johnson, G. D., N. D. Opdyke, S. K. Tandon and A. C. Nanda, The magnetic polarity stratigraphy of the siwalik group at Haritalyangar (India) and a new last appearance datum for Ramapithecus and Sivapithecus in Asia, Palaeogeogr. Palaeoclimatol. Palaeoecol., 44, 223-249, 1983.

Johnson, G. D., P. Zeitler, C. W. Naeser, N. M. Johnson, D. M. Summers, C. D. Frost, N. D. Opdyke, and R. A. K. Tahirkheli, The occurrence and fission track ages of late Neogene and Quaternary Volcanic sediments, Siwalik group, northern Pakistan, Palaeogeogr. Palaeoclimatol. Palaeoecol., 37, 63-93, 1982.

Johnson, N. M., N. D. Opdyke, G. D. Johnson, E. H. Lindsay, and R. A. K. Tahirkheli, Magnetic polarity stratigraphy and ages of Siwalik group rocks of the Potwar Plateau, Pakistan, Palaeogeogr. Palaeoclimatol. Palaeoecol., 37, 17-42, 1982.

Kaila, K. L., Deep seismic sounding studies in India, Geophys. Res. Bull., 20(3), 309-328, 1982.

Karner, G. D., and A. B. Watts, Gravity anoamlies and flexure of the lithosphere at mountain ranges, J. Geophys. Res., 88, 10,449-10,477, 1983.

Karner, G. D., M. S. Steckler, and J. A. Thorne, Long-term thermo-mechanical properties of the continental lithosphere, Nature, 304, 250-253, 1983.

Karunakaran, C., and A. Ranga Rao, Status of exploration for Hydrocarbons in the Himalayan Region--Contributions to Stratigraphy and Structure, Himalayan Geology Seminar, Section III, Oil and Natural Gas Resources, Geol. Surv. India Misc. Publ., 41, 1-66, 1979.

Kono, M., Gravity anomalies in East Nepal and their implications to the crustal structure of the Himalayas, Geophys. J. R. Astron. Soc., 39, 283-300, 1974.

Lyon-Caen, H., and P. Molnar, Constraints on the structure of the Himalaya from an analysis of gravity anomalies and a flexural model of the lithosphere, J. Geophys. Res., 88, 8171-8191, 1983.

Lyon-Caen, H., and P. Molnar, Gravity anomalies and the structure of Western Tibet and the Southern Tarim Basin, Geophys. Res. Lett., 11, 1251-1254, 1984.

Marussi, A., Geophysics of the Karakorum, Italian expeditions to the Karakorum (K^2) and Hindu Kush, Sci. Rep. 2, 1, 242 pp., 1964.

Mathur, L. P., and P. Evans, Oil in India, Proc. Int. Congr. XXII Sess. India, 1964, 1964.

Minster, J. B., and T. H. Jordan, The present-day plate motions, J. Geophys. Res., 83, 5331-5354, 1978.

Molnar, P., and W.-P. Chen, Focal depths and fault plane solutions of earthquakes under the Tibetan Plateau, J. Geophys. Res., 88, 1180-1196, 1983.

Molnar, P., and Q. D. Deng, Large earthquakes and the average rate of deformation in Asia, J. Geophys. Res., 89, 6203-6228, 1984.

Molnar, P., and P. Tapponnier, Late Cenozoic tectonics of Asia: Effects of a continental collision, Science, 189, 419-426, 1975.

Ni, J., and M. Barazangi, Seismotectonics of the Himalayan collision zone: Geometry of the underthrusitng Indian plate beneath the Himalaya, J. Geophys. Res., 89, 1147-1163, 1984.

Opdyke, N. D., E. Lindsay, G. D. Johnson, N. Johnson, R. A. K. Tahirkheli, and M. A. Mirza, Magnetic polarity stratigraphy and vertebrate paleontology of

the upper Siwalik subgroup of Northern Pakistan, Palaeogeogr. Palaeoclimatol. Paleocol., 27, 1-34, 1979.

Raiverman, V., Petrology of the Tertiary sediments of Sarkaghat anticline in the Himalayan foothills of Himachal Pradesh, Publ. Contrib. Adv. Study Geol., 5, 39-53, 1968.

Raiverman, V., S. V. Kunte, and A. Mukherjea, Basin geometry Cenzoici sedimentation and Hydrocarbon prospects in north western Himalaya and Indo-Gangetic Plains, in Petroliferons Basins of India, Petroleum Asia Journal, pp. 67-92, Dehra Dun, India, 1983.

Rao, Y. S. N., A. A. Rahman, and D. P. Rao, On the structure of the Siwalik range between rivers Yamuna and Ganga, Himalayan Geol., 4, 137-150, 1974.

Royden, L., and G. D. Karner, Flexure of the lithosphere beneath the Apennine and Carpathian fordeep basins, Nature, 309, 142-144, 1984.

Sahni, M. R., and L. P. Mathur, Stratigraphy of the Siwalik group, Proc. Int. Geol. Cong. XXII Sess. India, 1964, 24 pp., 1964.

Sastri, V. V., An overview of petroleum geotectonics of the region to the north and south of the Himalaya, Himalayan Geology Seminar, Section III, Oil and Natural Gas Resources, Geol. Surv. India Misc. Publ., 41, 247-276, 1979.

Sastri, V. V., L. L. Bhandari, A. T. R. Raju, and A.K. Datta, Tectonic framework and subsurface stratigraphy of the Ganga basin, J. Geol. Soc. India, 12, 222-233, 1971.

Seeber, L., J. Armbruster, and R. Quittmeyer, Seismicity and continental subduction in the Himalayan arc, in Zagros, Hindu-Kush, Himalaya, Geodynamic Evolution, Geodyn. Ser., vol. 3, A. G. U., Washington, D. C., 1981.

Tapponnier, P., and P. Molnar, Active faulting and tectonics in China, J. Geophys. Res., 82, 2905-2943, 1977.

Tapponnier, P., G. Peltzer, A. Y. Le Dain, R. Armijo, and P. Cobbold, Propagating extrusion tectonics in Asia: New insights from simple experiments with plasticine, Geology, 10, 611-616, 1982.

Tauxe, L., and N. D. Opdyke, A time framework based on magnetostratigraphy for the Siwalik sediments of the Khaur area, northern Pakistan, Palaeogeogr. Palaeoclimatol. Palaeoecol., 37, 43-61, 1982.

Van de Meulebrouck, J., Thèse de 3ème cycle, Univ. des Sci. et Tech. du Languedoc, Montpellier, France, 1984.

Van de Meulebrouck, J., P. Tarits, J. L. Le Mouel, and L. S. Men, New gravity measurements on the Tibetan Plateau (abstract), Terra Cognita, 3, 272, 1983.

Verma, R. K., and C. Subrahamanyam, Gravity anomalies and the Indian lithosphere: Review and analysis of existing gravity data, Tectonophysics, 105, 141-163, 1984.

Walcott, R. I., Flexural rigidity, thickness and viscosity of the lithosphere, J. Geophys. Res., 75, 3941-3954, 1970.

Warsi, W. E. K., and P. Molnar, Gravity anomalies and plate tectonics in the Himalaya, in Colloques Internationaux du CNRS, Himalaya: Sciences de la Terre, pp. 463-473, Editions du Centre National de la Recherche Scientifique, Paris, 1977.

Watts, A. B., and M. Talwani, Gravity anomalies seaward of deep-sea trenches and their tectonic implications, Geophys. J. R. Astr. Soc., 36, 56-90, 1974.

Woollard, G.P., The new gravity system: Changes in international gravity base values and anomaly values, Geophysics, 44, 1352-1366, 1979.

Figure captions

Fig. 1. Map of the Indo-Gangetic plains and the Himalaya with 1000 and 3000 m elevation contours and contours of Bouguer anomalies over the plains. For each of the profiles shown, the routes along which gravity measurements were made in the Himalaya are shown by a heavy line or by dots.

Fig. 2. (a) Mean topography along each profile in Figure 1. The northern edge of the Ganga Basin is at x=0. (b) Comparison of observed Bouguer gravity anomalies with anomalies computed assuming that the mean topography shown in Figure 2a is locally isostatically compensated by thickening of the crust from a reference thickness of 38 km beneath central India.

Fig. 3. Schematic cross section of the geometry used to calculate the shape of the flexed plate, and hence the shapes of the Ganga Basin and the Moho. In the first step, only a load between $0 < x < X_o$ is used and a straight line is drawn from the calculated depth of the Moho at $x = X_o$ to that beneath southern Tibet. In a second step, a short segment of plate is added, extending the plate to X_o'. The flexural rigidity D' of the segment between X_o and X_o' is smaller than D. The load is the weight of the entire range between $0 \leq x \leq X_o'$. Values for X_o', and both a bending moment M_o, and an external force F_o per unit length are then sought such that the computed and observed gravity anomalies match.

Fig. 4. Comparisons of observed and computed Bouguer anomalies and deflections of plates for profile 2. (a) A simple plate with a constant flexural rigidity is used here. X_o is fixed and the computed anomalies for three different values of the flexural rigidity D are shown. (b) the configuration model as in Figure 4a is used, but D is fixed and the computed

anomalies for three different values of X_o are shown. (c) The flexural rigidity of the plate is D for $x < X_o$ and D' for $Xo < x < X_o'$ (see Figure 3). The bending moment M_o and vertical force F_o are applied at X_o'. The dashed line shows computed Bouguer anomalies for the case including a small wedge of underthrust sediments as shown in Figure 4d. (d) The computed deflection of the plate is compared with a profile of Ganga Basin inferred from deep wells near the profile. Positions of deep wells are shown in Figure 10. Vertical exaggeration is 10 times.

Fig. 5. Comparisons of observed and computed Bouguer anomalies for profile 3. (a) Format same as Figure 4a but for profile 3. (b) Format same as Figure 4b but for profile 3. (c) Format same as Figure 4c but for profile 3.

Fig. 6. Comparisons of observed and computed Bouguer anomalies and of deflections of the Indian plate for profile 4. (a) Format same as Figure 4a but for profile 4. (b) Format same as Figure 4b but for profile 4. (c) Format same as Figure 4c but for profile 4. (d) Comparison of the computed deflection with the depth of the basement inferred by Raiverman et al. [1983]. Vertical exaggeration is 10 times.

Fig. 7. Comparisons of computed and measured Bouguer gravity anomalies and of delfections of the Indian plate for profile 5. (a) Format same as Figure 4a but for profile 5. (b) Format same as Figure 4b but for profile 5. (c) Format same as Figure 4c but for profile 5. (d) Comparison of the computed deflection of the plate using the parameters from Figure 7c with depths to various horizons obtained from deep wells. Vertical exaggeration is 10 times.

Fig. 8. Hypothetical, vertically exaggerated cross section of the Ganga Basin

and (top) plot of expected basement ages vs. distance from the southwest edge of the basin. The Himalaya would be to the right of the drawing, and coarse debris are shed southward from the range. The basement bends down and moves to the right (northward) beneath the Himalaya. Sediment is presumed to be deposited on the basement when the basement is flexed below the level of the plains on the left. As the basement moves to the right, it is buried by younger, coarser material. Facies boundaries are time transgressive so that age horizons, given by t_1 to t_5, cross such boundaries. The rate of convergence can be obtained from the ratio given by the distance to the edge of the basin divided by the age of the oldest post-Himalayan sediment overlying the basement.

Fig. 9. Simplified stratigraphic columns from deep wells and surface outcrops in the northwest Himalaya (Figure 10). Horizontal scale gives rough distances between sites. Sloping top surfaces on columns indicate that erosion has removed the upper parts of the section. Wells only at Zira, Adampur, and Janauri reached basement. The column at Sarkagat is inferred only from surface exposures. Note the time transgressive nature of facies changes; conglomerates were deposited only relatively close to the Himalaya.

Fig. 10. Map showing locations of deep wells, basement outcrops, and the line used to define the edge of the Ganga Basin for constructing Figure 11.

Fig. 11. Plot of inferred basement ages vs. distances from the edge of the Ganga Basin for deep wells in Figure 10. Uncertainties of 30 km are shown for all distances. Uncertainties in ages are discussed in the text. Solid circles, open circles, and the cross denote wells treated together as parts of profiles.

Fig. A1. Balanced cross section (top) and (bottom) palinspastically restored section across the Mohand anticline (see Figure 10 for approximate location). Following Raiverman et al. [1983], the stratigraphy is divided into layers according to grain size and heavy minerals. Strikes and dips given by Rao et al. [1974] were used to constrain the orientations at the surface.

Fig. A2. (top) Balanced cross section and (bottom) palinspastically restored section for the Janauri anticline (see Figure 10 for the approximate location.) We used stratigraphic data given by Karunakaran and Ranga Rao [1979] and surface mapping reported by Mathur and Evans [1964] to constrain the thicknesses and dips of various layers.

TABLE 1. Parameters Describing the Geometry and the Forces Acting on an Elastic Indian Plate, Inferred From the Gravity Anomalies

Profile	X_o, km	X_o', km	D, Nm	D', Nm*	M_o, N†	F_o, N/m†
1. Everest	130±10	200	$7(^{+13}_{-4})\times10^{24}$	2×10^{22}	4.0×10^{17}	3.0×10^{12}
2 India Nepal Border	130±10	190	$7(\pm3)\times10^{24}$	3×10^{22}	4.0×10^{17}	2.4×10^{12}
3. Rishikesh	100±30	230	$1(^{+2}_{-0.5})\times10^{24}$	3×10^{22}	4.0×10^{17}	4.0×10^{12}
4. Simla	70±20	240	$3(^{+4}_{-2})\times10^{24}$	3×10^{22}	3.5×10^{17}	3.4×10^{12}
5. Mandi-Leh	100±20	200	$0.5(^{+0.5}_{-0.3})\times10^{24}$	5×10^{22}	3.6×10^{17}	3.4×10^{12}

*Allowable values of D' probably lie within a factor 10 of those given here.
†Allowable values of Mo and Fo are probably within a factor of 2 of those given here.

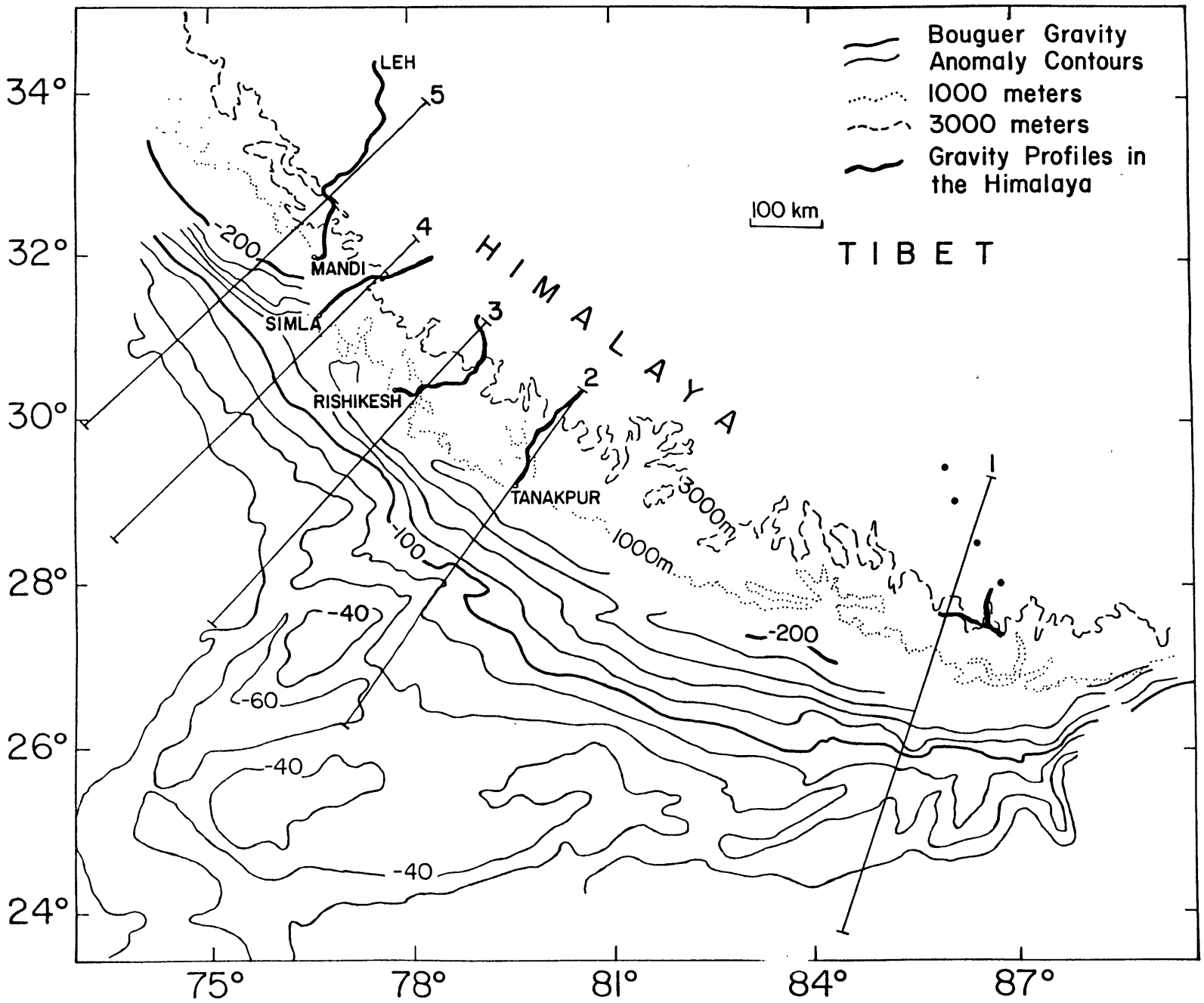
Bouguer Gravity Anomaly Contours
1000 meters
3000 meters
Gravity Profiles in the Himalaya
100 km
TIBET
HIMALAYA
LEH
MANDI
SIMLA
RISHIKESH
TANAKPUR
1
2
3
4
5
-200
-100
-60
-40
-40
-40
-200
1000m
3000m
34°
32°
30°
28°
26°
24°
75°
78°
81°
84°
87°

Figure 1

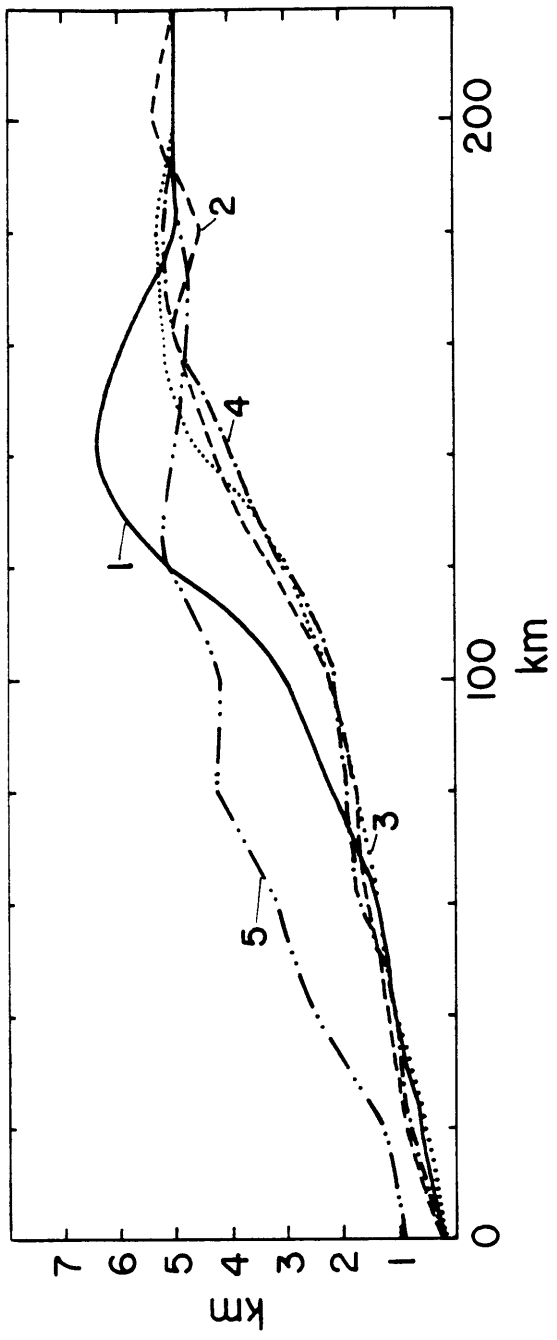

Figure 2a

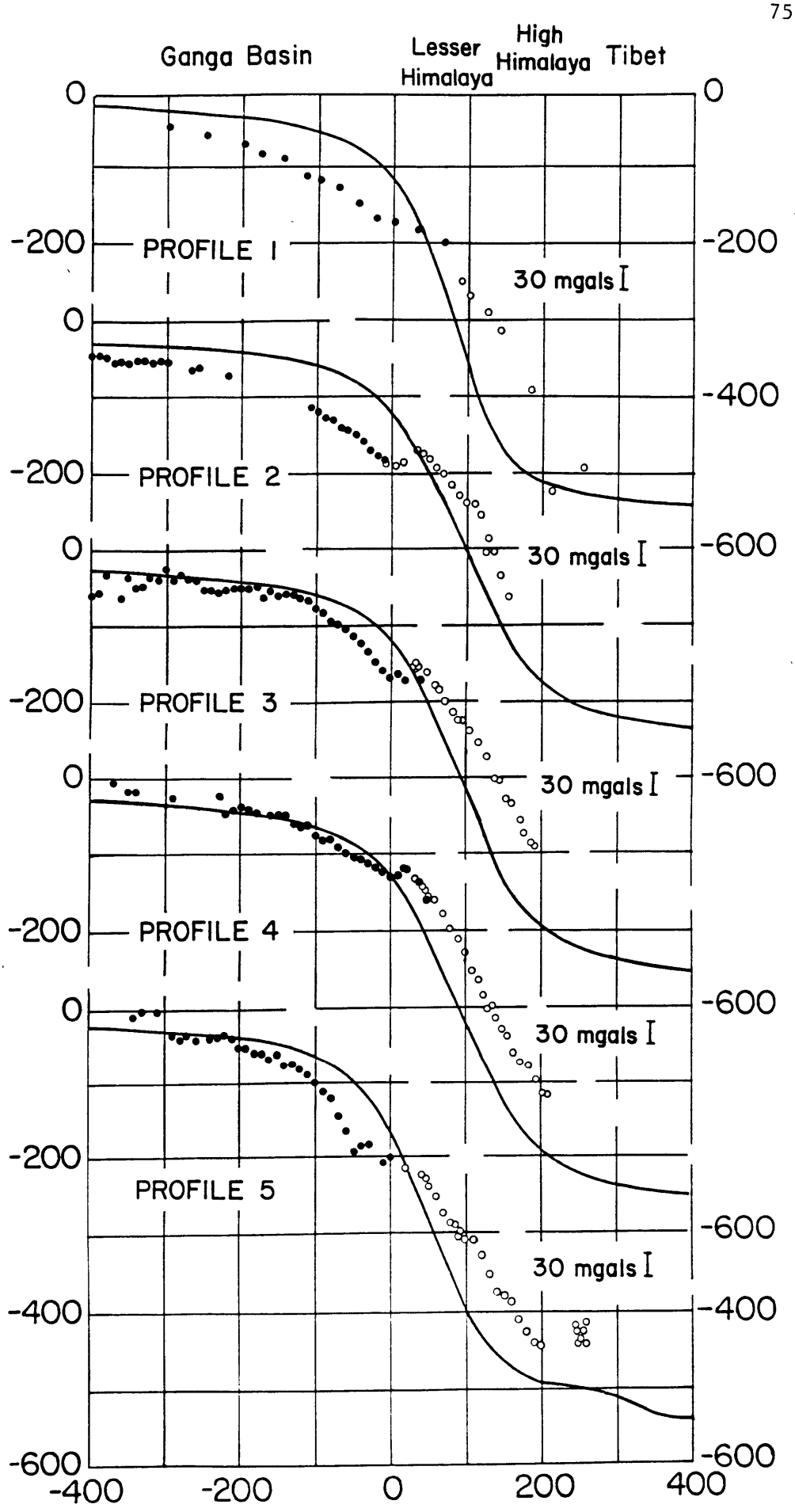
Ganga Basin
Lesser Himalaya
High Himalaya
Tibet
PROFILE 1
PROFILE 2
PROFILE 3
PROFILE 4
PROFILE 5
30 mgals
0
-200
-400
-600
-400
-200
0
200
400

Figure 2b

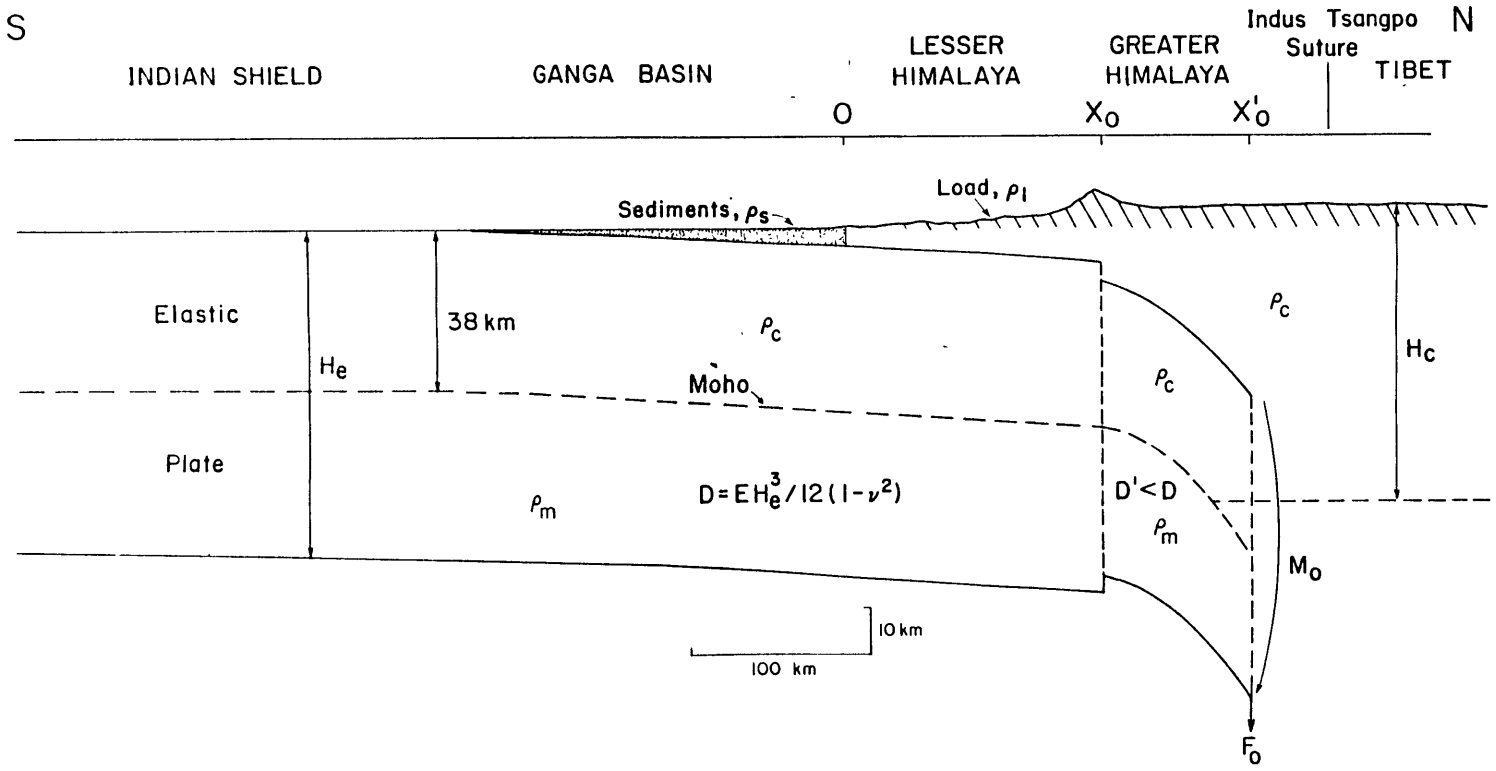
S
INDIAN SHIELD
GANGA BASIN
LESSER HIMALAYA
GREATER HIMALAYA
Indus Tsangpo Suture
N
TIBET
O
X_o
X'_o
Load, ρ_l
Sediments, ρ_s
Elastic
Plate
H_e
38 km
ρ_c
Moho
ρ_m
$D = EH_e^3/12(1-\nu^2)$
$D' < D$
H_c
M_o
F_o
10 km
100 km

Figure 3

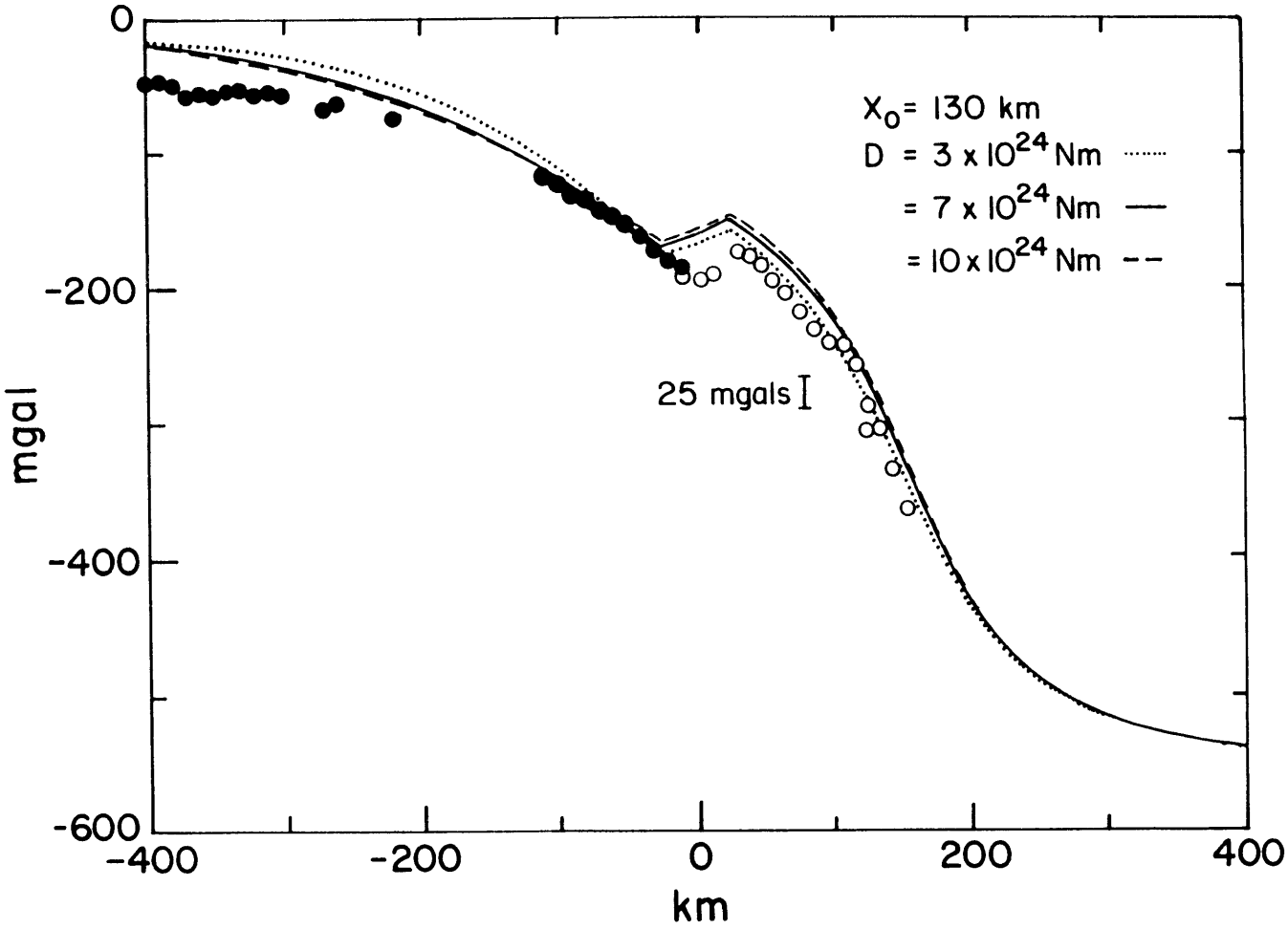
0
-200
-400
-600
mgal
-400
-200
0
200
400
km
X_0= 130 km
D = 3 x 10^{24} Nm
= 7 x 10^{24} Nm
= 10 x 10^{24} Nm
25 mgals

Figure 4a

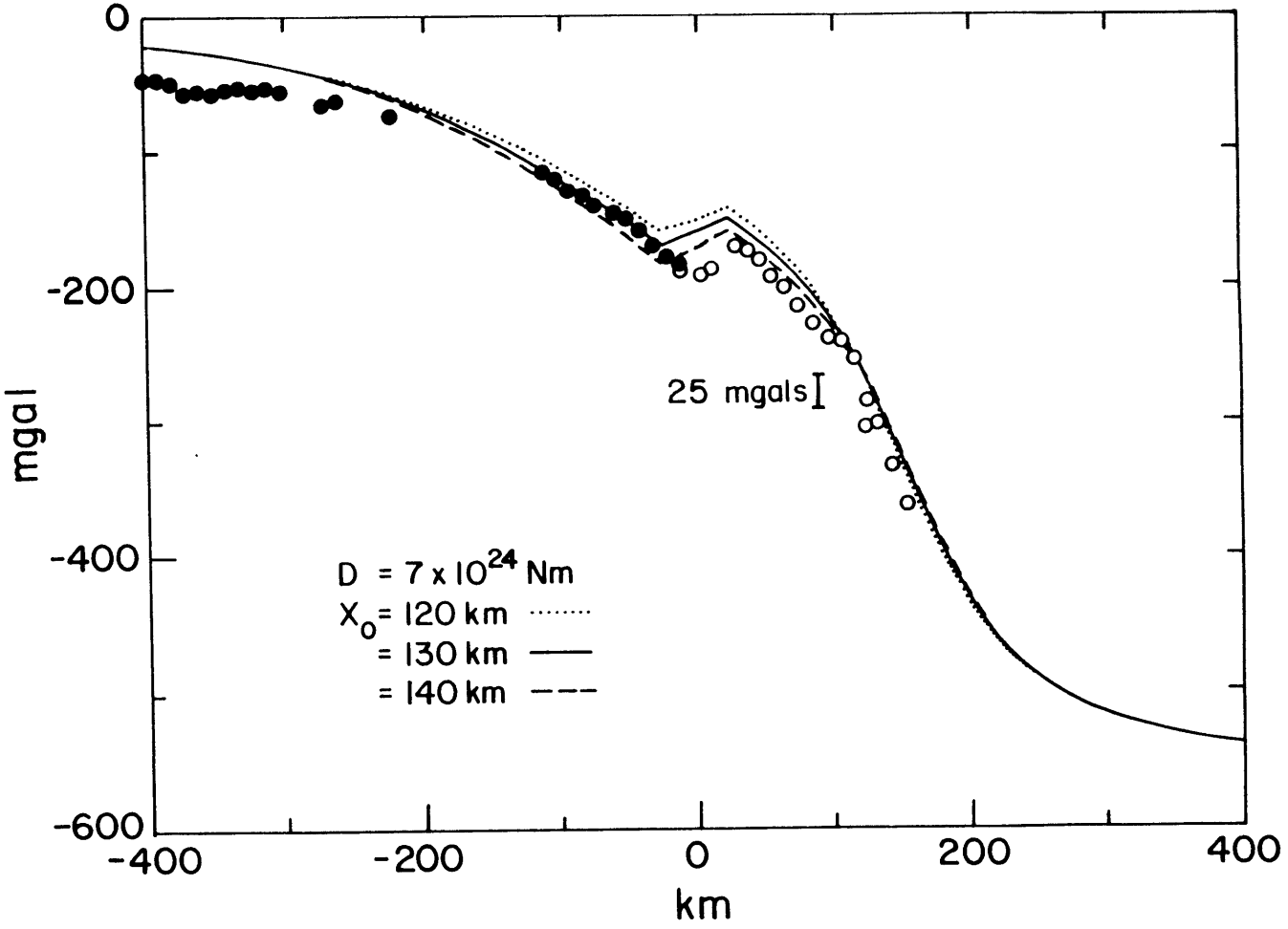
0
-200
-400
-600
mgal
-400
-200
0
200
400
km
25 mgals
D = 7 x 10^24 Nm
X0 = 120 km
= 130 km
= 140 km

Figure 4b

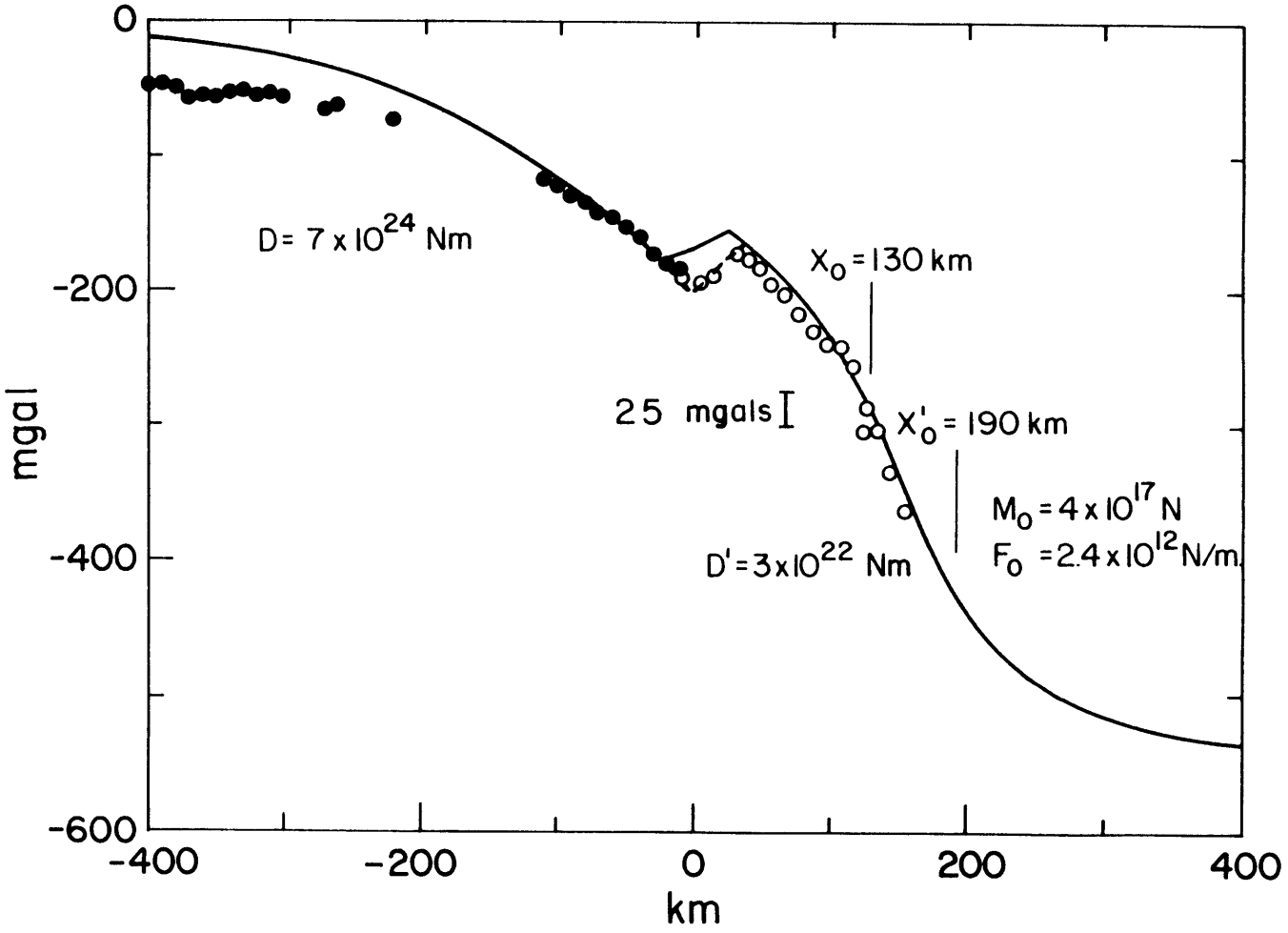
0
-200
-400
-600
mgal
-400
-200
0
200
400
km
D= 7 x 10^24 Nm
X0 = 130 km
25 mgals
X'0 = 190 km
M0 = 4 x 10^17 N
F0 = 2.4 x 10^12 N/m
D' = 3 x 10^22 Nm

Figure 4c

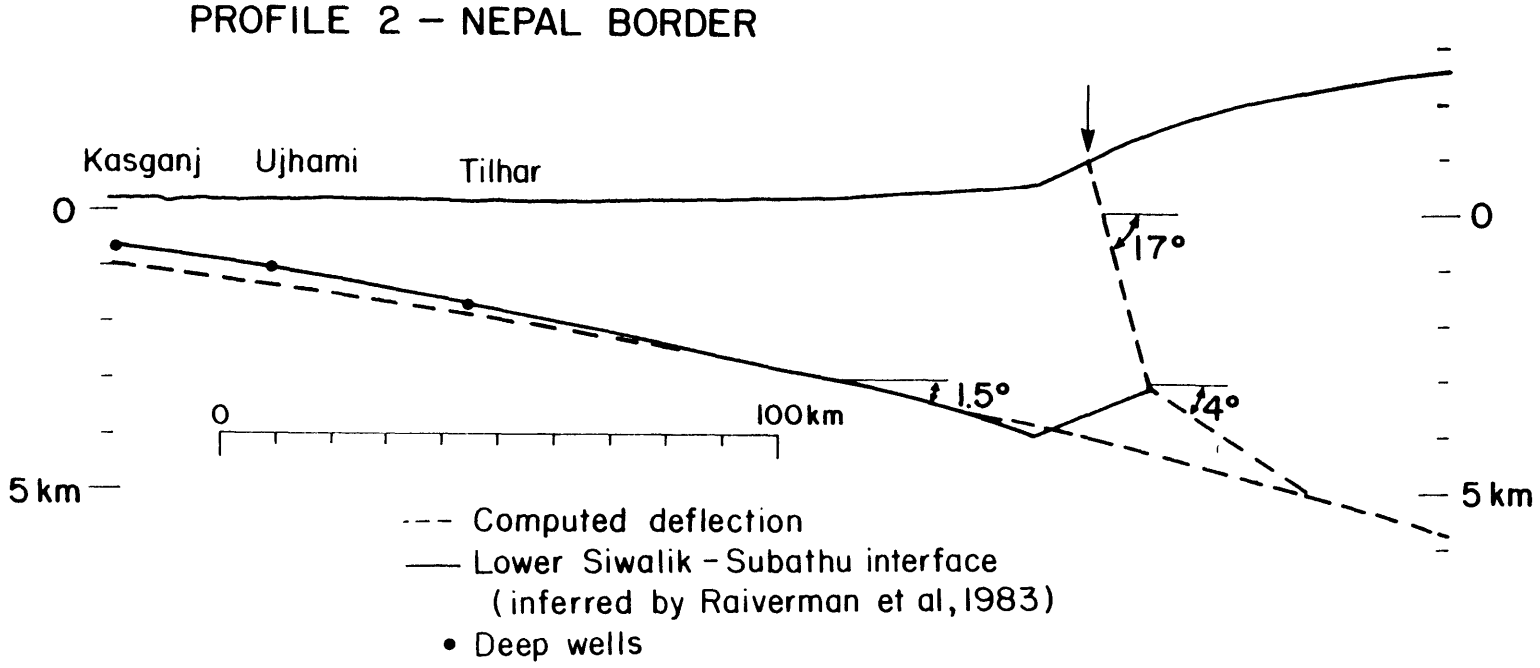
PROFILE 2 – NEPAL BORDER
Kasganj
Ujhami
Tilhar
0
0
17°
1.5°
4°
0
100km
5 km
5 km
--- Computed deflection
—— Lower Siwalik - Subathu interface
(inferred by Raiverman et al, 1983)
• Deep wells

Figure 4d

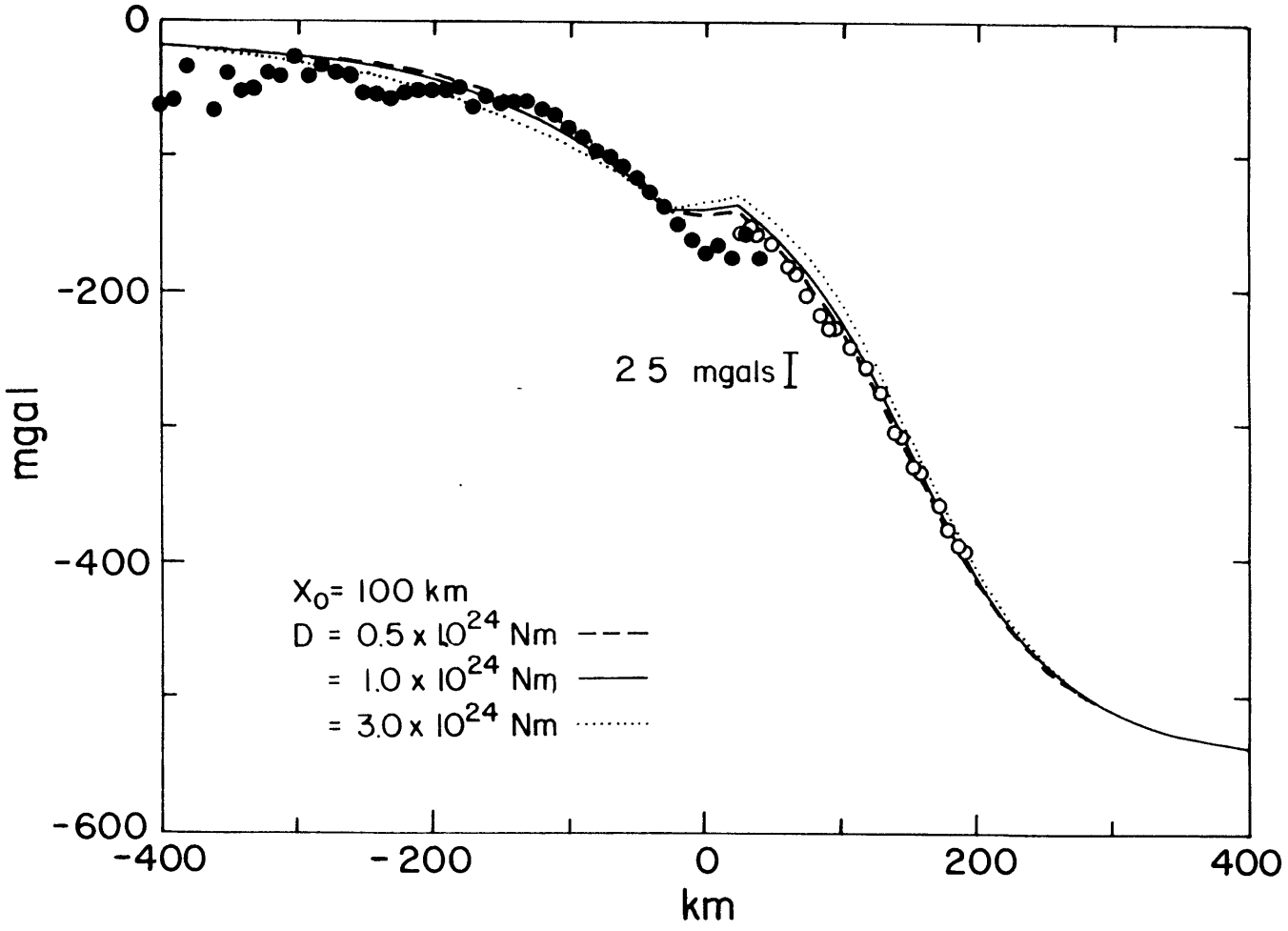
0
-200
-400
-600
mgal
25 mgals
X_0= 100 km
D = 0.5 x 10^{24} Nm
= 1.0 x 10^{24} Nm
= 3.0 x 10^{24} Nm
-400
-200
0
200
400
km

Figure 5a

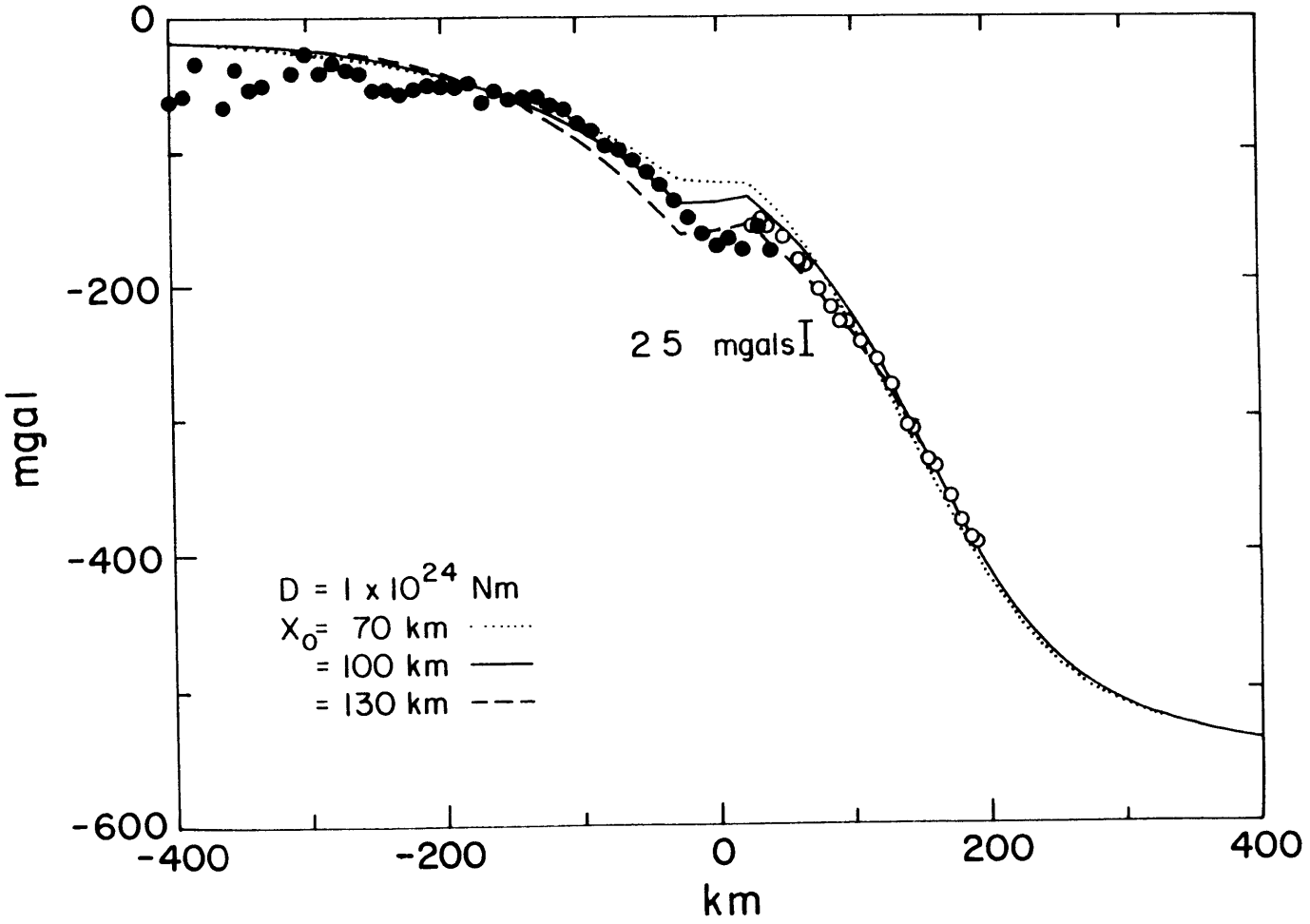
0
-200
-400
-600
mgal
25 mgals
D = 1 x 10^24 Nm
X0= 70 km
= 100 km
= 130 km
-400
-200
0
200
400
km

Figure 5b

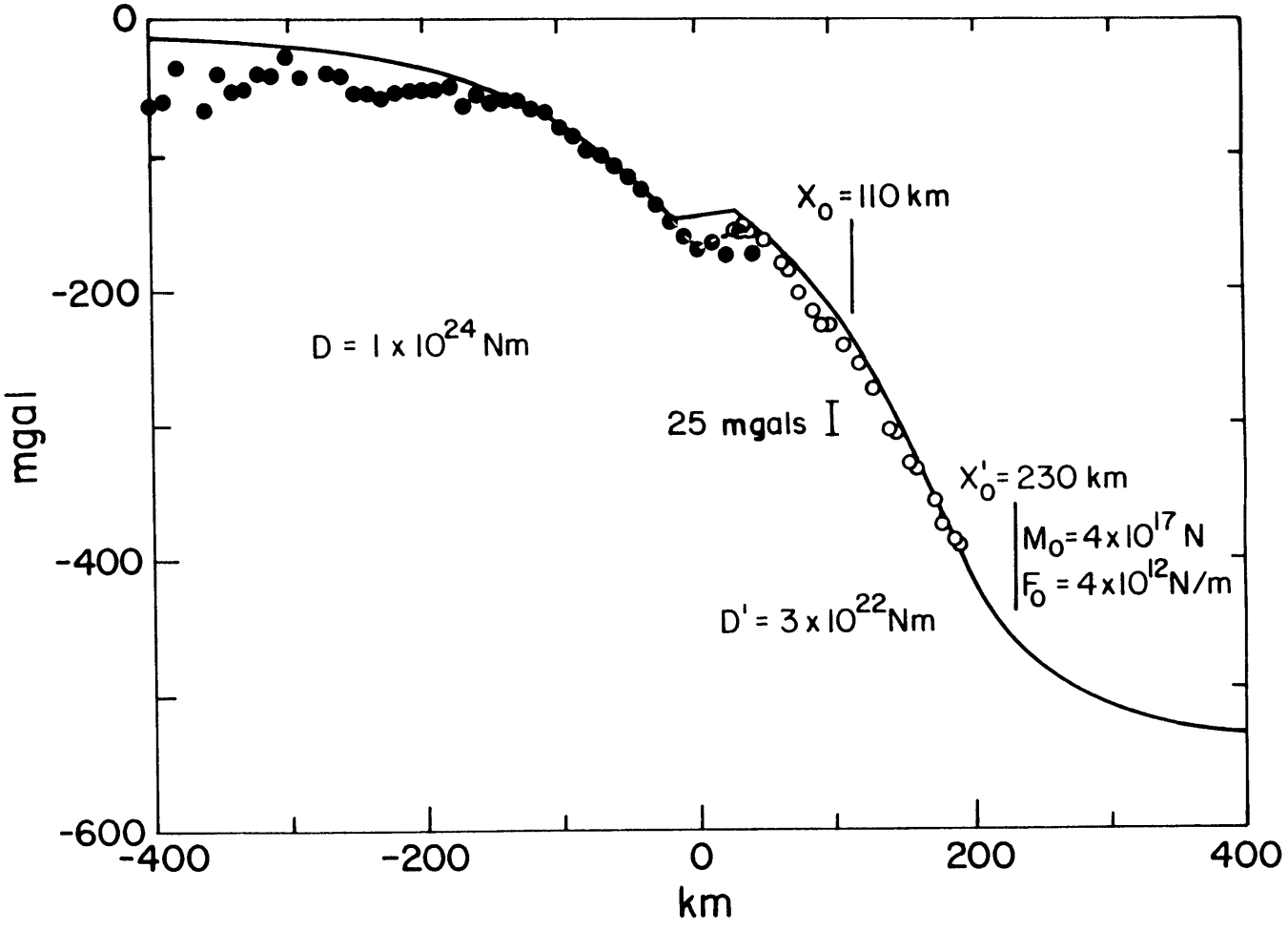
0
-200
-400
-600
mgal
-400
-200
0
200
400
km
X_0 = 110 km
D = 1 x 10^{24} Nm
25 mgals
X'_0 = 230 km
M_0 = 4 x 10^{17} N
F_0 = 4 x 10^{12} N/m
D' = 3 x 10^{22} Nm

Figure 5c

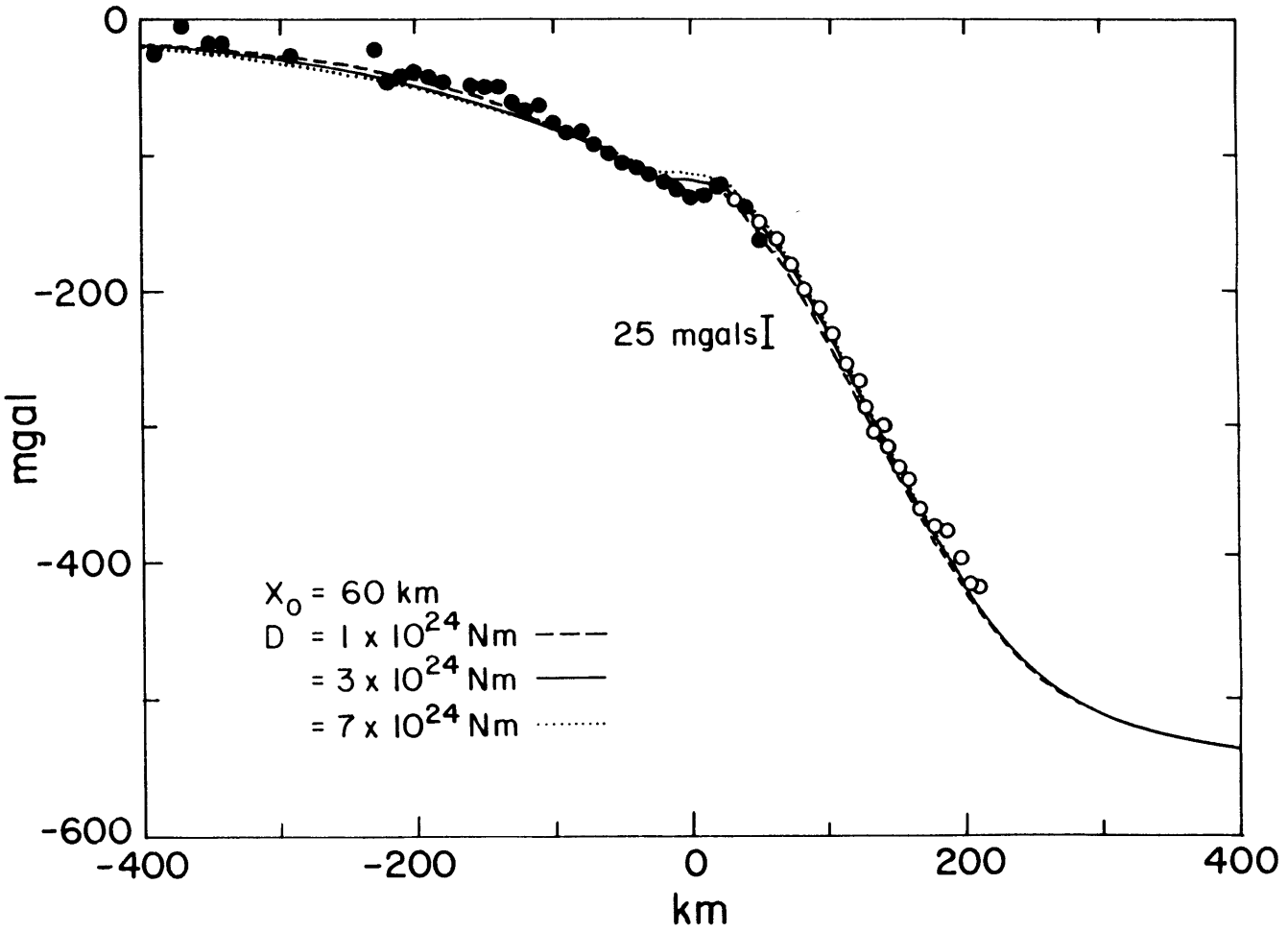
0
-200
-400
-600
mgal
25 mgals
X_o = 60 km
D = 1 x 10^{24} Nm
= 3 x 10^{24} Nm
= 7 x 10^{24} Nm
-400
-200
0
200
400
km

Figure 6a

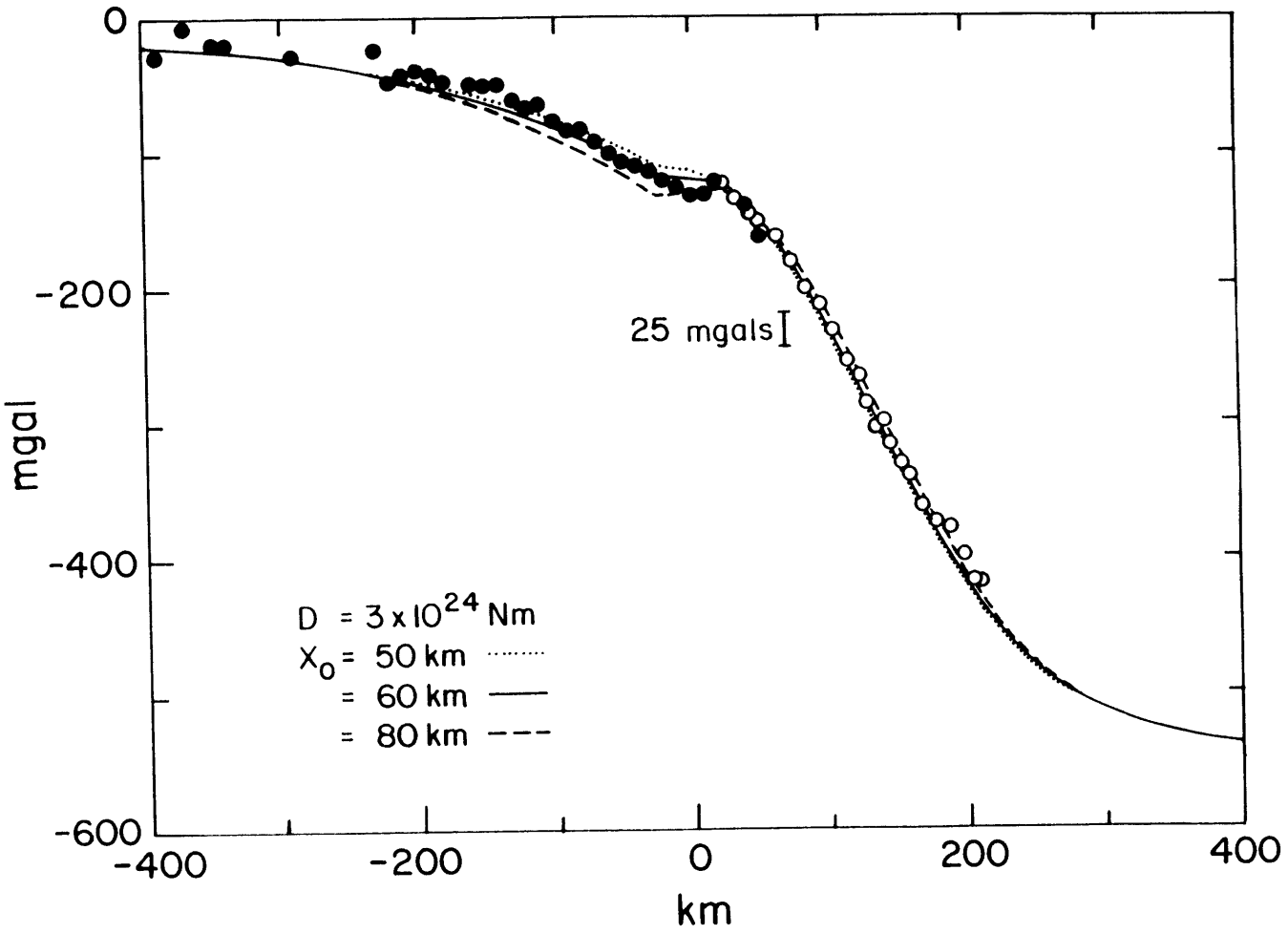
0
-200
-400
-600
mgal
25 mgals
D = 3 x 10^24 Nm
X0 = 50 km
= 60 km
= 80 km
-400
-200
0
200
400
km

Figure 6b

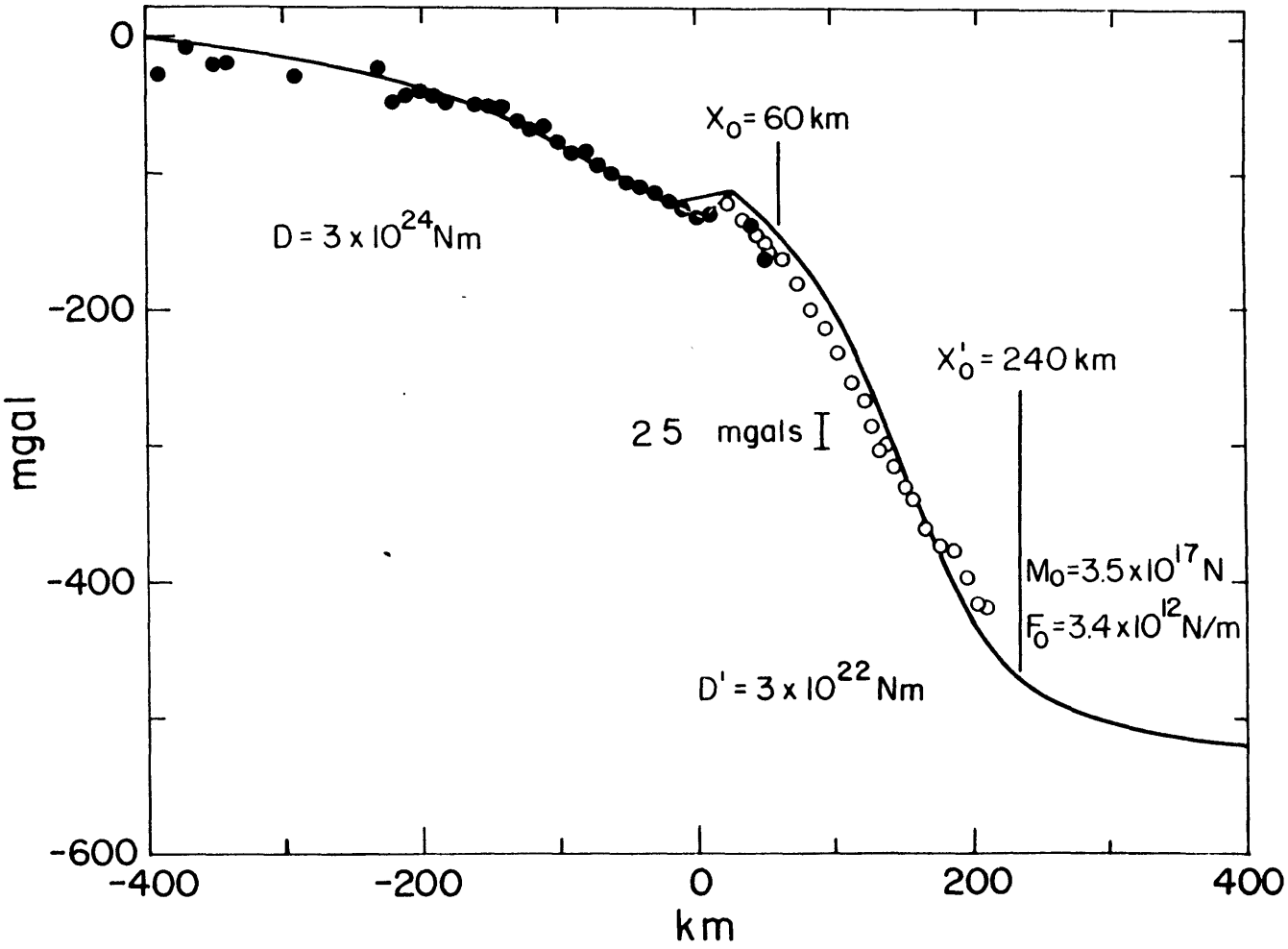
0
-200
-400
-600
mgal
-400
-200
0
200
400
km
X_0= 60 km
D = 3 x 10^{24} Nm
X'_0 = 240 km
25 mgals
M_0=3.5x10^{17} N
F_0=3.4x10^{12} N/m
D' = 3 x 10^{22} Nm

Figure 6c

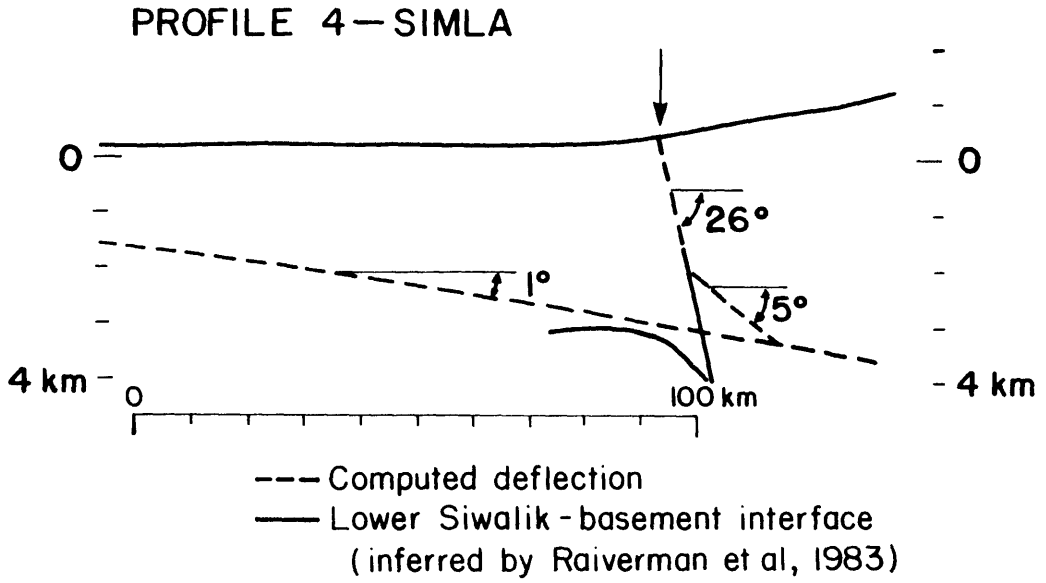
PROFILE 4—SIMLA
0
0
26°
1°
5°
4 km
0
100 km
4 km
---Computed deflection
——Lower Siwalik-basement interface
(inferred by Raiverman et al, 1983)

Figure 6d

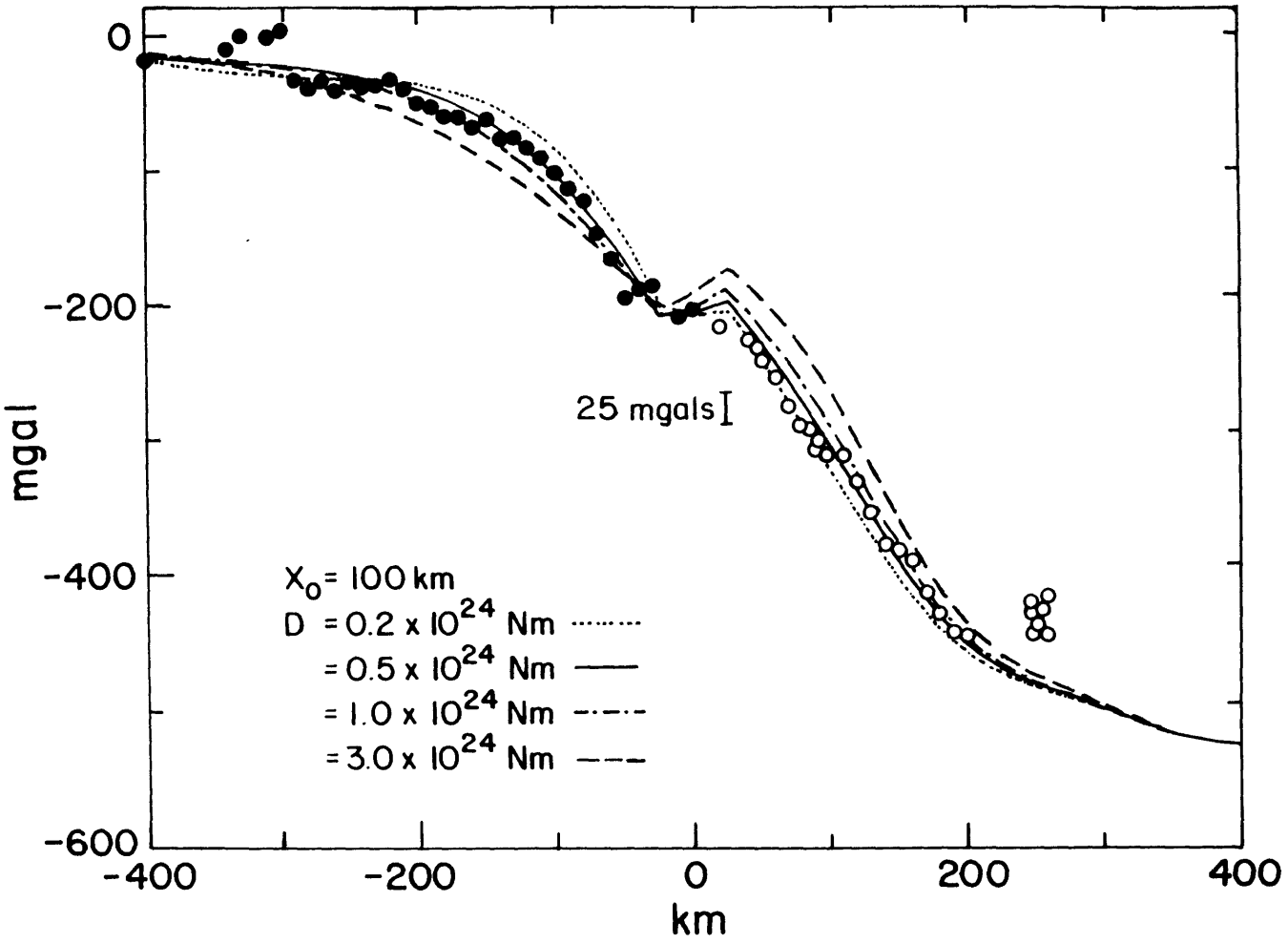
0
-200
-400
-600
mgal
25 mgals
X_o = 100 km
D = 0.2 x 10^{24} Nm
= 0.5 x 10^{24} Nm
= 1.0 x 10^{24} Nm
= 3.0 x 10^{24} Nm
-400
-200
0
200
400
km

Figure 7a

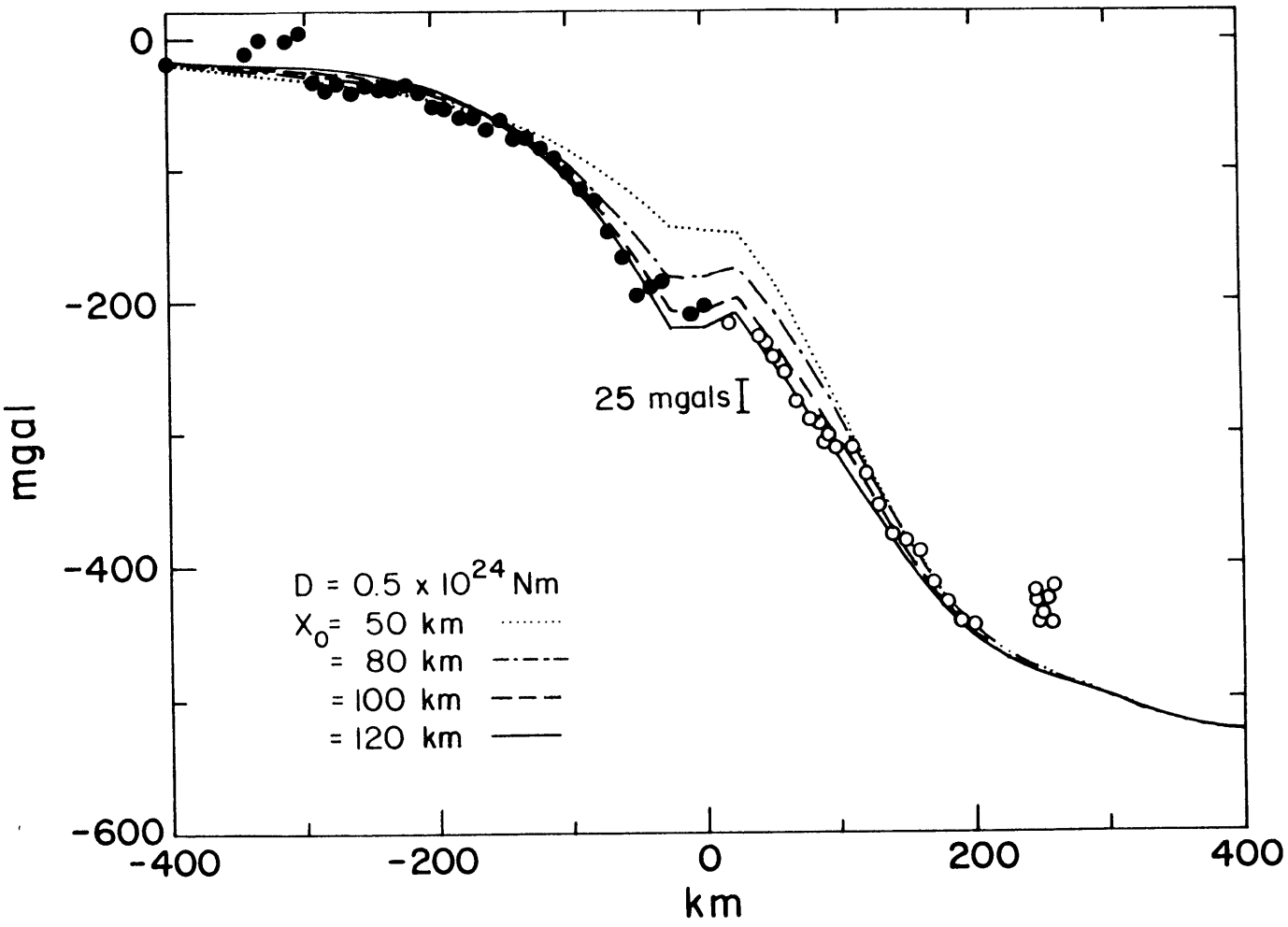
0
-200
-400
-600
mgal
25 mgals
D = 0.5 x 10^24 Nm
X0= 50 km
= 80 km
= 100 km
= 120 km
-400
-200
0
200
400
km

Figure 7b

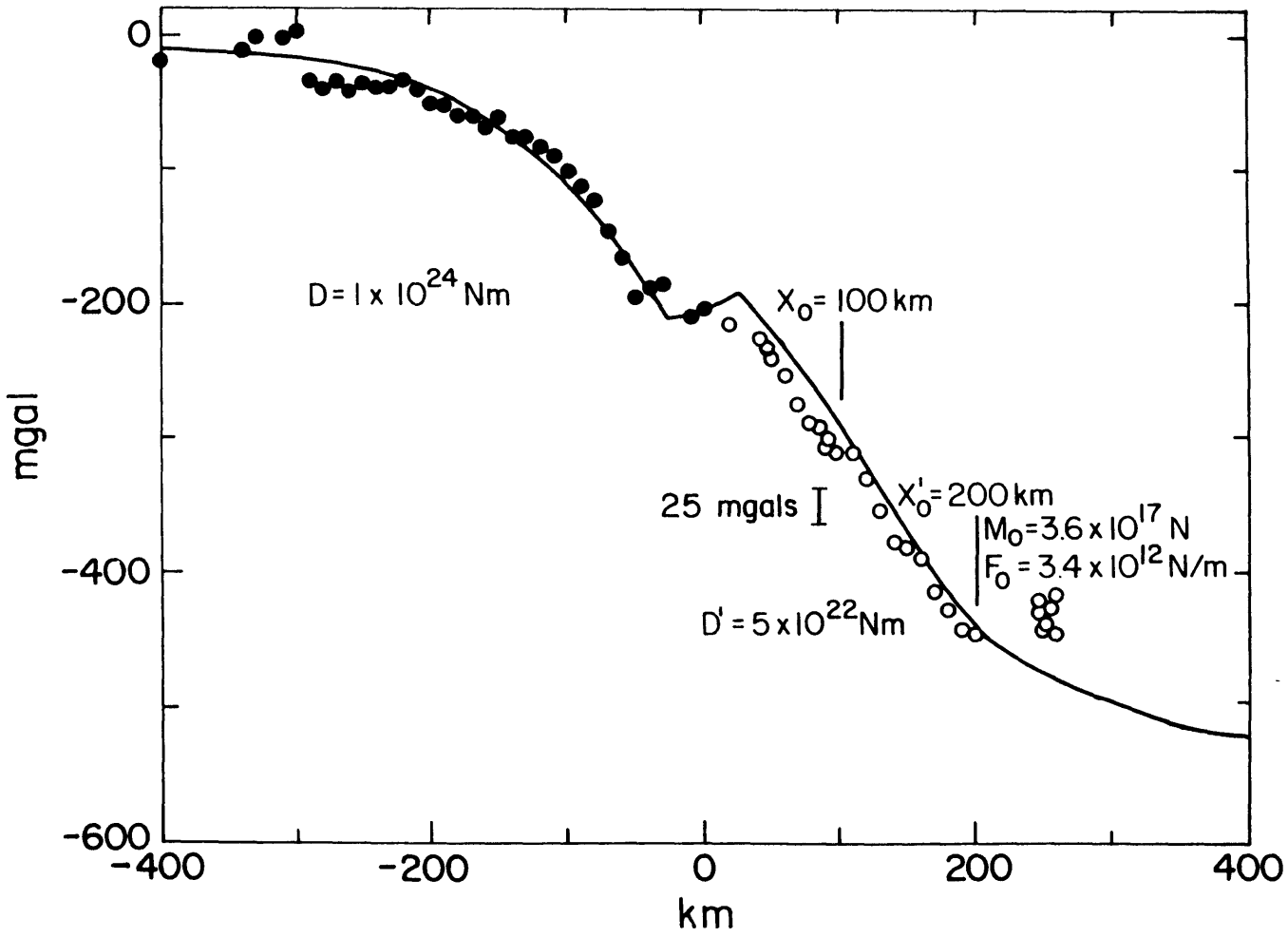
0
-200
-400
-600
mgal
-400
-200
0
200
400
km
D= 1 x 10^24 Nm
X0= 100 km
25 mgals
X'0= 200 km
M0=3.6 x 10^17 N
F0 = 3.4 x 10^12 N/m
D' = 5 x 10^22 Nm

Figure 7c

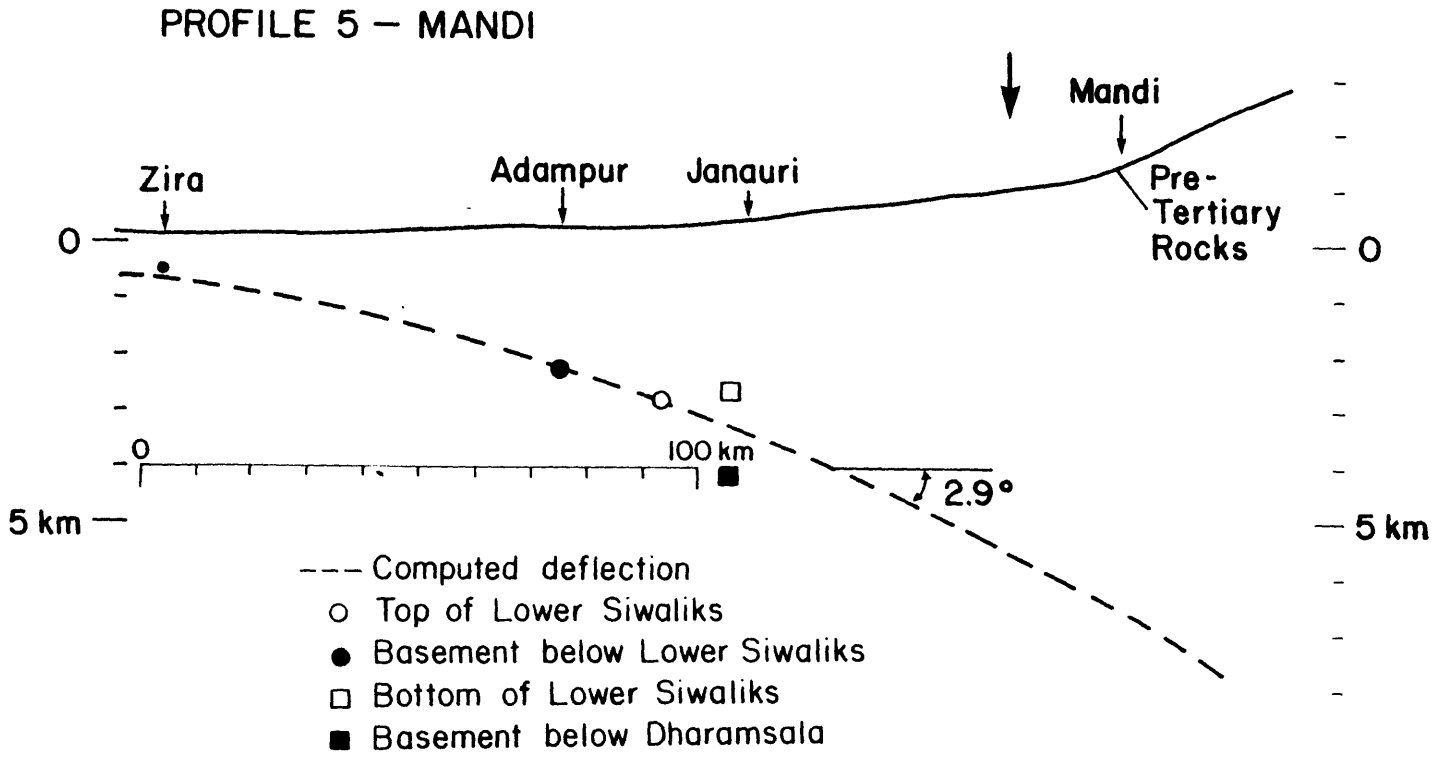
PROFILE 5 – MANDI
Mandi
Zira
Adampur
Janauri
Pre-
Tertiary
Rocks
0
0
100 km
2.9°
5 km
5 km
Computed deflection
Top of Lower Siwaliks
Basement below Lower Siwaliks
Bottom of Lower Siwaliks
Basement below Dharamsala

Figure 7d

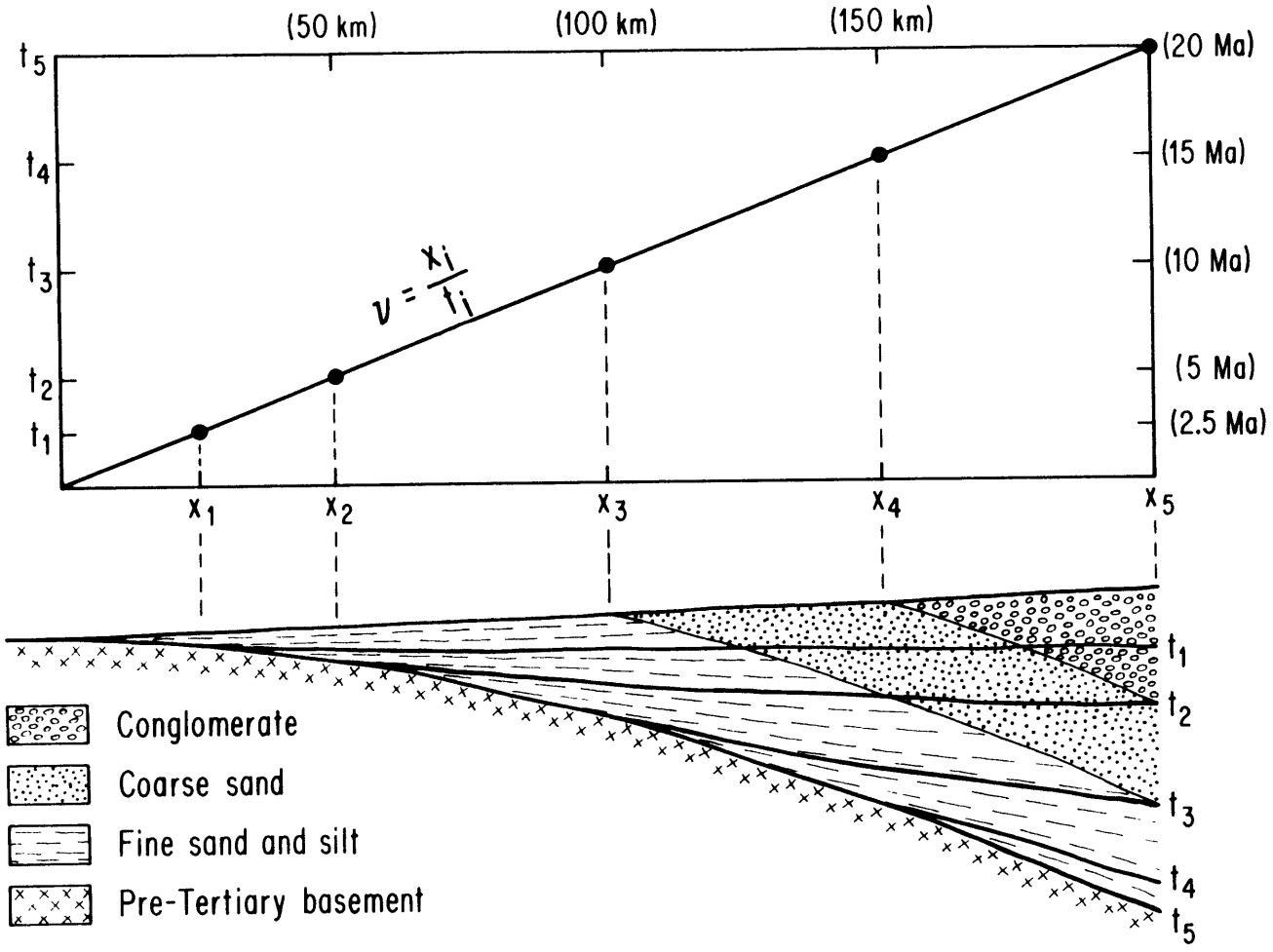
(50 km)
(100 km)
(150 km)
t5
t4
t3
t2
t1
(20 Ma)
(15 Ma)
(10 Ma)
(5 Ma)
(2.5 Ma)
v = xi / ti
x1
x2
x3
x4
x5
t1
t2
t3
t4
t5
Conglomerate
Coarse sand
Fine sand and silt
Pre-Tertiary basement

Figure 8

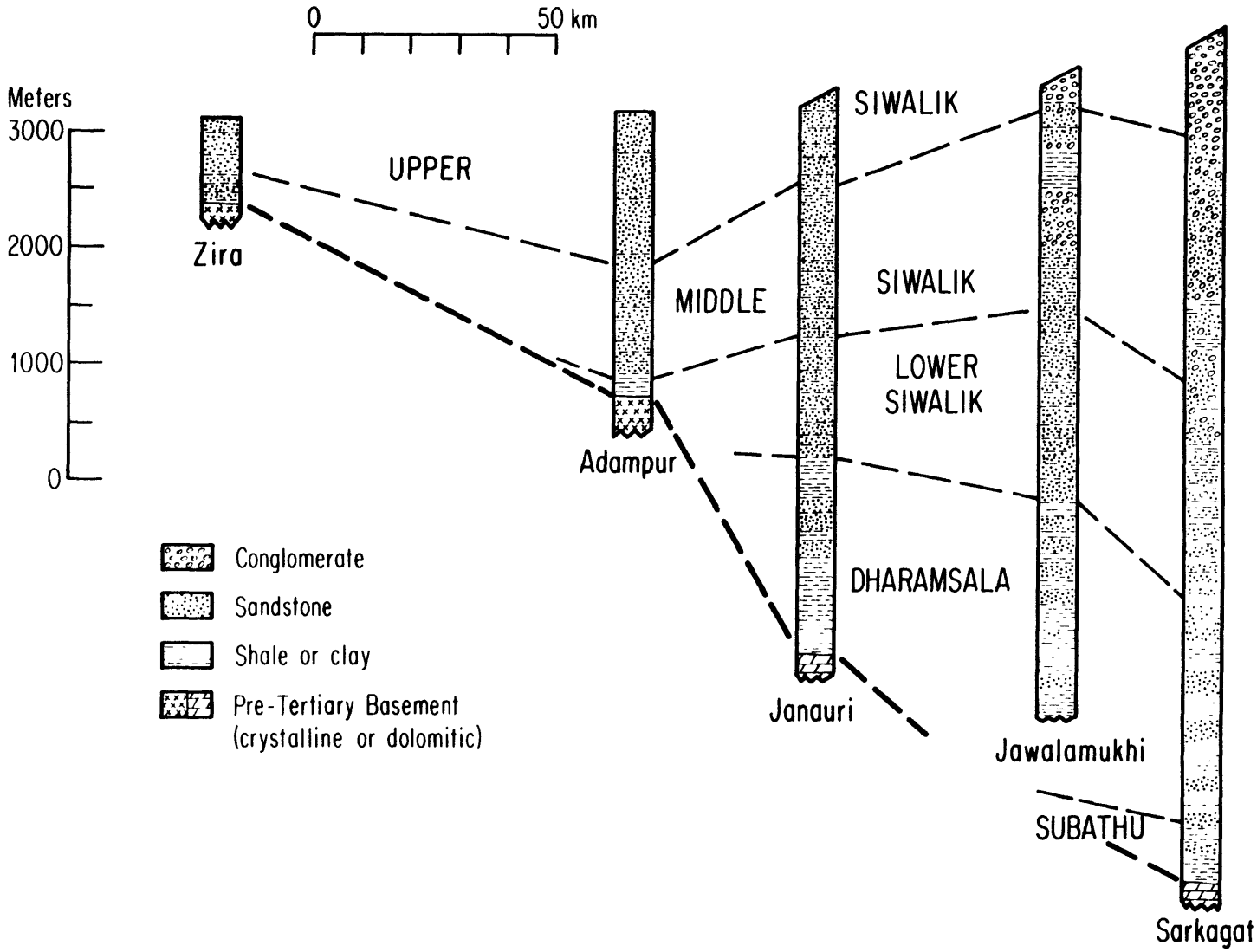
0
50 km
Meters
3000
2000
1000
0
Zira
UPPER
SIWALIK
MIDDLE
SIWALIK
LOWER
SIWALIK
Adampur
DHARAMSALA
Janauri
Jawalamukhi
SUBATHU
Sarkagat
Conglomerate
Sandstone
Shale or clay
Pre-Tertiary Basement
(crystalline or dolomitic)

Figure 9

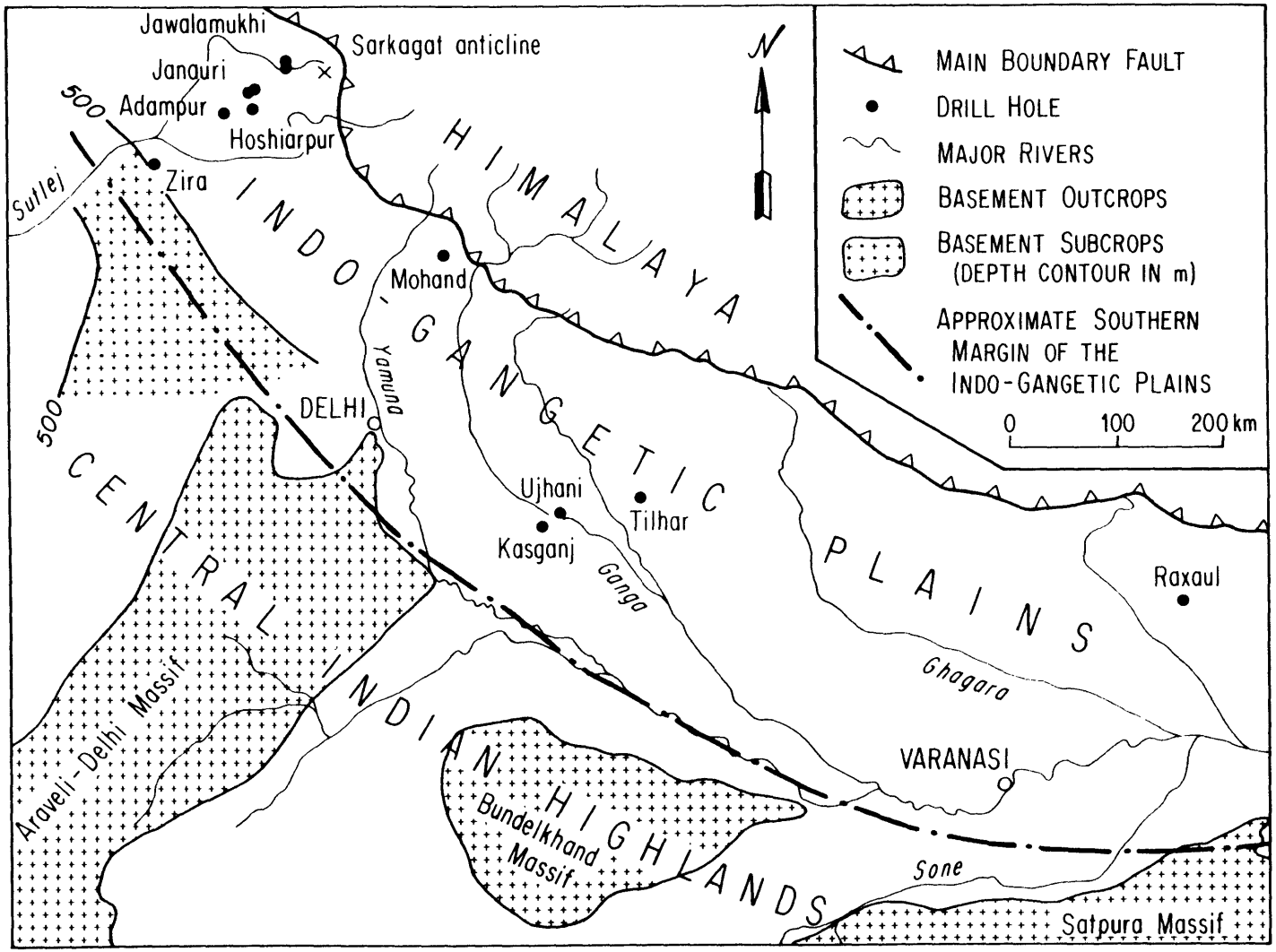
Jawalamukhi
Sarkagat anticline
Janauri
Adampur
Hoshiarpur
500
Zira
Sutlej
HIMALAYA
INDO-GANGETIC PLAINS
Mohand
Yamuna
DELHI
500
CENTRAL INDIAN HIGHLANDS
Ujhani
Tilhar
Kasganj
Ganga
Raxaul
Ghagara
VARANASI
Aravali-Delhi Massif
Bundelkhand Massif
Sone
Satpura Massif
N
MAIN BOUNDARY FAULT
DRILL HOLE
MAJOR RIVERS
BASEMENT OUTCROPS
BASEMENT SUBCROPS (DEPTH CONTOUR IN m)
APPROXIMATE SOUTHERN MARGIN OF THE INDO-GANGETIC PLAINS
0
100
200 km

Figure 10

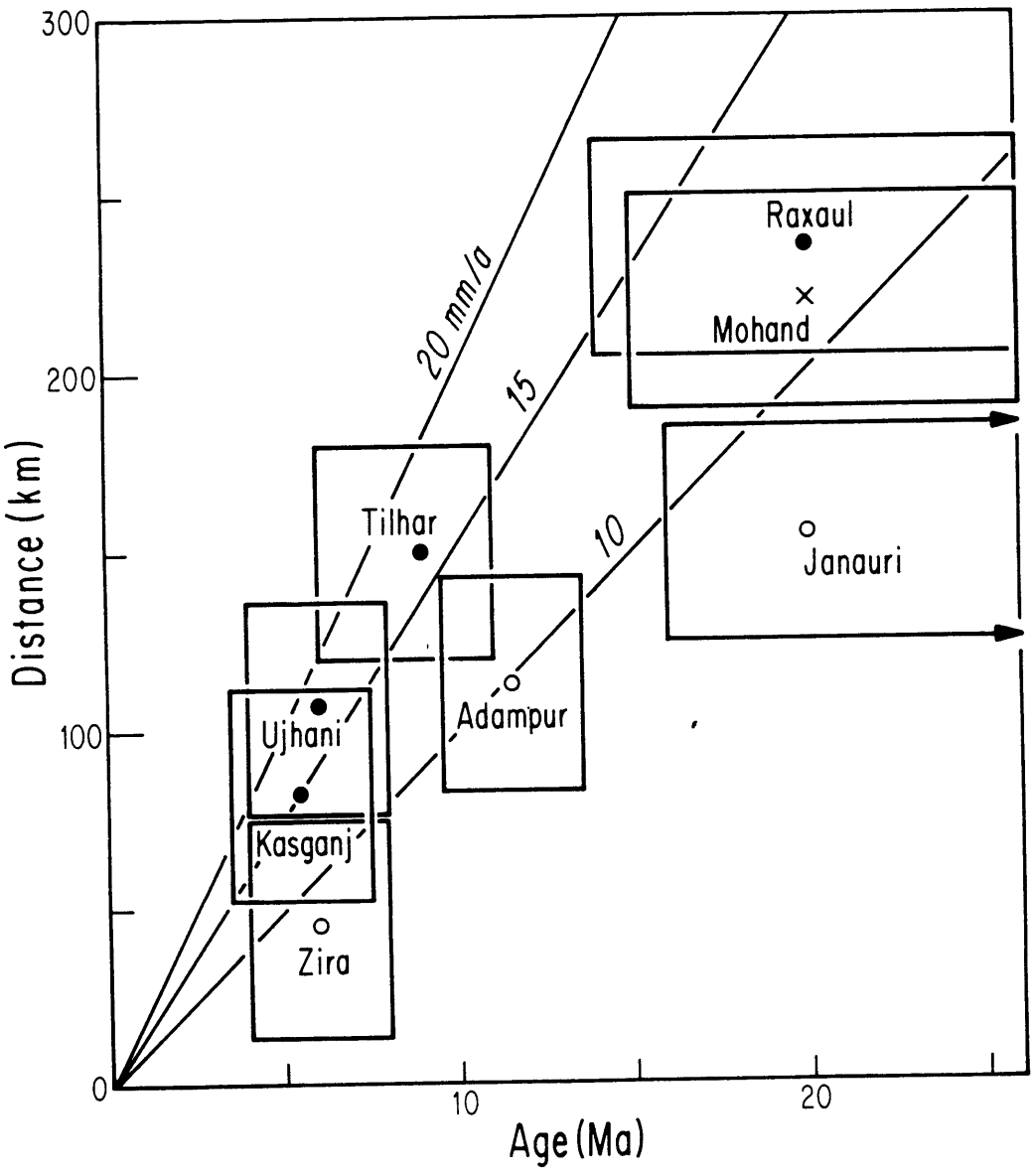
300
200
100
0
Distance (km)
10
20
Age (Ma)
20 mm/a
15
10
Raxaul
Mohand
Tilhar
Janauri
Adampur
Ujhani
Kasganj
Zira

Figure 11

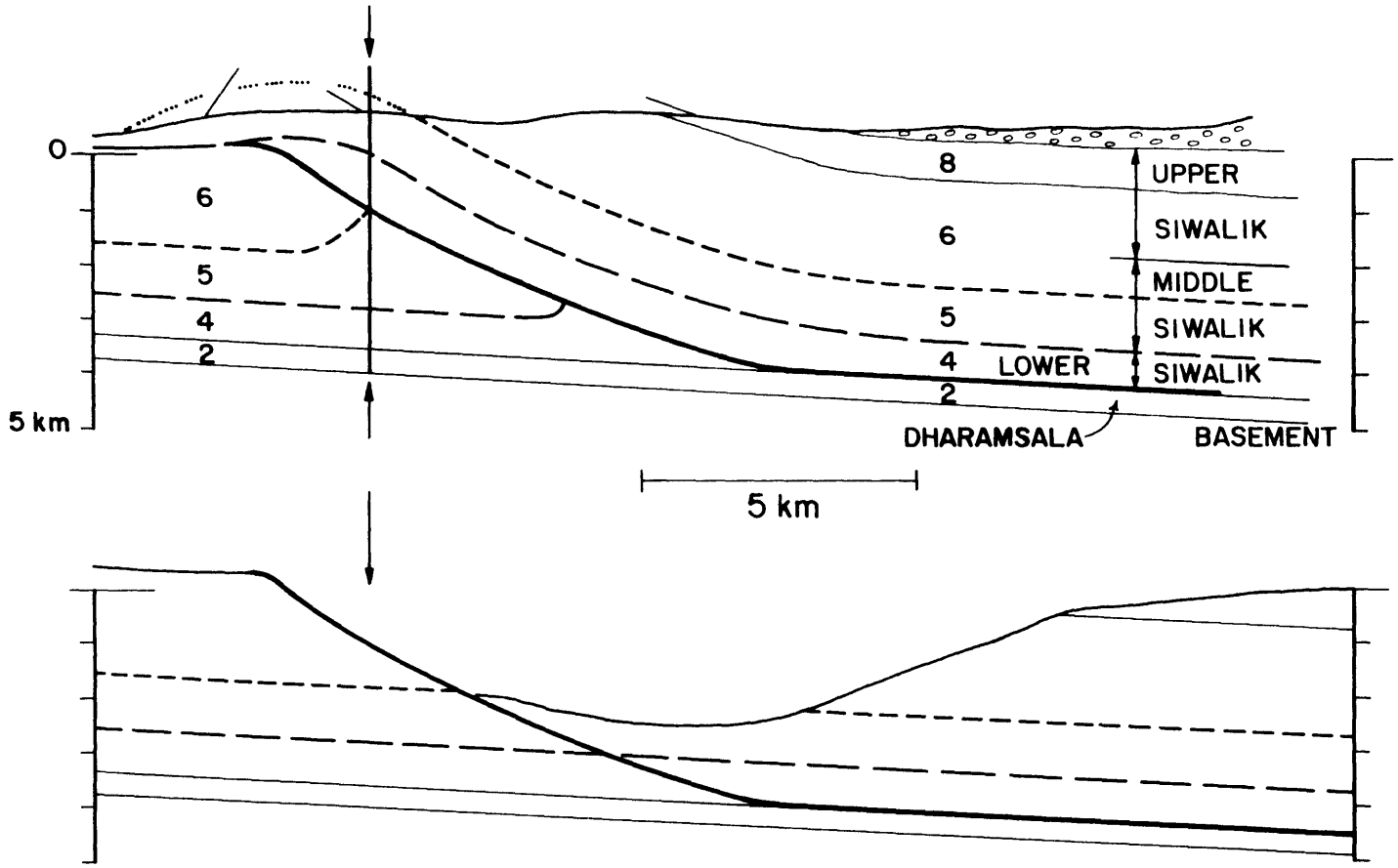
0
5 km
6
5
4
2
8
6
5
4
2
UPPER
SIWALIK
MIDDLE
SIWALIK
LOWER
SIWALIK
DHARAMSALA
BASEMENT
5 km

Figure A1

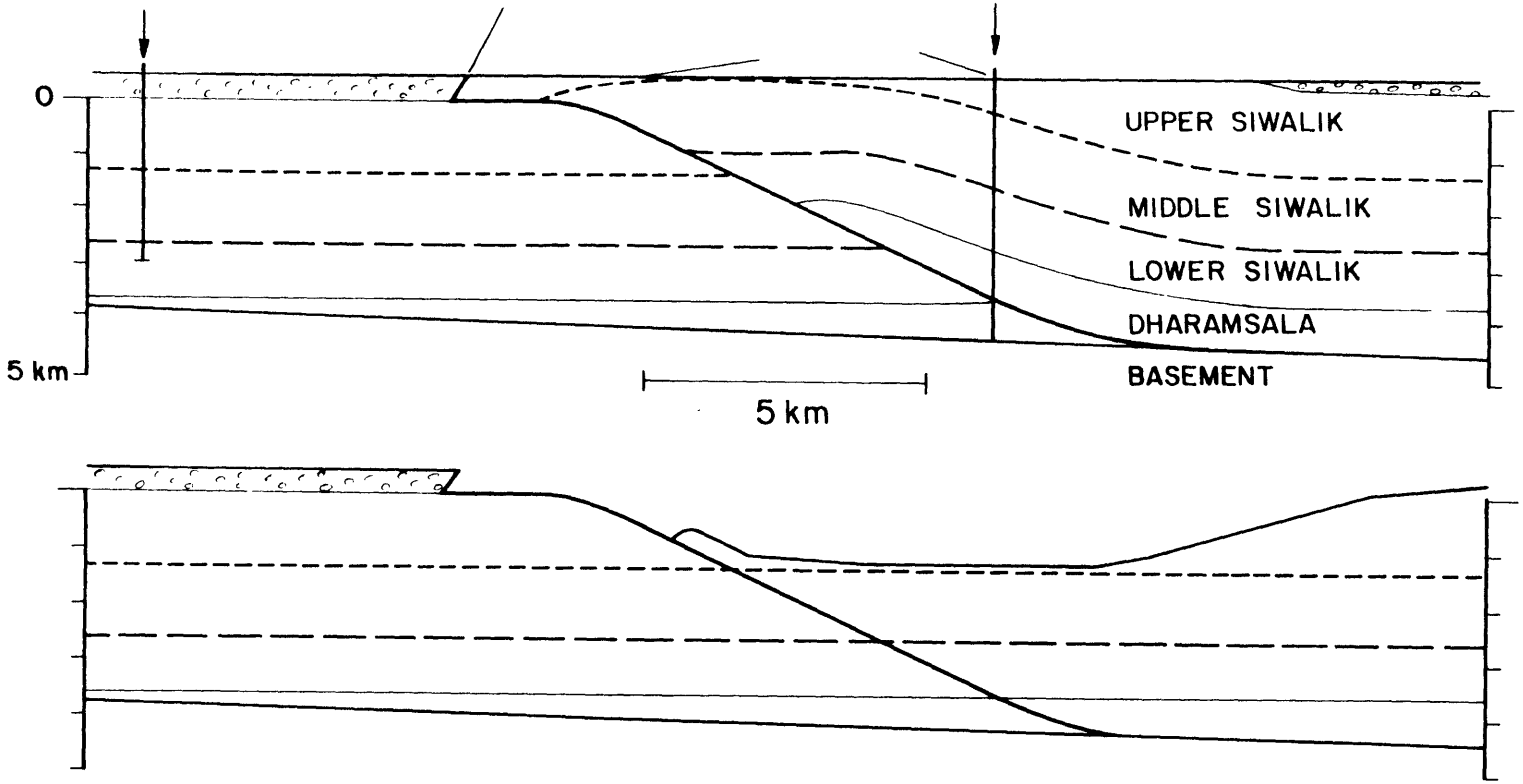
0
5 km
UPPER SIWALIK
MIDDLE SIWALIK
LOWER SIWALIK
DHARAMSALA
BASEMENT
5 km

Figure A2

CHAPTER III

GRAVITY ANOMALIES AND THE STRUCTURE OF WESTERN TIBET AND THE SOUTHERN TARIM BASIN

GEOPHYSICAL RESEARCH LETTERS, VOL. 11, NO. 12, PAGES 1251-1254, DECEMBER 1984

GRAVITY ANOMALIES AND THE STRUCTURE OF WESTERN TIBET AND THE SOUTHERN TARIM BASIN

Hélène Lyon-Caen and Peter Molnar

Department of Earth, Atmospheric, and Planetary Sciences, Massachusetts Institute of Technology, Cambridge, Massachusetts 02139

Abstract. Gravity anomalies across the western part of the Tarim Basin and the Kunlun mountain belt show that this area is not in local isostatic equilibrium. These data can be explained if a strong plate underlying the Tarim Basin extends southwestward beneath the belt at least 80 km and supports part of the topography of northwest Tibet. This corroborates Norin's inference that late Tertiary crustal shortening has occurred in this area by southward underthrusting of the Tarim Basin beneath the Kunlun. This study places a lower bound on the amount of underthrusting.

Introduction

The northern edge of the Tibetan plateau is bordered by the Kunlun mountain belt and is separated from the Precambrian shield of the Tarim Basin by the Altyn-Tagh fault (Figure 1). The Kunlun was the locus of late Paleozoic orogenic activity and has been reactivated since the collision of India with Eurasia whereas the Tarim Basin has remained almost undeformed. The transition from plateau to basin is best studied in western Tibet, where the mean elevation ranges from about 1300 m at the edge of the Tarim Basin to over 5000 m, 130 km south of the edge of the basin. At the edge of the basin, Tertiary sedimentary rocks dip to the south with dips ranging from 15° to 50° and are overthrust by Paleozoic rocks [Norin, 1946]. Young folds in the sedimentary cover of the Tarim Basin recognized by Norin [1946] near the front of the range can be seen on Landsat imagery (Figures 1 and 2). These observations suggest that the lithosphere below the Tarim Basin is strong [Molnar and Tapponnier, 1981] and that crustal shortening has occurred in western Tibet by underthrusting of part of the Tarim Basin to the south. Since the movement on the Altyn-Tagh fault is now left lateral strike-slip [Molnar and Tapponnier, 1975; Tapponnier and Molnar, 1977], part of the crustal shortening that occurred in the north-eastern part of Tibet is probably due to the same mechanism.

Data and Analysis

Our analysis is based on Amboldt's [1948] pendulum gravity measurements obtained by the Sino-Swedish Expedition (1929-1933) across the Tarim Basin and western Tibet (Figure 1), and we used the Bouguer anomalies published by Marussi [1964], who computed the Bouguer and terrain corrections for these measurements. The standard Bouguer correction, with a density of $2.67 g/cm^3$ was made, but we corrected the values of the Bouguer anomalies over the Tarim Basin, to account for the lower density of the sediments there. The value of $2.5 g/cm^3$, given by Amboldt [1948], was used; this decreases the computed Bouguer anomalies given by Marussi by about 10 mgals over the Tarim Basin. Terrain corrections are small (less than 8 mgals) but probably could be in error by as much as 10 mgals due to inaccurate locations and topography. The main source of error in these data is certainly the inaccurate knowledge of the elevation. We assume the uncertainties to be of the order of 20 mgals, corresponding to uncertainties in elevation of 100 m.

Figure 3 shows a comparison of the Bouguer gravity data with two calculated profiles of Bouguer anomalies that both assume local isostatic compensation of the topography. For this calculation we obtained the mean topography from the Aeronautical Navigation Charts over the gravity profile by averaging the elevation perpendicular to it over a width of 100 km on each side. The calculations were made assuming either that compensation occurs locally by variations in crustal thickness from a reference level of 40 km or that the compensation occurs in the Tarim Basin by variation in the thickness

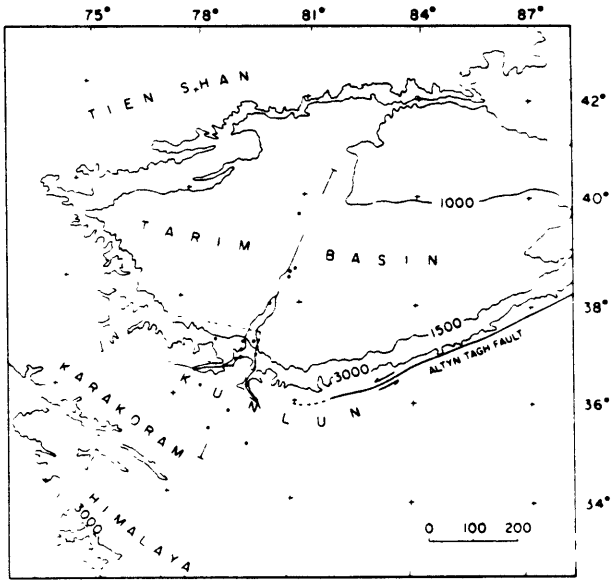

Fig. 1. Map of the Tarim Basin and western Tibet showing 1000, 1500 and 3000 m elevation contours and Amboldt's [1948] gravity stations (black dots). The location of the Landsat image shown in Figure 2 is enclosed by the dashed lines. The axis of projection of the gravity data is also indicated.

Paper number 4L6369.
0094-8276/84/004L-6369$03.00

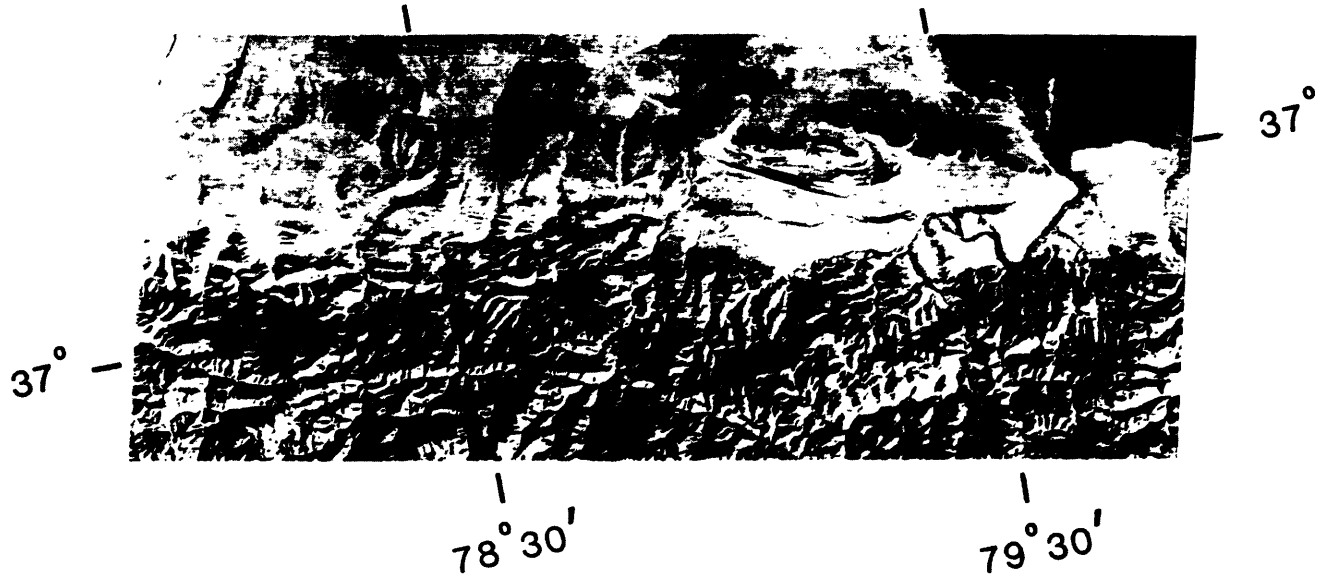

Fig. 2. Portion of Landsat image E-1457-04522 showing young folds on the southern edge of Tibet.

of sediments with the thickness of the underlying crust being constant and equal to 40 km. The difference between the two computed anomalies is negligible apart from an edge effect in the neighborhood of the southern border of the basin (x = 0). Comparison of the data with either of these curves shows that the Tarim Basin, from the front of the range to about 150 km north has a deficit of mass and that an excess of mass is present over a large part of the Kunlun mountains. Marussi [1964] found the same pattern of mass anomalies by computing standard isostatic anomalies.

Similar patterns of coupled mass deficiency and mass excess are present all along the Himalayan front, with the Ganga Basin having a deficit of mass and the Himalaya an excess of mass [Marussi, 1964]. They have been interpreted to be due to the flexure of the Indian plate under the load of the Himalayan topography [Karner and Watts, 1983; Lyon-Caen and Molnar, 1983]. Here we use the formulation described in Lyon-Caen and Molnar [1983] to analyze the gravity data: the Tarim Basin is treated as being underlain by an elastic plate that can

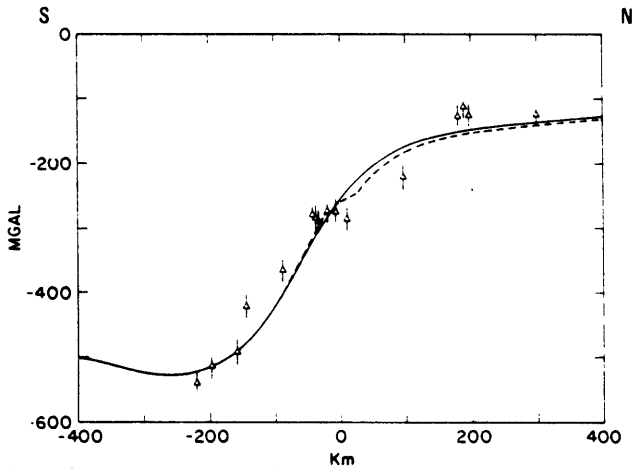

Fig. 3. Comparison of observed Bouguer anomalies with two calculated profiles assuming a local isostatic compensation. Solid curve is computed assuming that compensation occurs by variation of crustal thickness. Dashed curve is computed assuming that compensation occurs in the Tarim Basin by variation of the thickness of the sedimentary cover. The positive and negative abscissas cover the Tarim basin and the Kunlun and Karakorum belts, respectively.

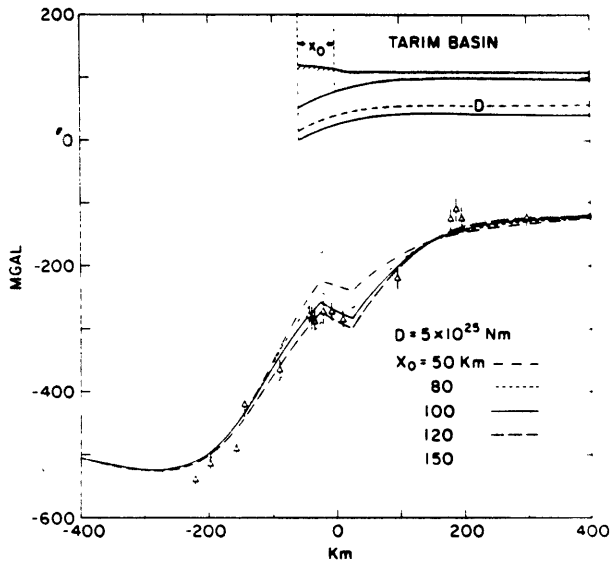

Fig. 4. Comparison of observed and calculated Bouguer anomalies for different values of the flexural rigidity, asssuming that the plate extends 100 km southwards beneath the range (X_0 = 100 km). For large D, the plate does not bend enough and calculated negative anomalies are too large in the Tarim Basin. For small D, the plate bends too much and the calculated anomalies north of the foot of the range are too small.

extend beneath the mountains a distance X_0 from the front of the mountains; the mass of these mountains then acts as a load on the plate. The trough created in front of the load is filled by sediments. From the calculated deflection of the plate the corresponding gravity anomalies are computed assuming that they are due only to mass anomalies caused by the deflections of the interfaces between the crust and mantle and between the sediments and crust, both of which are assumed to be parallel to the calculated deflection of the plate. Beyond the edge of the elastic plate, we assume a linear increase in the depth of the Moho, from its calculated depth at X_0 to the depth (67 km) corresponding to isostatic equilibrium at X = -170 km. Beyond that point a structure similar to the one used in the isostatic calculation is assumed.

Results

Essentially two parameters are needed to describe the shape of the plate: the flexural rigidity of the plate, D, and the distance X_0 to which the elastic plate extends beneath the range. The wavelength of the gravity anomalies over the basin is mainly constrained by the flexural rigidity and the value of the anomaly at the edge of the basin is constrained by X_0, which parameterizes the magnitude of the load on the Indian plate. Other parameters that can be varied are the density contrasts among the mantle, crust, and sediments, but they are not important for the calculations of the gravity anomalies [Lyon-Caen and Molnar, 1983]. The assumed values of densities are 3.35 g/cm^3 for the mantle, 2.8 g/cm^3 for the crust, and 2.5 g/cm^3 for the sediments. Because there is a mean thickness of sediments of about 1300 m above sea level in the Tarim basin, these sediments act as a small load on this part of the plate. Thus the calculated deflection of the plate will depend

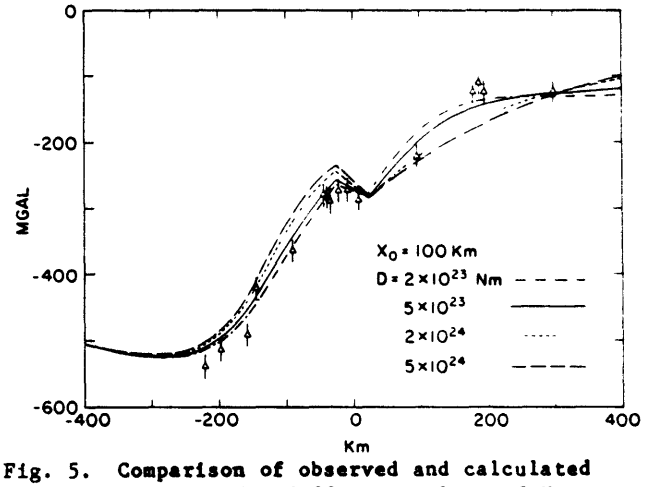

Fig. 5. Comparison of observed and calculated Bouguer anomalies for different values of X_0, assuming the flexural rigidity of the plate is D = 5 × 10^{23} Nm. The configuration of the plate is sketched at the top. For small values of X_0, calculated anomalies are too small; the plate is not flexed down enough. For large values of X_0, the heavy load of the Kunlun mountains flexes the plate too much and the calculated anomalies are too large.

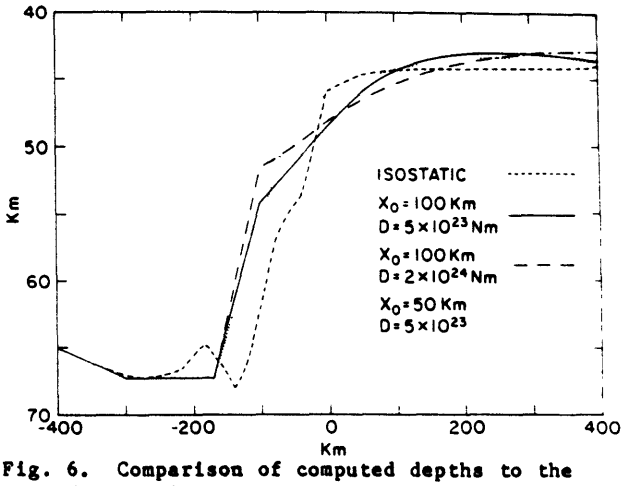

Fig. 6. Comparison of computed depths to the Moho for local isostatic compensation and different plate flexure models. Isostatic compensation predicts a Moho beneath the mountains that is too deep.

on the density of the sediment, both above and below sea level, and the calculated gravity anomalies might also. We show here results computed with a value of 2.5 g/cm^3 (Figures 4, 5, and 6), but calculations made using 2.3 g/cm^3 show that, in fact, the main characteristics of the computed gravity anomalies remain the same.

An elastic plate with a constant flexural rigidity of about 5 x 10^{23} Nm (corresponding to an elastic plate thickness of about 40 km) and that extends at least 80 km and no more than 120 km beneath the range is adequate to explain the deficit of mass over the Tarim Basin and the excess of mass over the range (Figures 4 and 5). A comparison of the shape of the Moho for the model assuming local isostatic compensation with those computed with an elastic plate with different parameters (Figure 6) illustrates clearly how a flexed plate can account for the observed data where local isostatic compensation does not. With a flexural rigidity of 5 x 10^{23} Nm and a density of sediments of 2.5g/cm^3, predicted maximum depths below sea level of the Pre-Tertiary surface of the basin are 7.6 km and 8.4 km for plates extending 80 or 100 km beneath the Kunlun. The misfit of the data near the center of the basin (x ~ 200 km) is probably a consequence of the assumptions of two-dimensional geometry, of a semi-infinite extent of the plate, and of no external forces acting on the plate. Clearly these are not strictly valid here. The Tien Shan, for example, probably acts as a load on the northern edge of the Tarim Basin and creates a sedimentary trough similar to the one on its southern edge [Marussi, 1964]. In this case the plate beneath the middle part of the basin would be flexed up more than predicted by the calculations here, and consequently the computed Bouguer anomaly would be smaller there.

We have shown that the southwestern part of the Tarim Basin and the Kunlun belt are not in isostatic equilibrium, with the basin being over compensated and the belt undercompensated. This can be explained if a strong plate

underlying the Tarim Basin extends at least 80 km southwest beneath the Kunlun. Part of the topography of the Kunlun is thus supported by the strength of this plate. This result, together with the geological evidence of young folds in the Tarim Basin at the front of the mountains, suggests that probably a minimum of about 80 km of crustal shortening has occurred by underthrusting of the Tarim Basin below the Kunlun belt. This implies a comparable value for the minimum amount of strike-slip displacement on the Altyn Tagh strike-slip fault. Moreover, given the lack of detailed geologic work in most of northern Tibet, we probably should not dismiss the possibility that much of northern Tibet was underthrust by the Tarim Basin earlier in the Tertiary era before the Altyn Tagh fault formed.

Acknowledgements. This research was supported by NASA and NSF. We thank S. Luria for the typing of the manuscript, and P. England for critically reviewing it.

References

Amboldt, N., Relative schwerkraftsbestimmungen mit pendeln in Zentral Asien, 2 reports from scientific expedition to northwestern provinces of China under leadership of Dr. Sven Hedin, Publ. 30, III Geodes., Tryckeri Aktiebolaget Thule, Stockholm, 1948.

Karner, G. D., and A. B. Watts, Gravity anomalies and flexure of the lithosphere at mountain ranges, J. Geophys. Res., 88, 10449-10477, 1983.

Lyon-Caen, H., and P. Molnar, Constraints on the structure of the Himalaya from an analysis of gravity anomalies and a flexural model of the lithosphere, J. Geophys. Res, 88, 8171-8192, 1983.

Marussi, A., Italian expeditions to the Karakorum (K^2) and Hindu Kush, Sci. Rep. II, Vol. I, Geophysics of the Karakorum, 242 pp., E. J. Brill, Leiden, 1964.

Molnar, P., and P. Tapponnier, Cenozoic tectonics of Asia: Effects of a continental collision, Science, 189, 419-426, 1975.

Molnar, P., and P. Tapponnier, A possible dependence of tectonic strength on the age of the crust in Asia, Earth and Planet. Sci. Lett, 52, 107-114, 1981.

Norin, E., Geological explorations in western Tibet, Reports from the scientific expedition to the northwestern provinces of China under the leadership of Dr. Sven Hedin, Publ. 29, III Geology, Tryckeri Aktiebolaget Thule, Stockholm, 1946.

Tapponnier, P., and P. Molnar, Active faulting and tectonics in Asia, J. Geophys. Res., 82, 2905-2930, 1977.

(Received October 1, 1984;
Accepted October 24, 1984)

CHAPTER IV

COMPARISON OF THE UPPER MANTLE SHEAR VELOCITY STRUCTURE OF THE INDIAN SHIELD AND THE TIBETAN PLATEAU AND TECTONIC IMPLICATIONS

Hélène Lyon-Caen

INTRODUCTION

The Tibetan Plateau is one of the major products of the collision of India with Eurasia. Although many recent studies have brought information on the geological structure and active deformation of its southern part and a better knowledge of the suture zone north of the Himalaya, the dynamic processes that lead to the formation and maintain the mean elevation of 4500 m over the plateau are not well understood and are controversial. Because of its obvious importance for constraining these deep processes, the seismic velocity structure of the Tibetan Plateau has been the subject of many studies. These studies have consistently used group and phase velocities of fundamental mode surface wave [e.g., Chen and Molnar, 1981; Romanowicz, 1983; Jobert et al., 1985] and observations of P_n and S_n waves [Ni and Barazangi, 1983; Chen and Molnar, 1981]. The best resolved features outlined by these studies are: a thick crust of 70±10 km (see also Hirn et al., 1984) with a low mean crustal shear wave velocity of 3.4 to 3.5 km/s and high uppermost mantle P_n and S_n velocities of at least 8.1 and 4.7 km/s underneath most of the plateau.

Barazangi and Ni [1982] used the evidence of high P_n and S_n velocities to infer the existence of a thick, high velocity lid beneath the plateau and to argue that the structure of the plateau is that of a shield, like India. They interpreted this as an indication that the Indian plate as a whole is now underthrusting beneath the entire plateau and is responsible for the formation of the 70 km thick crust and high elevation. If this were true, the mean mantle velocity in the upper 200 km or so of the Tibetan Plateau should be relatively high and comparable to that of the Indian Shield. Unfortunately, dispersion of fundamental mode surface waves lacks resolution of the velocity structure below 100 or 150 km, and trade-offs occur when trying to constrain

various parameters such as the crustal thickness and the mean upper mantle velocity [Chen and Molnar, 1981]. In contrast, Chen and Molnar [1981] argued that the high P_n and S_n velocities do not require a particularly cold and strong upper-mantle. Moreover S-P residuals calculated from the Jeffreys-Bullen tables for earthquakes within the plateau, indicate that the mean shear velocity in the upper 400 km of the mantle is quite lower than that beneath the Himalaya [Molnar and Chen, 1984]. Their studies, however, do not provide any constraint on the depth range of material with these apparently low velocities.

The purpose of this study is to constrain the shear wave velocity structure of both the Indian Shield and the Tibetan Plateau down to a depth of about 400 km. The dispersion of higher mode surface wave could provide such constraints, but higher modes are difficult to isolate, in particular on the short paths confined exclusively to Tibet. Recent work using long period body waves data have demonstrated that the travel times and waveforms of SH waves recorded at distances up to 30° and of SS recorded between 30° and 60° can provide tight constraints on the large scale velocity structure of the upper 670 km of the mantle and particularly of the upper 400 km [e.g. Grand and Helmberger, 1984; Rial et al., 1984; Given, 1984]. In this distance range the waveforms are controlled by the interference of phases created by first order velocity discontinuities in the uppermantle. Specifically, the distinction between a structure with a thick lid and a poorly developed low velocity zone and a structure with a pronounced low velocity zone can easily be made by measuring SS-S travel times, relative amplitudes of SS to S waves and by synthesizing waveforms [Grand and Helmberger, 1984]. I first present an analysis of long period SH phases for the Indian Shield, then show some evidence that the upper mantle velocity beneath the Tibetan Plateau is

significantly slower than that beneath the Indian Shield and try to put bounds on the velocities there.

DATA COLLECTION AND PROCEDURE

Seismograms from earthquakes at the border of the Indian Shield, mainly in Burma and the Himalaya, and recorded at the WWSSN stations on the shield (HYB, KBL, KOD, LAH, NDI, NIL, QUE, SHL) were selected to study the Indian Shield (Table 1). To study the plateau, seismograms from earthquakes within the Tibetan Plateau or at the edge of it were selected (Figure 1; Table 2). I collected long period S waves with a large signal to noise ratio from simple, shallow, moderate-sized earthquakes ($m_b \simeq 5.5$ to 5.9) with, in most cases, reliable focal mechanisms and simple source time functions. In addition I also used some seismograms from the People's Republic of China network with stations equipped with intermediate period pendulums (12.5s) and galvanometers (1.2s).

Because it is necessary to identify phases created by discontinuities in the velocity structure, I avoided using complex earthquakes. The best way to know if an earthquake has a simple source time function is to analyse the teleseismic P waveforms. Such analysis has been done for some of the earthquakes used here [Molnar and Chen, 1983; Baranowski et al., 1984]. For other earthquakes I looked at a few teleseismic P or S waves to check that the signal was not complicated and to estimate the width of the time function. Some earthquakes were too small, and for such events I picked the S waves when the signals looked simple or resembled signals at similar epicentral distances. In any case, in the period range used here (esentially longer than 10s for the seismograms from the WWSSN stations), small earthquakes are very likely to have simple time functions. Moreover, because of the higher attenuation of shear waves than longitudinal waves, S waveforms are less

sensitive to small details of the source time function than are the P waveforms. Stations from the People's Republic of China network have a flat response in displacement from about 1s to 12s. Thus the seismograms recorded at those stations are usually not as simple as those from the WWSSN stations.

First, a travel time curve was constructed by directly measuring the S wave arrival time on the long period seismogram. I corrected the origin times of the earthquakes given by the ISC in such a way that they all would have occured at 10 km depth, assuming a vertical slowness of 0.15 s/km, which is appropriate for a ray leaving the source with an angle of incidence of 25.8° and a P-wave velocity of 6 km/s at the source. For a couple of reasons it seems more appropriate to proceed in this way rather than correcting each observed phase with its own slowness: First, the depths of the earthquakes are almost certainly between 0 and 20 km [Molnar and Chen, 1983] and were an ISC depth in this range correct, the difference in the depth corrections using 0.15 s/km for slowness or using the appropriate slowness of the phase would at most be 0.5s for S_n phases refracted at the Moho, which would be the extreme case. Second, depths assigned 30 km by the ISC reflect unconstrained depths, and because these events are located essentially only with arrival times from stations at distances between about 40° and 70°, a correction of 0.15 s/km seems appropriate. Since most of the earthquakes used here are corrected to a shallower depth, the time correction is almost always in the same sense, and errors in the correction would introduce only a systematic shift in travel times. Because the main interest is to compare the travel time curve of the Indian Shield with that of Tibet, this procedure should not affect the conclusions of the study. Moreover, errors involved in the depth corrections are of the same order of magnitude as those due to measuring arrival times and

probably are smaller than those due to mislocation of events, which are likely to be systematic also. Mislocation by 10 km can introduce errors in travel times as large as 2 or 3s.

Synthetic seismograms were computed using the WKBJ method [Chapman, 1978]. This technique has been compared to the more exact generalized ray method by Grand and Helmberger [1984] and Given [1984]. The WKBJ method does not account for diffracted energy, which leads to an inaccurate calculation of amplitudes beyond the end of triplication branches. A detailed study of the velocity structure near discontinuities would require the use of a more exact technique, but since this study concentrates on the large scale features, the WKBJ method is sufficient. The Green's functions calculated by the WKBJ method are then convolved with the instrument response, with the source time function, and with an anelastic attenuation operator [Futterman, 1962] that is commonly used in the synthesis of body waves and for which most of the attenuation is assumed to occur in the upper part of the mantle. For shallow earthquakes, usually a trade-off occurs between the duration of the time function and the assumed focal depth. When computing synthetic seismograms I generally found that changing the earthquake's source parameters changed the details of the waveforms but did not affect the more prominant features that are controlled by the triplication of the travel time curve.

Since the number of clear waveforms for both the Indian Shield and the Tibetan Plateau is quite small (15 each) and the distance coverage sparse, only gross features of the velocity structure can be resolved. By keeping some parameters fixed I concentrated on those features that have the clearest signature in the waveforms. Specifically, I started from the structure derived by Grand and Helmberger (1984) for the Canadian Shield from a large data set and perturbed it until it yielded a good match to the travel time

curve and the waveforms for the Indian Shield. In doing this the structure below 400 km and the position and size of the 400 km discontinuity were kept fixed. Since the main features in the signals could be explained by perturbing only the structure in the upper 400 km and since studies using the same technique as the one used here to compare areas as different as the Canadian Shield [Grand and Helmberger, 1984] and the Alpine belt [Rial et al., 1984], have not yet revealed resolvable heterogeneities below 400 km, this is probably a good approach. In addition, inversion for the velocity structure of the western United States on a data set similar to that used here [Given, 1984] shows that long period body waves cannot resolve the position of a discontinuity to better than 10 or 20 km.

INDIAN SHIELD

After correcting for focal depth there remains some scatter in the travel times (Figure 2). Nevertheless the characteristics of a structure with a high velocity lid are easily seen : at distance of 10° to 20°, the first arrival is the S_n phase that propagates with an apparent velocity equal to the S wave velocity in the lid and is the long period component of the short period S_n phase observed by Ni and Barazangi [1983] and Huestis et al [1973]. The velocity in the lid is about 4.7 km/s in agreement whith estimates from those two studies.

A second strong arrival created by reflections from the 400 km discontinuity, follows the S_n arrival by about 20s at a distance of 17.5° (Figure 2). (See also Figure 20 of Grand and Helmberger [1984] to observe the similarity between seismograms from the Canadian Shield and the Indian Shield at those distances.) The time separation between S_n and the reflection from the 400 km discontinuity fixes the mean velocity in the mantle shallower than 400 km.

The mean velocity between 250 and 400 km, however, should be constrained by the observation of the 400 km branch beyond 24° because the corresponding ray spends most of its time in this depth range and the phase starts to be well separated from the two first phases corresponding to rays bottoming below and above the 660 km discontinuity . The velocity gradient in that depth range should be constrained by the amplitude of the arrival and by the maximum distance where it can be seen . There is, however, only one good observation recorded at 26.6° (Figure 3). The seismogram recorded at 28.2° is not of very good quality, but it seems that the 400 km branch is either small or absent (Figure 3). If this is true, the velocity gradient between 250 and 400 km should be fairly high to end the 400km branch near 28°. At the same time the mean velocity in the upper 250 km should be high enough to satisfy the travel times between 15° and 20°. The combination of these two constraints seem to indicate that the lid is fairly thick (~100-130 km) with a velocity near 4.7 km/s. The thickness of the lid, however, cannot be well resolved by this study . After different trials the mean velocity at depths of 40 to 250 km is constrained to lie between about 4.58 and 4.68 km/s if the velocity structure deeper than 400 km is fixed. These two extreme values correspond to a variation of 4.5s in the arrival time of the reflection from the 400 km discontinuity at 17.5°.

The lower value of 4.58 km/s is consistent with an SS-S time difference observed from an earthquake in Pakistan and recorded at station KMI (Figure 4), while the higher value of 4.68 km/s yields a calculated SS-S time difference about 7s too small. For this path neither the epicenter nor the recording station are on the shield, and the bounce point is in the Ganga Basin where the SS phase can easily be delayed by 2 to 3s in the thick pile of

sediments. Additional delay because part of the path is not beneath the shield is likely. In summary, 4.58 and 4.68 km/s are bounds consistent with both S and SS-S travel times for the velocity between 40 and 250 km in the Indian Shield. More precisely, the mean velocity between 40 and 140 km is very likely to be between 4.65 and 4.7 km/s.

Synthetic seismograms computed using the velocity structure listed on Table 3 are compared to observations for a wide range of distances (Figure 3). The seismograms most important in constraining the velocity structure in the upper 400 km are those recorded at distance of 15°, 17.5° and 26.6°, which were discussed above.

No noticeable difference in travel times or waveform can be found between the paths that sample the Indian Shield and those that sample a large part of the Himalaya, and they have been studied together. Assuming a 55 km thick crust beneath the Himalaya with a velocity structure otherwise similar to that of the Indian Shield, the S_n wave should be delayed by about 2s and the reflection from the 400 km discontinuity by about 1.5s at distance of 15 to 20°. These delays are within the scatter of the arrival times, and even if they were present, they could not be detected. Thus, the data collected for this study do not show evidence that the structure beneath the Himalaya is different from that of the Indian Shield. The arrival times, however, would also be consistent with a mean velocity slightly higher beneath the Himalaya than beneath the Indian Shield.

COMPARISON OF S WAVES ACROSS THE INDIAN SHIELD AND TIBET

SS Phases:

First order differences in upper mantle velocity structure can be quickly observed by comparing SS-S differential travel time and amplitude ratios of SS to S waves, as clearly demonstrated by Rial et al.'s [1984] study of paths

sampling the Alpine belt and the European platform or by Grand and Helmberger's [1984] comparison of the structure of the Canadian Shield and the Western United States. The effect of local structure at the epicenter or at the receiver is largely, but not completely, eliminated by using the differential time SS-S, because the angles of incidence of the S and SS rays do not differ much. Thus large anomalies in SS-S time differentials can be attributed to the structure along the SS paths but not very close to the epicenter or receiver. Because lateral heterogeneities tend to decrease with depth, large anomalies are likely to be due to relatively shallow structures and thus to be created by structures more concentrated near the bounce point. Amplitude ratios of SS to S waves can change very rapidly with distance because constructive interference occurs near triplications that are located at different distances depending on the velocity structure.

A good coverage of distances from 30° to 60° is needed to make a detailed study such as Grand and Helmberger's [1984]. Because of the epicenter-station geometry, SS phases that bounce beneath the Indian Shield or beneath Tibet are very few, and we show here (Figure 4) the only ones that we could collect. They do not sample a large distance range but provide good evidence for a slower upper mantle beneath the Tibetan Plateau than beneath the Indian Shield.

At the top of Figure 4, a comparison of two SS waveforms is shown, one bouncing beneath the Ganga Basin and with a large part of the path beneath the shield, the other one sampling the northern part of Tibet. They have traveled almost the same distance, but their SS-S time differentials differ by about 25s. At a distance of 37.5°, the first ray with a large amplitude in the SS waveform is a ray bottoming near the 400 km discontinuity, and this is the one delayed by about 25s in the Tibetan path compared to that in the Indian Shield

path.

To compare directly delays along these two paths, it is necessary to evaluate the delay created at a bounce point beneath Tibet due to the presence of a thick crust with a lower mean velocity than that of the Indian Shield. This was done by comparing S travel times calculated for the structure obtained for the Indian Shield with those for a structure having the same upper mantle velocities but with a Moho at a depth below sea level of 70 km and a mean crustal velocity of 3.45 km/s. For rays bottoming near the 400 km discontinuity, the difference in S wave travel times is about 9s at distances of 17° to 20°. The same difference will also exist between SS phases bouncing off the top of these structures and recorded at distances of 34 to 40°. One also must account for the delay due to the extra 4500 meters of topography in Tibet. Assuming a low velocity of 2.55 km/s in these 4500 meters [Chen and Molnar, 1975], an upper bound on the delay is 4s. Thus an upper bound on the difference in SS-S time differential expected from the difference in crustal structure is 13s.

This estimate was obtained assuming a crustal structure for Tibet with a mean velocity lower than the bounds obtained from studies of surface wave dispersion. With the addition of the 4500 m, the crust is 74.5 km thick and the mean velocity is 3.4 km/s while studies of surface wave dispersion suggest ranges from 3.43 to 3.5 km/s [Chen and Molnar, 1981; Romanowicz, 1983]. Most of the delay, apart from that due to excess topography, is not due to a longer time spent in the upper 70 km but to a longer path in the upper mantle below 70 km; because of the lower velocity in the Tibetan crust, the angle of incidence in Tibet is smaller than that in the Shield and the time spent by the ray in the Tibetan crust down to a depth of 70 km is almost the same as the time spent by the same ray through the crust and upper mantle of the

Indian shield down to 70 km. The horizontal distance traveled by the ray, through the 70 km, however, is less for the Tibetan crust than for the Indian Shield crust and uppermantle.

The differences in arrival times of SS and S in Figure 4 show that the SS phase that bounces beneath Tibet is delayed by at least 12 s in the upper mantle compared to the one bouncing beneath the shield. Probably part of this delay is localized in the area near WHN, where surface wave dispersion suggests mean upper mantle velocities equal to or less than 4.5 km/s [Wier, 1982; Feng, 1982]. Nevertheless for a velocity structure to yield the observed SS-S time of about 185 s, the mean upper mantle velocity from 70 to 250 km depth cannot be larger than 4.4 km/s if the mean velocity from 250 to 400 km is not lower than that beneath the Indian Shield. A mean velocity of 4.4 km/s predicts an SS-S time of 183s at 37.5° while a mean velocity of 4.5 km/s predicts an SS-S time of 177s. The difference in arrival times of S and SS for another path at a distance of 35.8° recorded at LZH (Figure 4) and bouncing beneath northern Tibet requires the same low average upper mantle velocity of 4.4 km/s.

Evidence that the mean velocity between depths of 250 to 400 km beneath the Tibetan Plateau is not lower than that beneath the Indian Shield comes from travel times and waveforms of direct SH phases and is described below.

The large amplitudes of SS compared to those of S at distances of 41° and 44° also indicates the presence of a low upper mantle velocity. The large amplitudes of SS cannot be explained by a structure similar to that of the Indian Shield down to 400 km (model SH on Figure 5 and Table 4) nor by a structure similar to that of the Indian Shield down to 250 km and with a lower mean velocity between 250 and 400 km (model TIL on Figure 5 and Table 4). A structure with a low velocity zone between 120 and 250 km, however, can

explain both the amplitudes and shapes fairly well (model TI on Figure 5 and Table 4). In this case the large amplitude is created by the combination of two rays, one reflected from the 400 discontinuity and the other bottoming below the low velocity zone between 250 and 300 km. In the case of model TIL and SH there is no ray bottoming in this depth range. It is not possible to constrain the extent of or the velocity in the low velocity zone because no ray bottoms inside it, but the mean velocity from 70 to 250 km should be between 4.45 and 4.5 km/s to match both the arrival times and amplitudes of SS. This is somewhat higher than the 4.4 km/s required by the SS phases recorded at 37.5°and 35.9° (Figure 4). A mean velocity of 4.4 km/s would predict SS-S times about 4s longer than those observed for the paths in Figure 4. This kind of difference in travel time has been observed on paths through much more homogeneous structure than those studied here [Grand and Helmberger, 1984] and may be due to localized heterogeneities at the bounce point . Alternatively delays of 4s could result from the two receivers (KBL and QUE) being located in areas with higher velocities than the area around LZH or WHN. In fact, the two SS phases with the largest delays (to WHN and LZH, Figure 4) sample the northern most part of Tibet where Ni and Barazangi [1983] found that S_n waves do not propagate efficiently and where Molnar and Chen [1984] observed the largest S-P residuals.

Thus the travel times and amplitudes of SS require a low velocity zone in the upper mantle of northern and central Tibet of 4.4 to 4.5 km/s. But by themselves they are not sufficient to put tight constraint on the velocity in the uppermost mantle of Tibet.

SH Phases:

A comparison of SH phases recorded at distances of about 17.5° and sampling different regions provides constraints on the upper mantle velocity

beneath Tibet (Figure 6). On the seismograms shown, an S_n phase with a small amplitude is followed by a large signal that represents energy reflected from the 400 km discontinuity. The seismograms are aligned with a reduced time calculated assuming a 4.7 km/s velocity. For the two paths that cross only part of Tibet (to HYB and to QUE) the arrival from the 400 km discontinuity is delayed about by 8 to 9s compared to that for a path purely in the Indian Shield (to NDI). In contrast, note that the two paths from earthquakes in the Tien Shan to SHL do not sample the uppermost part of the mantle beneath Tibet and the arrival from the 400 km discontinuity comes almost at the same time as that for the Indian Shield path. The change in travel time of the reflected phase from 400 km is about 2.8s per degree. Thus the reflected phase from the 400 km discontinuity at SHL (Δ = 17.89°) should arrive about 1.3s earlier there than at NDI (Δ = 17.46°) if the mean uppermantle velocities were the same. In fact it arrives about 2s earlier (Figure 6). If the delays along paths from the Tibetan earthquakes were due only to the crustal structure there, either the crust would be 70 km thick with a mean crustal S wave velocity less than 3 km/s or 100 km thick with a mean S wave velocity of 3.46 km/s. Clearly these structures are not compatible with surface wave dispersion and a maximum delay of 4.5 s is calculated assuming the crustal structure listed in Table 4. Because part of the delay due to the crustal structure is already taken into account in the origin time of the earthquakes, the delay of 4.5s is a maximum delay. Assuming a P wave velocity of 6.8 km/s in the lower crust and of 8 km/s in the uppermost mantle, the delay in the P arrival time due to a crust 30 km thicker than normal and for a ray traveling a distance of 40°, is of the order of 1s. Thus the origin times of the Tibetan earthquakes given by the ISC are probably about 1s too late and the correction of the S wave travel time due to the Tibetan crustal structure

should not be larger than 3.5s. Therefore, from the 8s delay observed for the paths to HYB or QUE, a minimum delay of 3.5s, and more likely of 4.5s, must have its source in the upper mantle of Tibet. Furthermore the delay must occur in the uppermost part of the mantle because 1) the path to HYB samples Tibet only in the first 250 km or so and 2) the paths to SHL are not delayed and sample Tibet mostly at depths from 250 to 400 km.

Again a 3.5s delay implies a mean velocity of about 4.45 km/s between 70 and 250 km, if the mean velocity in the Indian Shield is assumed to be 4.65 km/s between 40 and 250 km. The SS phases presented above were delayed at least 12s in the upper mantle for a path sampling northern Tibet, which would correspond to a 6s delay for a single S wave. This is not inconsistent with the 3.5 to 4.5s minimum delay found here since the SS travel time can be affected by other heterogeneities and heterogeneities within the plateau are very likely [Molnar and Chen, 1984; Ni and and Barazangi, 1982].

A seismogram with a path sampling part of Tibet from an earthquake in the central part of Tibet to KOD, recorded at distance of 24.5° (Figure 7) also shows evidence for a delay in the arrival from the 400km discontinuity. At this distance, the first arrival is a direct ray bottoming below the 660 km discontinuity followed by the arrival from a ray bottoming above the 660 km discontinuity, which creates the complication in the beginning of the waveform. There is another separate phase arriving in the latter part of the seismogram that is not distinct on the synthetic seismogram computed for a pure Indian Shield structure (Figure 7) . It is explained here as being created by the arrival from the 400 km discontinuity, which for the shield structure arrives earlier and cannot be observed as a separate phase on the seismogram. The mean velocity between 40 and 250 km used here is 4.53 km/s which is intermediate between the shield and Tibetan velocities inferred from above. Note that this mean velocity is dirived from the relative timing

between the 660 km and the 400 km discontinuity arrivals rather than from the absolute arrival time of the SH phase like those discussed above.

PATHS ACROSS THE TIBETAN PLATEAU

Because most of the collected seismograms do not correspond to pure paths and sample areas with large heterogeneities, the travel times are quite scattered (Figure 8) and the seismograms are not as easy to interpret as those for the Indian Shield. For example, as shown in Figure 6, travel times for paths across Tibet but from earthquakes outside Tibet can be quite different from those from earthquakes within Tibet that travel the same distance, just because of the effect of the thick Tibetan crust. Thus, rather than trying to obtain a good fit to all travel times and waveforms, I tried to isolate the features in the travel time curve and in the waveforms that would give the most information about the large scale structure of the upper 400 km and I discuss these below by comparing observed seismograms with calculated ones for only a few assumed structures.

An S_n phase can be observed on most paths from 7° to 20°, implying the existence of a lid with an apparent velocity between 4.65 and 4.8 km/s, in agreement with previous studies [Chen and Molnar, 1981; Ni and Barazangi, 1983]. Although quite scattered, the travel times of S_n are about 10 to 12s longer than those for the pure Indian Shield paths. This is true for paths with both epicenter and receiver within Tibet as well as for paths with the epicenter in Tibet and the receiver on the Indian Shield. A maximum delay of only 7s is calculated to be due to a one way path within the slow and thick crust of Tibet, assuming an uppermost mantle velocity of 4.7 km/s. An extremely low crustal velocity (< 3 km/s) or a very thick crust (100 km or so) would be required to explain the 10-12s delay if it occurred solely within the Tibetan crust. Those hypotheses are ruled out by surface wave dispersion

curves . Probably strong lateral heterogeneities and changes in crustal thickness may affect the S_n propagation, but it is difficult to imagine that they could cause an additional, systematic delay of 3 to 5s. Thus it seems impossible for the delay of 10 to 12s to occur solely in the Tibetan crust, especially since the crustal velocities for Tibet used here are already among the slowest allowed by the surface wave dispersion accros Tibet. Probably the velocity in the lid beneath Tibet is slower by a few hundredths of km/s than that in the lid beneath the Indian Shield; a difference of 0.02km/s will cause a difference in travel time of 1 or 2s at 1000 or 2000km respectively. If the S_n velocity is 4.7 km/s beneath the Indian Shield, it should be between 4.65 and 4.7 km/s beneath Tibet.

The travel times of clear phases interpreted as reflections from the 400 discontinuity are from 5 to 12s longer than those of the corresponding phases from the Indian Shield (Figure 9) . If a 4s delay is attributed to the extra thickness of crust beneath Tibet, the delay in the upper-mantle is only 1 to 8s. The paths with only 1s delay are from earthquakes in eastern Tibet (15.08.67, 22.05.71, 22.07.72, Table 2) where Molnar and Chen [1984] found relatively small S-P residuals of 1.5 to 1.9s. The largest delays are for paths from earthquakes in central or northern Tibet to the shield and from events in southern Tibet to LZH and XAN. In contrast, along four paths that cross Tibet from north to south from earthquakes in the Tien Shan to SHL, delays are only 2s or less as discussed above (see also Figure 6). Thus the phases reflected from 400 km again indicate that some low velocity material is present beneath most of Tibet, except possibly beneath the eastern part, and that this material is between depths of 70 and 250 km.

In general, waveforms at distances of 20° to 25° are not very sensitive to the presence or absence of a low velocity zone in the upper part of the

mantle. They are, however, sensitive to the mean velocity between 250 and 400 km, as shown by synthetic seismograms computed for distances of 20.1 and 24.0° (Figure 9). If the mean velocity between 250 km and 400 km is low (4.63 km/s in TIL instead of 4.68 km/s in TI, Figure 9) rays traveling below and above the 400 km discontinuity arrive at different times and appear as two distinct phases on the synthetic seismogram at distance of 20.1°. For model TI, however, they both arrive at the same time and form a large amplitude signal. The arrival reflected from the 660 km discontinuity arrives in the latter part of the seismogram, and its timing relative to the arrival from the 400 km discontinuity is also predicted by model TI. This indicates that the mean velocity between 400 and 660 km is not very different from that for both TI and SH, and therefore that no resolvable heterogeneities can be detected in this depth range.

At a distance of 24.0°, the arrival from above the 400 km discontinuity, which spends most of its time between 250 and 400km , arrives in the latter part of the S phase and forms the last large downward half cycle. The difference in arrival time of this phase and that from the 660 km branch is well predicted by model TI (Figure 9). In contrast, model TIL with a lower velocity between 250 and 400 km leads to an arrival 2.5 to 3s too late. This again indicates that the velocity between 250 and 400 km beneath Tibet is comparable to that beneath the Indian Shield in the same depth range and is not unusually low.

The waveforms at KBL and QUE (Figure 10) result from the interference of three rays: one bottoming below and one just above the 660 km discontinuity and a third one bottoming just above the 400 km discontinuity. This third arrival spends most of its time beneath Tibet between depths of 250 and 400 km. At station KBL the relative timing of this last ray with respect to the

other two earlier ones is well explained by model SH but is too large for model TI (Figure 10). The amplitude of the phase is, however, too large, as for the waveforms calculated for the Indian Shield (Figure 3). This may indicate a higher gradient between 250 and 400 km than that of model SH. In contrast the relative timing of these three arrivals at QUE from an earthquake within Tibet is better explained by model TI than by model SH capped by a crustal structure like that of Tibet. In this case the path beneath Tibet samples depths of 10 to 400 km. The difference in the two paths (to KBL and QUE) is mainly in the upper 250 km and it can be explained by model TI that is about 4% slower than model SH between 70 and 250 km.

The waveform at LZH at a distance of 18.4° from an earthquake in south-west Tibet (Figure 9) seems to require a low velocity zone with somewhat lower velocities than that in model TI (model TIS, Table 4), with a mean velocity of 4.45 km/s between 70 and 250 km and apparently with no lid or a very thin lid . This path has a larger part within Tibet than those at distance of 20.1° or 24.0°, which are from earthquakes in the northern part of the Himalaya and with no part within the Indian Shield. Thus 4.45 km/s is probably an upper bound for the mean velocity beneath Tibet between 70 and 250 km.

The match of both the relative timing and amplitudes (Figure 11) of the two phases from below and above the 660 km discontinuity from an earthquake with a focal depth of 95 km beneath the Karakorum area and recorded at distance of 26.2 and 27.2° (see Figure 9 for the path), indicates that both the amount of velocity change near the discontinuity and the gradient above it cannot, with data presently available, be distinguished from those beneath the Canadian Shield and Western United States [Grand and Helmberger, 1984] which are assumed here.

DISCUSSION

The travel times and waveforms presented in this study show: 1) India as well as the Himalaya are underlain by a shield structure with a relatively thick high velocity ($\beta_{Sn} \approx 4.7$ km/s) lid (probably at least 100 km thick) and a mean velocity between 40 and 250 km of 4.58 to 4.68 km/s. 2) There is a high velocity lid beneath most of Tibet with an apparent velocity between 4.65 and 4.8 km/s, but this lid cannot be thick because the mean velocity between 70 and 250 km is about 4.45 ± 0.05 km/s. This mean velocity is lower by 4% or more than that beneath the Indian Shield. Only in southern and eastern Tibet might the mean velocity be more nearly that beneath India. The extent of the low velocity zone and the exact depth dependence of the velocity in the low velocity zone are not well constrained, but the low velocity zone cannot extend much below 250 km. 3) No resolvable large scale differences in the velocity structure of the Indian Shield and the Tibetan plateau could be found below 250 or 300 km (Figure 12).

The results are consistent with positive S-P residuals obtained by Molnar and Chen [1984] for earthquakes in Tibet and show that the source of the observed delays is essentially in the upper 250 km beneath Tibet. They are consistent with the idea that the Indian plate is now underthrusting beneath the Himalaya [e.g. Baranowski et al, 1984; Barazangi and Ni, 1982; Molnar et al, 1977; Seeber et al, 1981] but indicate that India is not being underthrust as a whole beneath the Tibetan Plateau at the present time, as suggested by Barazangi and Ni [1982] and Seeber et al [1981]. If it were, we would expect the mean velocity down to about 200 km to be about the same in the two areas because heating by conduction solely is a very slow process and would take over 80 Ma. Moreover, the effect of increased pressure on the underthrust shield would actually tend to increase the velocities in the underthrust plate (Chen and Molnar, 1981).

However if the lower part of the lithosphere had been stripped of its upper part, heating by convection could become effective and could occur as a relatively rapid process [e.g., Houseman et al., 1981]. Thus we cannot completely rule out the possibility that the Indian Shield has underthrust beneath part of Tibet after the collision, but if it did, the lower part of its lithosphere must have been removed so that a rapid heating could occur.

Present underthrusting of the Indian Shield beneath Tibet [Barazangi and Ni, 1982], however, seems to be ruled out by our results because the high shield velocity does not extend beneath Tibet as thought by Barazangi and Ni [1982] . This is in agreement with the analysis of gravity anomalies in the Himalaya and southern Tibet, that indicates that the strength of the Indian plate does not support the load of Tibet at all [Lyon-Caen and Molnar, 1983; 1985]. If the Indian plate has been underthrusting Tibet, it should have become very weak there and lost its strength. Moreover, some cold and dense material beneath southern Tibet, presumably representing the detached lower part of the Indian lithosphere, seems to be required to support the load of the High Himalaya [Lyon-Caen and Molnar, 1983; 1985]. The results of this study do not give evidence for or against this hypothesis. The few paths that largely sample the Himalaya or southern Tibet indicate only upper mantle velocities comparable to that of the Indian Shield and the technique used probably cannot detect relatively small blocks of high velocities that may not be a continuous structure and may be quite localized in space.

SUMMARY

Travel times and waveforms of SH and of SS phases were used to constrain the large scale features of the upper mantle velocity structure of the Indian Shield and to compare it to that of the Tibetan Plateau. Both areas are underlain by high velocity lids with velocities close to 4.7 km/s. The mean velocity between 70 and 250 km beneath Tibet, however, is constrained by both sets of data to be 4% or more slower than that beneath the Indian Shield and no large differences between the two structures are required below 250 km. The implications are that the present deep structure of the Tibetan Plateau is not that of a shield and thus that the Indian Shield is not underthrusting the entire Tibetan Plateau at the present time .

Acknowledgments: I thank S. Grand for guiding me at the begining of this study and allowing me to use his WKBJ computer program. He also pointed out a few seismograms used here. I thank P. Molnar for encouragements. S. Grand and P.Molnar made helpful suggestions on the manuscript. I also thank M. Barazangi for a constructive critical review. This research was supported by NASA Grant NAG5-300 and NSF Grant EAR-8121184 and was completed at the Massachusetts Institute of Technology .

References

Baranowski, J., J. Armbruster, L. Seeber and P. Molnar, Focal depths and fault plane solutions of earthquakes and active tectonics of the Himalaya, J. Geophys. Res., 89, 6918-6928, 1984.

Barazangi, M. and J. Ni, Velocities and propagation characteristics of P_n and S_n beneath the Himalayan arc and Tibetan plateau: possible evidence for underthrusting of Indian continental lithosphere beneath Tibet, Geology, 10, 179-185, 1982.

Chapman, C.H., A new method for computing synthetic seismograms, Geophys. J. R. astr. Soc., 54, 481-518, 1978.

Chen, W.P. and P. Molnar, Short-period Rayleigh wave dispersion across the Tibetan plateau, Bull. Seism. Soc. Amer., 65, 1051-1057, 1975.

Chen, W.P. and P. Molnar, Constraints on the seismic wave velocity structure beneath the Tibetan plateau and their tectonic implications, J. Geophys. Res., 86, 5937-5962, 1981.

Chen, W.P., and P. Molnar, Focal depths of intracontinental and intraplate earthquakes and their implications for the thermal and mechanical properties of the lithosphere, J. Geophys. Res., 88, 4183-4214, 1983.

Feng, C., A surface wave study of crustal and upper mantle structures of Eurasia, Ph.D. Thesis, University of Southern California, 1982.

Given, J., Ph. D. Thesis, California Institute of Technology, 1984.

Grand, S. and D.V. Helmberger, Upper mantle shear structure of North America, Geophys. J.R. Astr. Soc., 76, 399-438, 1984.

Hirn, A. et al., Lhasa block and bordering sutures - a continuation of a 500 km Moho traverse through Tibet, Nature, 307, 25-27, 1984.

Houseman, G. A., D. P. McKenzie, and P. Molnar, Convective instability of a

thickened boundary layer and its relevance for the thermal evolution of continental convergent belts, J. Geophys. Res., 86, 6115-6132, 1981.

Huestis, S., P. Molnar and J. Oliver: Regional S_n velocities and shear velocity in the upper mantle, Bull. Seism. Soc. Am., 63, 469-475, 1973.

Jackson, J. and D. McKenzie, Active tectonics of the Alpine-Himalayan belt between western Turkey and Pakistan, Geophys. J.R. astr. Soc., 77, 185-264, 1984.

Jobert, N., B. Journet, G. Jobert, A. Hirn and K.Z. Sun, Deep structure of southern Tibet inferred from the dispersion of Rayleigh waves through a long period seismic network, Nature, 313, 386-388, 1985.

Kaila, K.L., Deep seismic sounding studies in India, Geophys. Res. Bull. 20, 309-328, 1982.

Le Dain, A.Y., Tapponnier, P. and P. Molnar, Active faulting and tectonics of Burma and surrounding regions, J. Geophys. Res., 89, 453-472, 1984.

Lyon-Caen, H. and P. Molnar, Constraints on the structure of the Himalaya from an analysis of gravity anomalies and a flexural model of the lithosphere, J. Geophys. Res., 88, 8171-8191, 1983.

Lyon-Caen, H. and P. Molnar, Gravity anomalies, flexure of the Indian plate and the structure, support and evolution of the Himalaya and Ganga Basin, Tectonics, 4, 513-538 1985.

Molnar, P. and W.P. Chen, Focal depths and fault plane solutions of earthquakes under the Tibetan Plateau, J. Geophys. Res., 88, 1180-1196, 1983.

Molnar, P. and W.P. Chen, S-P wave travel time residuals and lateral inhomogeneity in the mantle beneath Tibet and the Himalaya, J. Geophys. Res., 89, 6911-6917, 1984.

Ni, J. and M. Barazangi, High frequency seismic wave propagation beneath the Indian Shield, Himalayan arc, Tibetan Plateau and surrounding regions: high uppermost mantle velocities and efficient S_n propagation beneath Tibet, Geophys. J. R. astr. Soc., 72, 665-681, 1983.

Ni, J. and M. Barazangi, Seismotectonics of the Himalayan collision zone: Geometry of the underthrusting Indian plate beneath the Himalaya, J. Geophys. Res., 89, 1147-1163, 1984.

Rial, J.A., S. Grand and D.V. Helmberger, A note on lateral variation in upper mantle shear wave velocity across the Alpine front, Geophys. J.R. astr. Soc., 1985.

Romanowicz, B., Constraints on the structure of the Tibet plateau from pure path phase velocities of Love and Rayleigh waves, J. Geophys. Res., 87, 6865-6883, 1982.

Tapponnier, P. and P. Molnar, Active faulting and tectonics of China, J. Geophys. Res., 82, 2905-2930, 1977.

Tapponnier, P. and P. Molnar, Active faultings and Cenozoic tectonics of the Tien Shan, Mongolia and Baykal Region, J. Geophys. Res., 84, 3425-3459, 1979.

Turcotte, D.L. and G. Schubert, Geodynamics, John Wiley, 450pp, New York, 1982.

Seeber, L., J.G. Armbruster, and R.C. Quittmeyer, Seismicity and continental subduction in the Himalayan arc, Zagros, Hindu-Kush, Himalaya, Geodynamic evolution, Geodynamics Series, Vol. 3, American Geophysical Union, Washington, D.C., 215-242, 1981.

Wier, S., Surface wave dispersion and earth structure in southeastern China, Geophys. J.R. astr. Soc., 69, 33-47, 1982.

Table 1. Earthquakes and stations used to study the Indian Shield

	N°	Date	Lat (°N)	Long (°E)	*	Stations	Δ(°)
HIMALAYA	1	01-09-64	23.12	92.26	1	QUE	22.41
	2	21-10-64	28.04	93.75	2	LAH	17.21
	3	29-09-66	27.49	92.61	1	QUE	22.63
	4	16-12-66	29.62	80.79	2	HOW	9.85
						POO	12.72
						KOD	19.53
	5	14-03-67	28.41	94.29	2	NDI	15.01
						LAH	17.57
						QUE	23.89
						KOD	24.01
	6	15-09-67	27.42	91.86	1	QUE	21.99
	7	20-05-79	29.93	80.27	1	QUE	11.54
						SHL	11.17
	8	19-11-80	27.4	88.8	1	KBL	18.36
						QUE	19.35
BURMA	9	05-02-66	26.4	103.21	3	NDI	23.18
						POO	28.16
	10	04-01-70	24.12	102.49	3	NDI	23.07
	11	30-05-71	25.2	96.41	4	NDI	17.46
						KBL	25.42
	12	31-05-71	25.22	96.51	4	NDI	17.54
						NIL	21.9
						QUE	26.6
	13	21-07-76	24.78	98.69	4	NDI	19.55
OTHERS	14	24-01-66	29.9	69.7	5	NDI	6.75
						HYB	17.4
						KOD	20.9
	15	08-09-73	33.29	86.82	6	KOD	24.51
						HYB	17.47
	16	04-10-74	26.38	66.65	5	NDI	9.65
	17	01-10-79	26.55	60.95	5	SHL	14.53
						NDI	27.72
	18	22-02-80	30.55	88.65	1	HYB	15.99

* Reference to fault plane solution:
1 Ni and Barazangi (1984)
2 Baranowski et al. (1984)
3 Tapponnier and Molnar (1977)
4 LeDain et al. (1984)
5 Jackson and McKenzie (1984)
6 Molnar and Chen (1984)

Table 2. Earthquakes and stations used to study the Tibetan Plateau

N°	Date	Lat (°N)	Long (°E)	*	Stations	Δ(°)
19	15-08-67	31.05	93.56		NDI	14.37
20	22-12-68	36.25	101.83		KBL	26.66
21	04-03-71	32.16	94.99	1	NDI	15.72
					NIL	18.32
					QUE	24.05
22	22-05-71	32.36	92.11	2	NIL	15.88
					KBL	19.37
					QUE	21.6
23	09-04-72	42.09	84.58	3	SHL	17.55
24	22-07-72	31.38	91.41	2	NIL	15.49
					KBL	19.03
					QUE	21.04
25	30-08-72	36.65	96.35	1	NIL	19.11
					KBL	22.28
					QUE	25.31
26	30-08-72	36.56	96.35	1	KBL	22.29
					QUE	25.30
27	07-07-73	31.5	100.33	1	NDI	20.19
					NIL	22.90
28	14-07-73	35.21	86.54	1	QUE	17.23
29	07-04-74	45.21	93.86	3	NDI	21.11
30	04-01-75	38.58	97.46		NIL	20.14
31	18-03-75	35.12	86.54		QUE	17.21
32	05-05-75	33.13	92.84		NIL	16.38
33	10-01-76	42.05	83.35		SHL	17.89
34	21-08-76	32.59	104.24	4	NDI	23.55
35	01-01-77	38.19	90.97		SHL	12.61
36	20-05-79	29.93	80.27		LSA	9.5
					XAN	24.6
37	06-01-80	38.91	95.6		LSA	9.9
38	13-02-80	36.4	76.8		XAN	26.2
					GYA	27.2
39	29-09-80	29.34	81.21		LSA	8.7
					LZH	20.17
					XAN	24
40	23-01-81	30.89	101.15		NDI	20.88
					NIL	23.72
					KBL	27.2
41	09-06-81	34.51	91.42		SHL	8.93
					KBL	18.44
					WHN	19.7
42	23-01-82	31.68	82.29		LSA	7.9
					LZH	18.4
					KMI	19.1
43	15-06-83	34.19	92.82		LSA	4.7

* Reference to fault plane solution:
1 Tapponnier and Molnar (1977)
2 Molnar and Chen (1984)
3 Tapponnier and Molnar (1979)
4 Romanowicz (1982)

Table 3. Shear velocity structure for model SH

Depth (km)	Vs (km/s)
0.	3.7
35.	3.86
38.	4.7
140.	4.7
155.	4.68
175.	4.61
235.	4.61
250.	4.61
275.	4.64
300.	4.67
325.	4.70
350.	4.72
375.	4.75
405.	4.78
406.	5.00

Table 4. Shear velocity structure for model TI, TIL and TIS

Depth (km)	Vs (km/s)		
	TI	TIL	TIS
0.	3.2	3.2	3.2
9.	3.4	3.4	3.4
49.	3.4	3.4	3.4
51.	3.7	3.7	3.7
68.	3.8	3.8	3.8
70.	4.7	4.7	4.7
95.	4.7	4.7	4.5
115.	4.4	4.7	4.4
155.	4.4	4.68	4.4
175.	4.4	4.61	4.4
195.	4.45	4.61	4.4
217.	4.50	4.61	4.46
235.	4.56	4.61	4.53
250.	4.60	4.61	4.60
275.	4.64	4.61	4.64
300.	4.67	4.61	4.67
325.	4.70	4.61	4.70
350.	4.72	4.63	4.72
375.	4.75	4.70	4.75
405.	4.78	4.75	4.78
406.	5.00	5.00	5.00

Figure Captions

Figure 1. Map of Asia with simplified 1.0 and 3.0 km elevation contours. The black dots show the location of the earthquakes used in this study and the open dots show the location of the seismological stations. The paths used in this study are listed in Table 1 and Table 2.

Figure 2. Travel times vs. epicentral distance of S waves for paths across the Indian Shield, reduced with a velocity of 4.7 km/s. The paths used are shown in the lower left corner and listed in Table 1. Some typical waveforms of SH components, identified by the earthquake's number and the station's name (see Table 1), are shown on the profile to the right. The waveforms are also aligned using a velocity of 4.7 km/s. Arrows identify phases. Only the arrival times of the first phase and of the reflection from the 400 km discontinuity between 15° and 20° can be measured. At distances greater than 24° secondary phases can be identified but their onset times cannot be measured. Different symbols are used depending on the path: (Δ) for path almost completely in the Indian Shield, (□) for path partly within the Himalaya or Tibet. Open symbols are readings of first arrivals, closed symbols are readings of secondary arrivals. The travel time curve plotted is calculated using the velocity structure SH listed in Table 3.

Figure 3. Comparison of observed SH waveforms for the Indian Shield with waveforms computed using the velocity structure SH listed in Table 3. The first arrivals for the synthetic and the observed seismograms have been aligned. Each waveform is identified by the earthquake's number and the recording station (Table 1).

Figure 4. Comparison of the SH component of S and of SS phases that were reflected beneath the Indian Shield and beneath Tibet. The map shows the paths with the bounce points indicated by a plus sign. The source time functions of earthquakes 1 and 2 are not simple, and the intervals between SS and S cannot be measured precisely. Nevertheless they differ by at least 25s. S and SS phases for the path from earthquake 4 to LZH also show a large time differential which is compatible with that from earthquake 2 to WHN. See Figure 5 for the seismograms from earthquake 3.

Figure 5. Comparison of observed SH component of S and SS phases from earthquake 3 (see Figure 4 for the location of the path) to KBL and QUE with synthetic seismograms computed using a structure with a shallow low velocity zone (TI, Table 4), with low velocities below 250 km (TIL, Table 4), and with a shield structure (SH, Table 3) modified by replacing the 38 km crustal thickness by a crustal structure for Tibet such as that used in TI (Table 4). Note that model TI, with a shallow low velocity zone can explain the relative amplitudes of S to SS waves better than does SH or TIL. This is due to the interference of the ray bottoming near the 400 km discontinuity with a ray bottoming below the low velocity zone .

Figure 6. Comparison of observed seismograms at distances of 17.21 to 17.90° and sampling different areas. The seismograms are aligned along a constant reduced time, using 4.7 km/s. The first arrival, indicated by a tick, is the S_n phase. The second tick indicates the arrival from the 400 km discontinuity. The vertical lines are separated by 4s, and the first such line is aligned with the arrival from the 400

km discontinuity at NDI. This path is purely in the Indian Shield. The arrivals from the 400 km discontinuity to HYB and QUE from earthquake in Tibet clearly are delayed by about 8 and 9s respectively. The ray reflected from the 400 km discontinuity to SHL apparently are not delayed. These rays do not sample the uppermost part of the mantle beneath Tibet. These data indicate low velocities beneath Tibet shallower than 400 km.

Figure 7. Comparison of an observed seismogram recorded at KOD at distance of 24.5° (see map on Figure 6 for the path) with synthetic seismograms computed using a shield structure SH (bottom) and a structure with upper mantle velocities intermediate between those of TI and SH (top) for which the mean velocity between 40 and 250 km is 4.53 km/s. For the shield structure the ray from the 400 km branch arrives too early to be seen as a separate arrival in the waveform.

Figure 8. Travel times vs. epicentral distance of S waves for paths across the Tibetan Plateau, reduced with a velocity of 4.7 km/s. The paths are shown on the left corner and are listed in Table 2. Different symbols are used depending on the paths: (▽) to Indian Shield and GYA and KMI, (△) to LZH and XAN and LSA, (□) for north-south paths. The travel time curve plotted is that for the Indian Shield (Figure 2) but delayed by 8s for the S_n branch and 4s for the later ones. These are expected delays due only to the thick crust of Tibet with a low average crustal velocity. Note that most arrivals from the 400 km discontinuity are late but those from the north-south paths (■) originating in the Tien Shan, passing beneath Tibet and recorded at stations in India are on time or earlier.

Figure 9. Comparison of observed and synthetic seismograms for different structures listed in Table 4. Synthetic seismograms using TIL, with a mean velocity between 250 and 400 km lower than model TI but with higher velocity above 250 km, do not match the observed waveforms at distance of 20.1 and 24.0°: at 24° the arrival time from the 400 km branch, which is the last large downward phase, is late and at 20.1°, because of the low velocity above 400 km, the two rays that contribute to the first arrival, bottoming below and above the 400 km discontinuity, arrive at different time and form the complicated waveform at the beginning of the seismogram. Also, because the overall mean velocity in the upper 400 km is larger in TIL than in TI, the arrival from the 660 km branch is earlier in TIL than in TI. The waveform at distance of 18.4° is better explained by model TIS (Table 4) which has no lid and a lower mean velocity than model TI between 70 and 250 km. These data show that heterogeneities are present within Tibet but in all cases a mean velocity of 4.45 km/s or less at depths between 70 and 250 km can better explain the waveforms.

Figure 10. In the lower figure the waveform at KBL shows that the relative arrival time of the ray from the 400 km branch with that of the direct ray and that of the 660 km branch can be accounted for by a structure such as SH but is too large if the mean velocity in the upper 400 km of the mantle is lower as in TI. In contrast, the waveform at QUE in the upper figure shows that the arrival time of the ray from the 400 km branch can be accounted for better by TI than by SH. Note the difference in the depth sampling of Tibet between the two paths: while the path to QUE samples the entire upper mantle beneath Tibet,

the path to KBL only samples depths of 250 to 400 km. Thus this indicates that the mean velocity beneath Tibet between 250 and 400 km is comparable to that beneath the Indian Shield and that the low velocity zone is mostly confined to the region above 250 km.

Figure 11. Comparison of observed and synthetic seismograms for an earthquake that occured at a depth of 95 km beneath the Karakorum (13 February 1980, 36.4° N, 76.8° E) for which the paths pass beneath northern Tibet (XAN) and southern Tibet (GYA) (Figure 9). The two phases observed and indicated by arrows are rays bottoming below and above the 660 km discontinuity. The agreement of both the time separation and relative amplitude of the two phases with observations , indicates an absence of resolvable differences between the structure beneath the Canadian Shield, the Indian Shield or the Tibetan Plateau deeper than 500 km.

Figure 12. Summary of average upper mantle S waves velocities beneath the Indian Shield and the Tibetan Plateau.

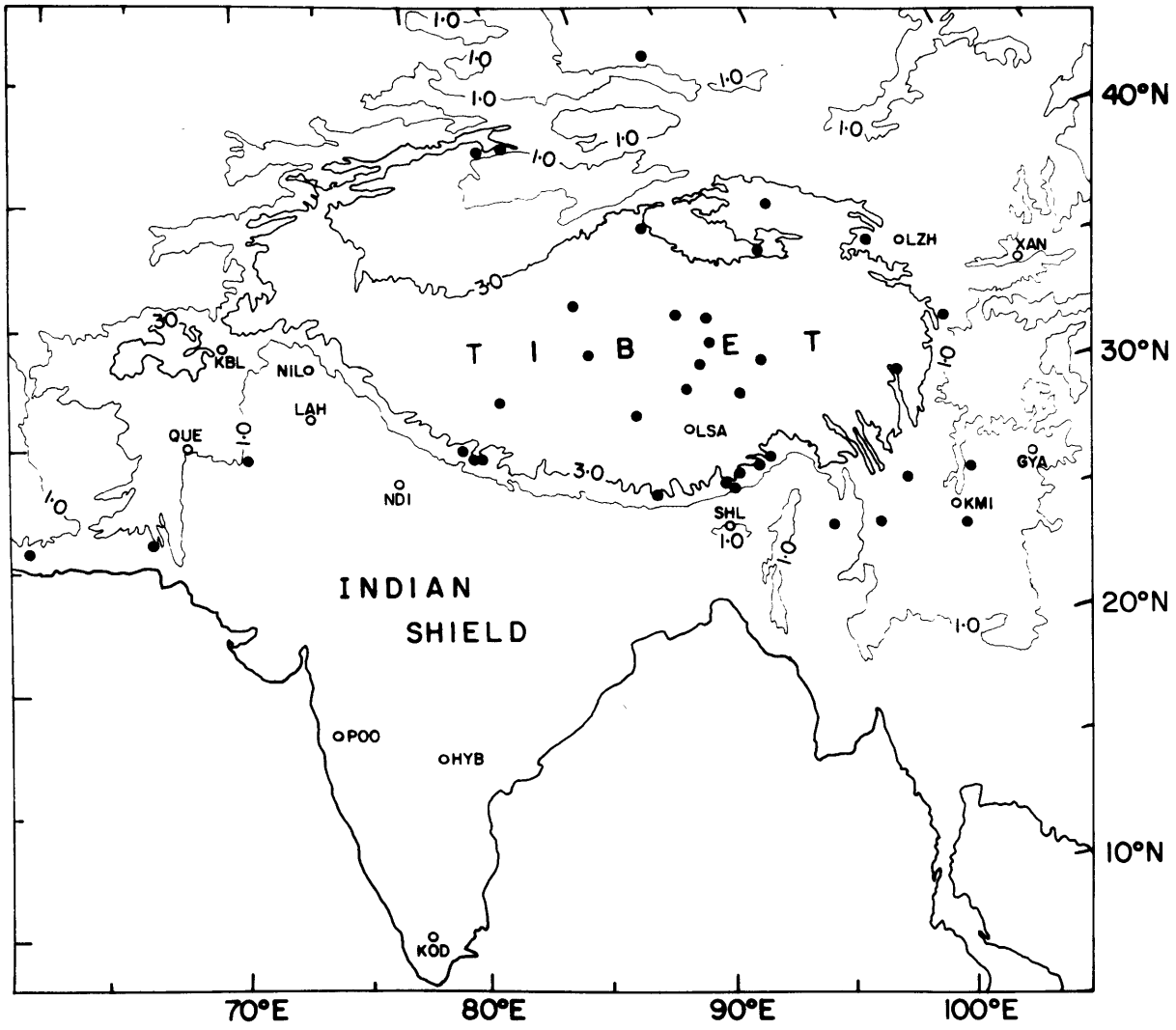
1·0
3·0
TIBET
INDIAN
SHIELD
KBL
NILO
LAH
QUE
NDI
OLSA
SHL
OLZH
XAN
GYA
OKMI
OPOO
OHYB
KOD
40°N
30°N
20°N
10°N
70°E
80°E
90°E
100°E

Figure 1

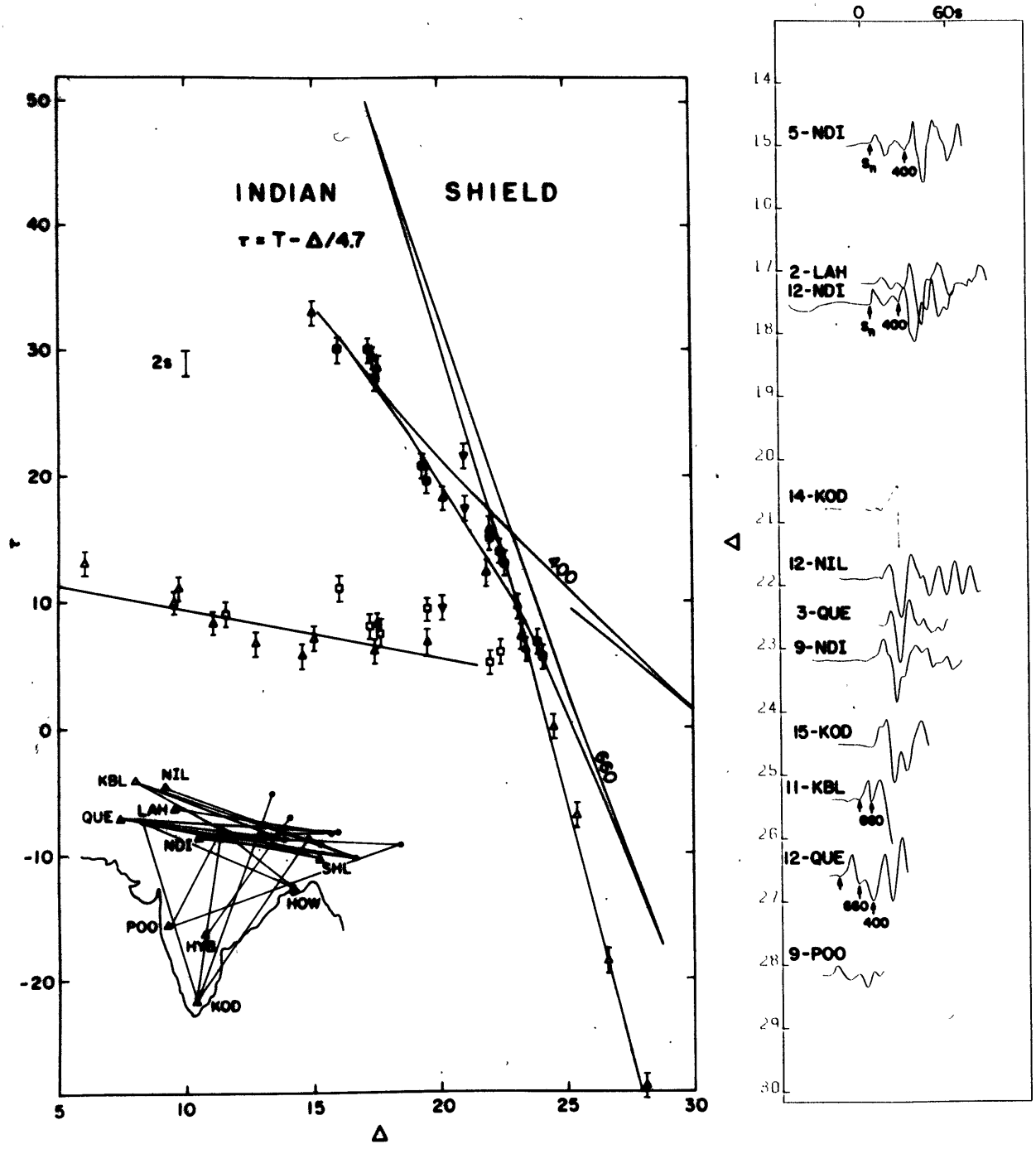
INDIAN SHIELD
τ = T - Δ/4.7
2s
τ
Δ
KBL
NIL
QUE
LAH
NDI
SHL
HOW
POO
HYB
KOD
660
400
0
60s
5-NDI
2-LAH
12-NDI
14-KOD
12-NIL
3-QUE
9-NDI
15-KOD
11-KBL
12-QUE
9-POO

Figure 2

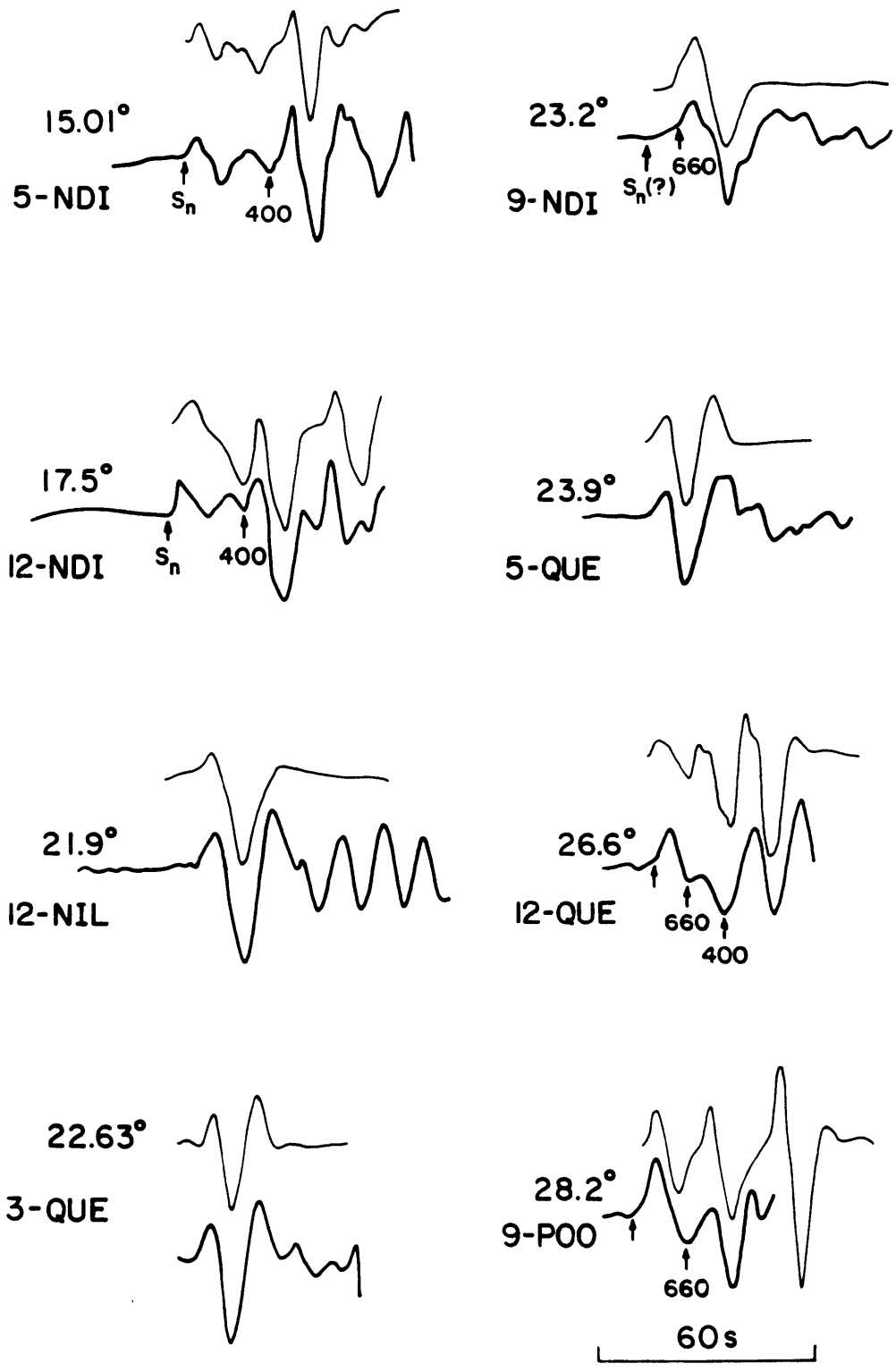
INDIAN SHIELD
15.01°
5-NDI
Sn
400
23.2°
9-NDI
Sn(?)
660
17.5°
12-NDI
Sn
400
23.9°
5-QUE
21.9°
12-NIL
26.6°
12-QUE
660
400
22.63°
3-QUE
28.2°
9-POO
660
60s

Figure 3

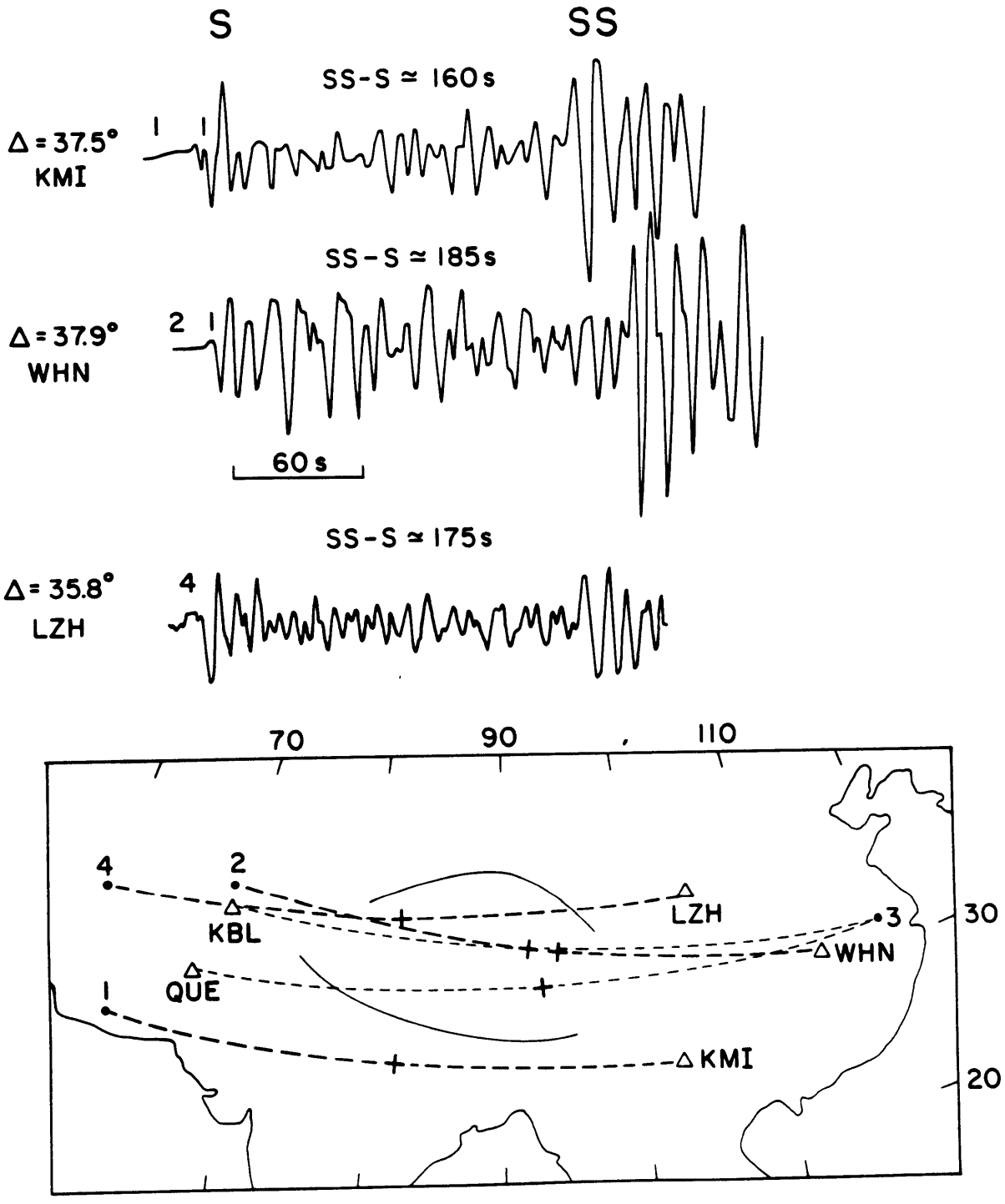
S
SS
SS-S ≃ 160 s
Δ = 37.5°
KMI
1
SS-S ≃ 185 s
Δ = 37.9°
WHN
2
60 s
SS-S ≃ 175 s
Δ = 35.8°
LZH
4
70
90
110
4
2
KBL
LZH
3
WHN
QUE
1
KMI
30
20

Figure 4

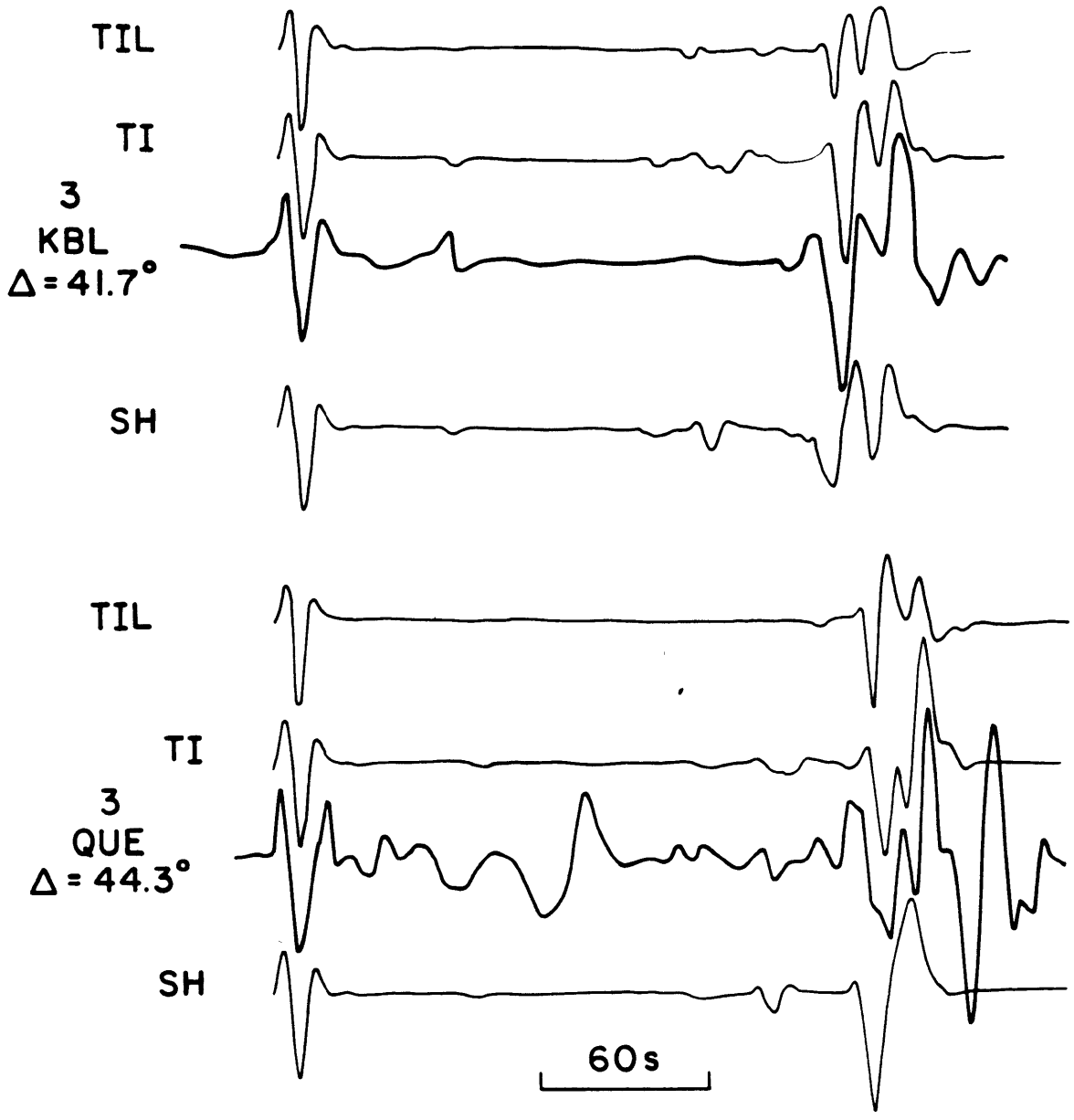

Figure 5

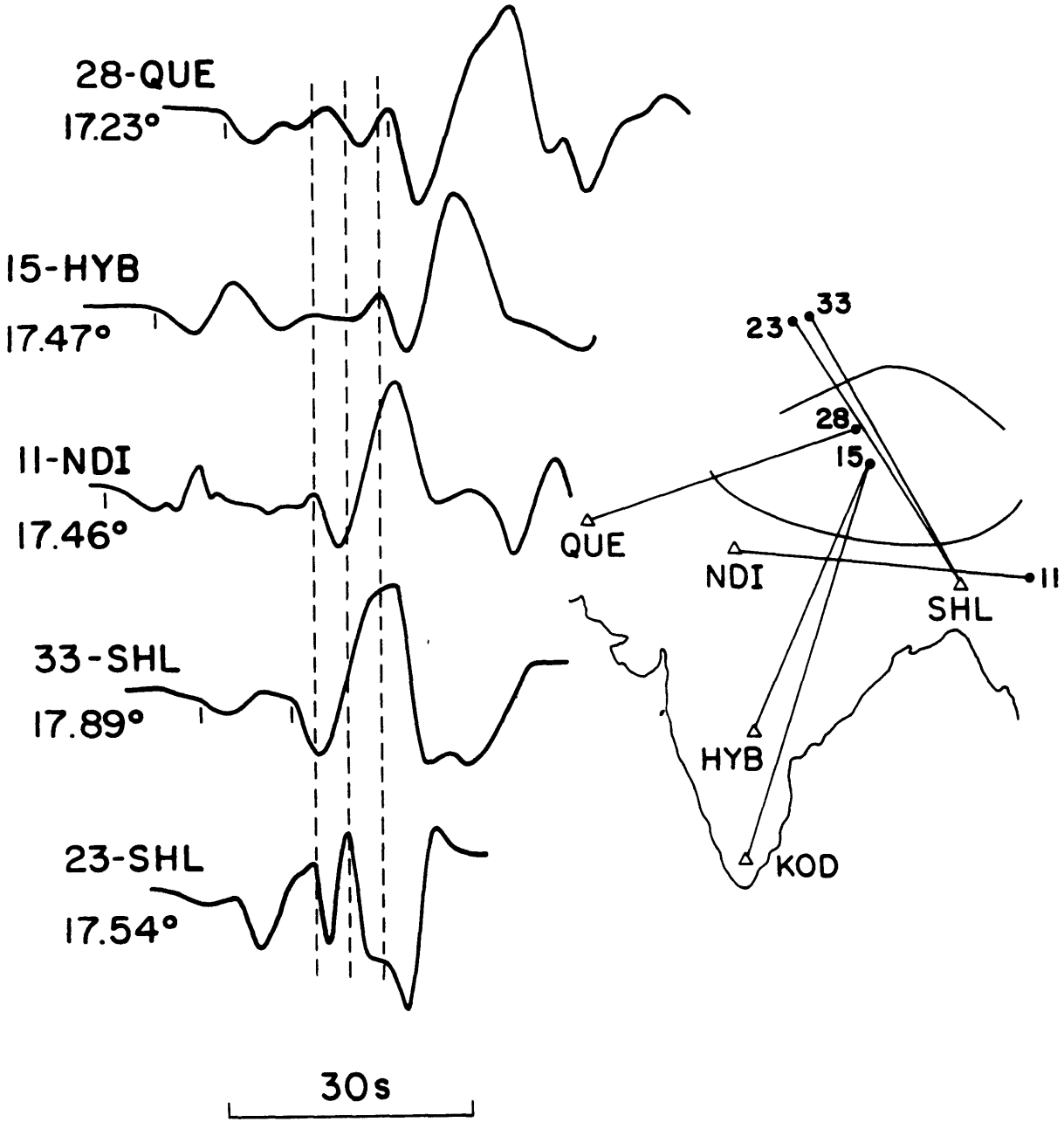
28-QUE
17.23°
15-HYB
17.47°
11-NDI
17.46°
33-SHL
17.89°
23-SHL
17.54°
30s
33
23
28
15
QUE
NDI
11
SHL
HYB
KOD

Figure 6

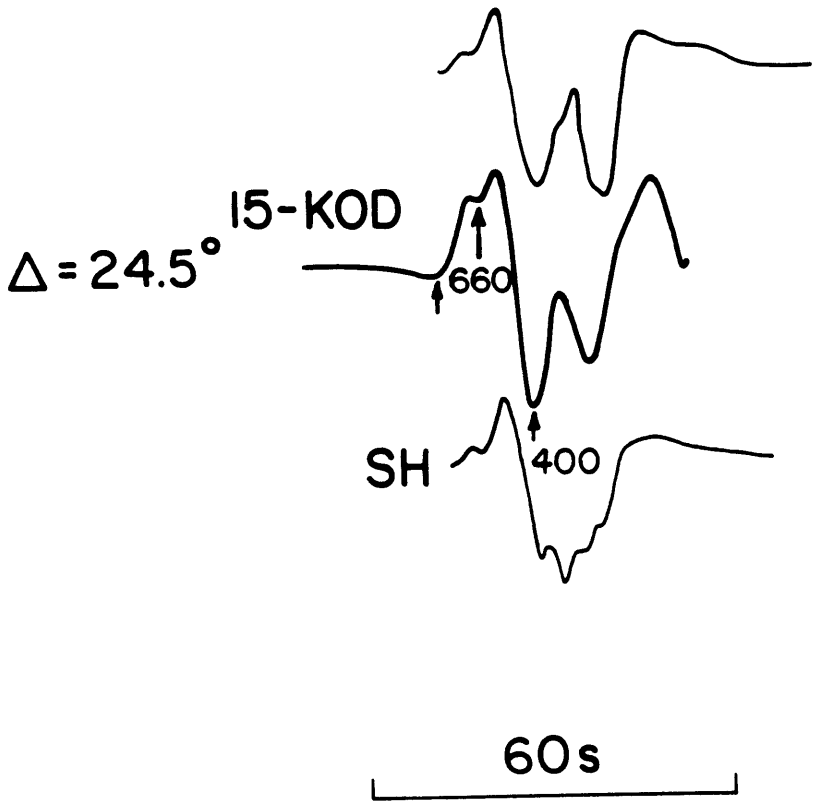

Figure 7

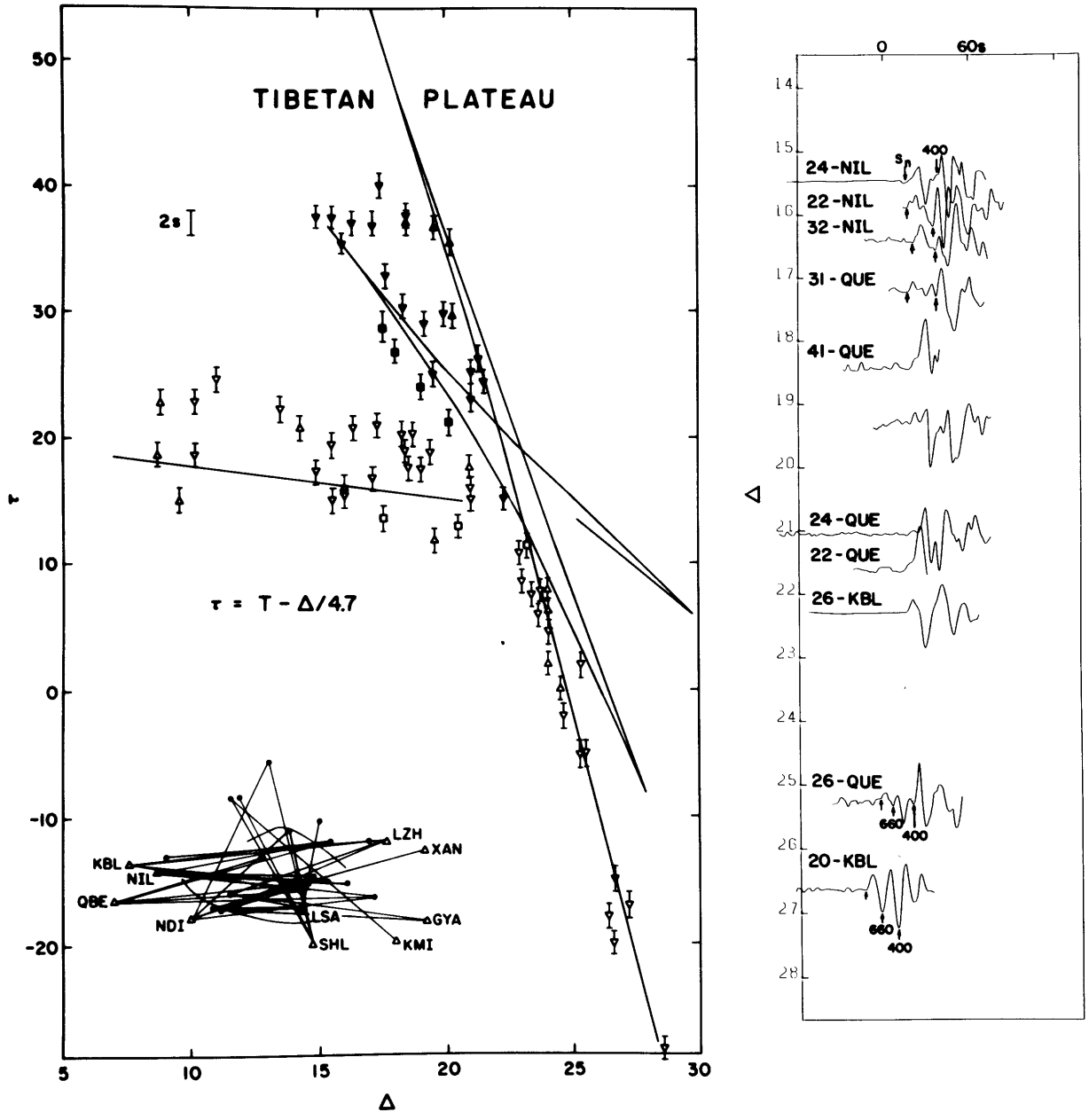
TIBETAN PLATEAU
2s
τ = T - Δ/4.7
τ
Δ
50
40
30
20
10
0
-10
-20
5
10
15
20
25
30
KBL
NIL
QBE
NDI
LZH
XAN
LSA
GYA
SHL
KMI
0
60s
14
15
16
17
18
19
20
21
22
23
24
25
26
27
28
24-NIL
22-NIL
32-NIL
31-QUE
41-QUE
24-QUE
22-QUE
26-KBL
26-QUE
20-KBL
400
660

Figure 8

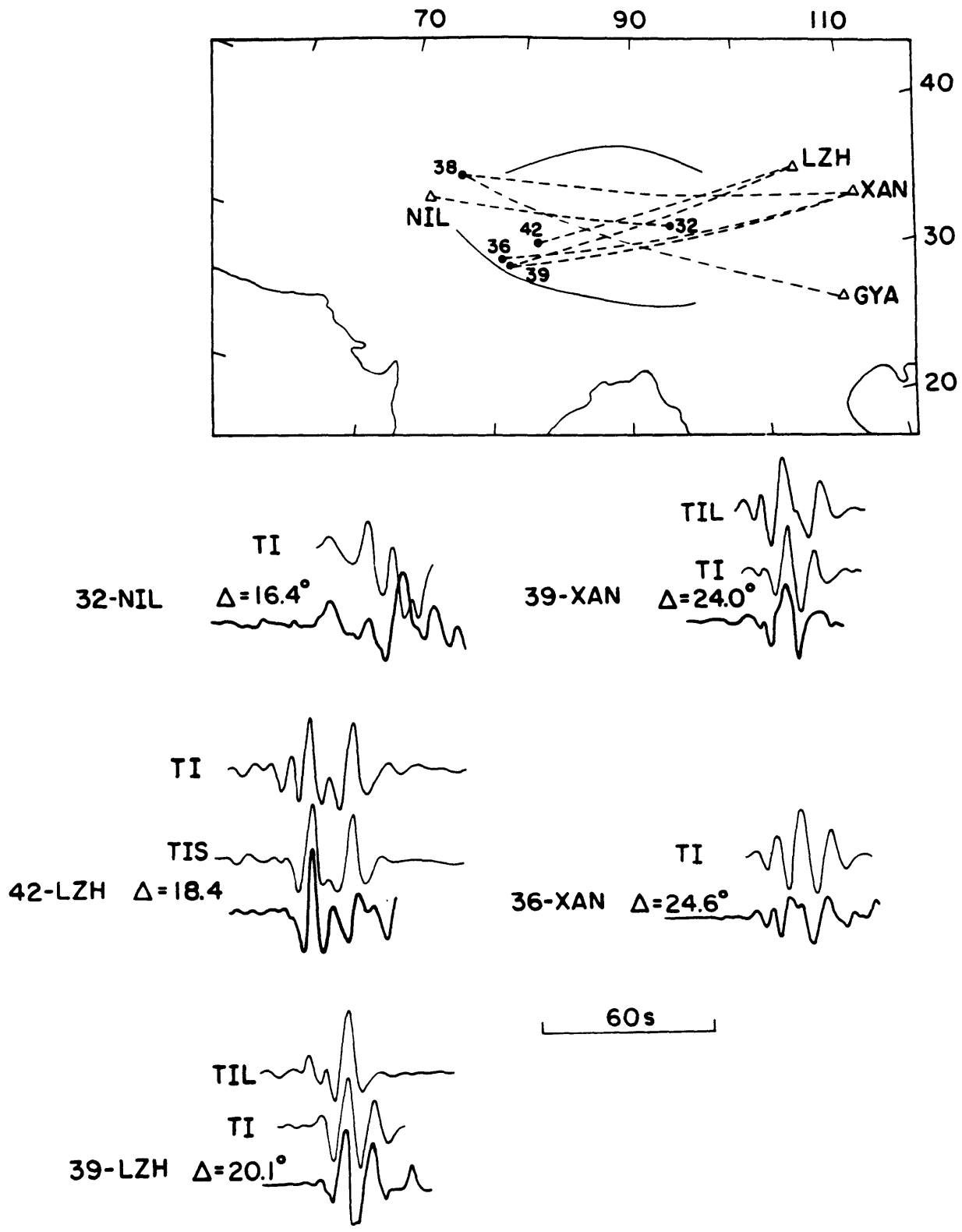
70
90
110
40
30
20
38
LZH
XAN
NIL
42
32
36
39
GYA
TI
32-NIL Δ=16.4°
TIL
TI
39-XAN Δ=24.0°
TI
TIS
42-LZH Δ=18.4
TI
36-XAN Δ=24.6°
60s
TIL
TI
39-LZH Δ=20.1°

Figure 9

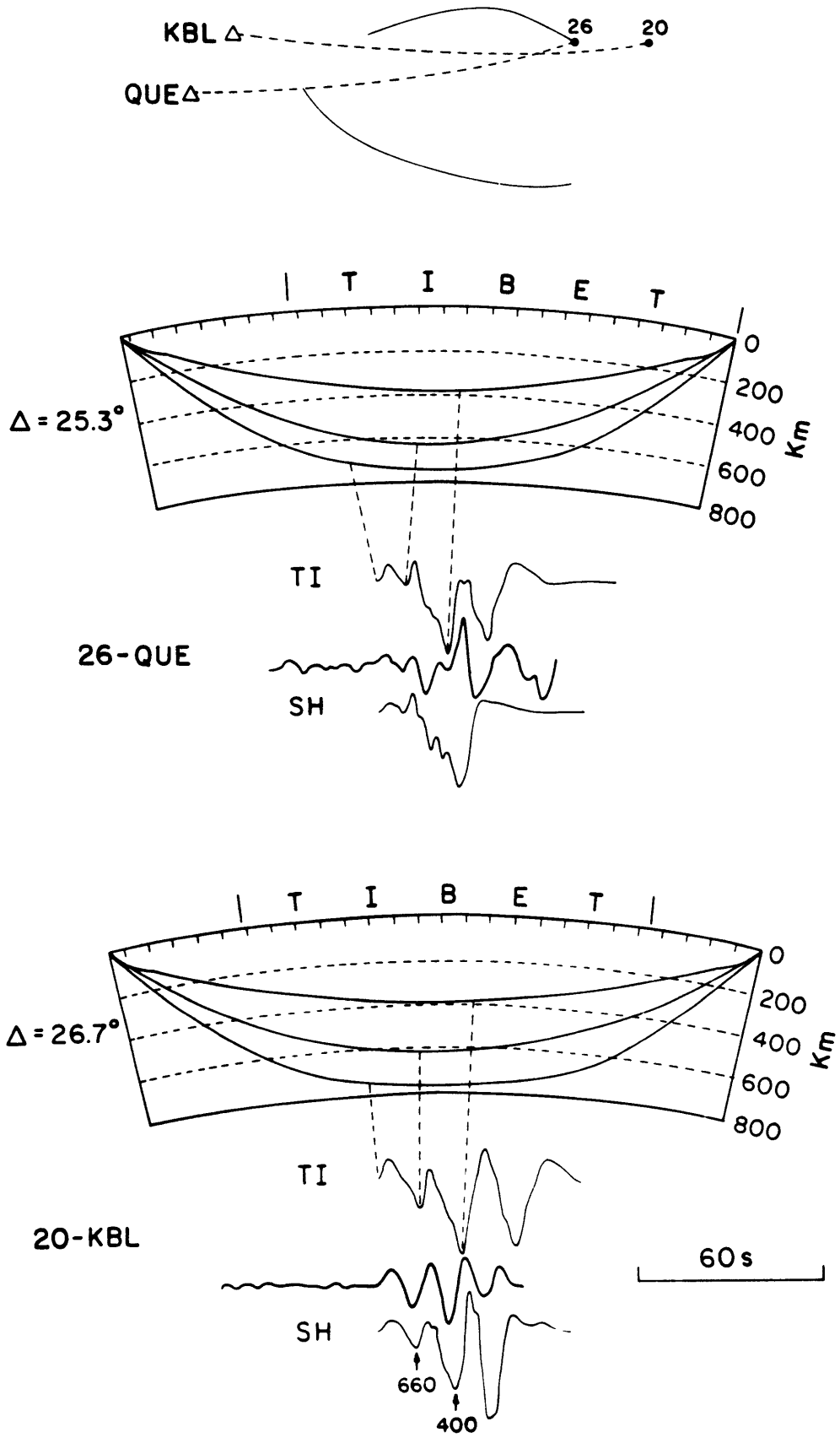
KBL Δ
26
20
QUE Δ
T I B E T
0
200
400
600
800
Km
Δ = 25.3°
TI
26-QUE
SH
T I B E T
0
200
400
600
800
Km
Δ = 26.7°
TI
20-KBL
60 s
SH
660
400

Figure 10

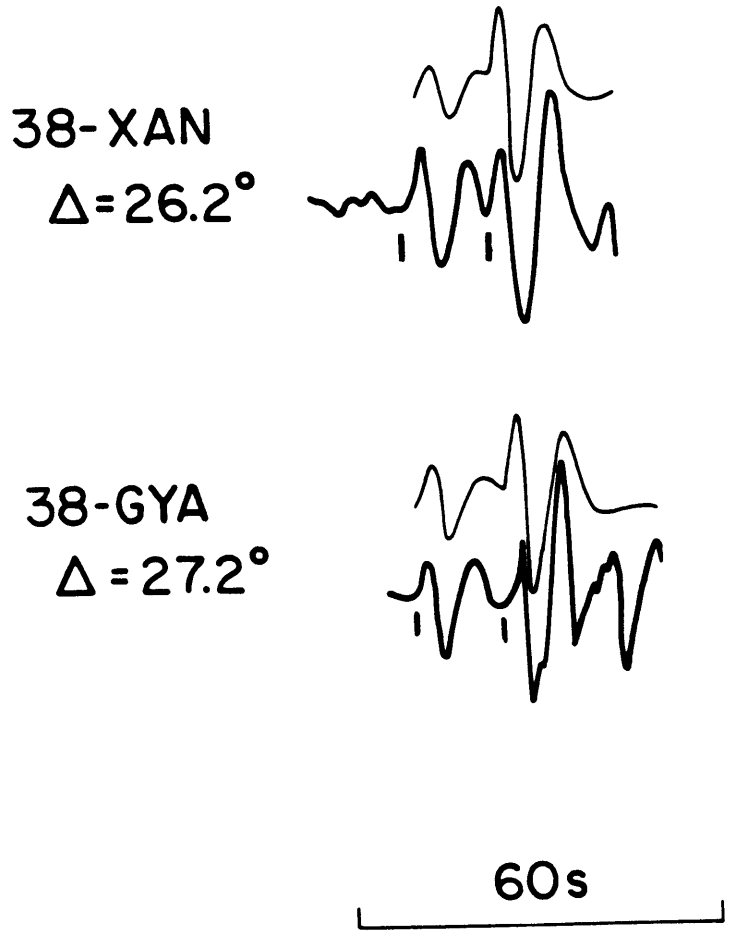

Figure 11

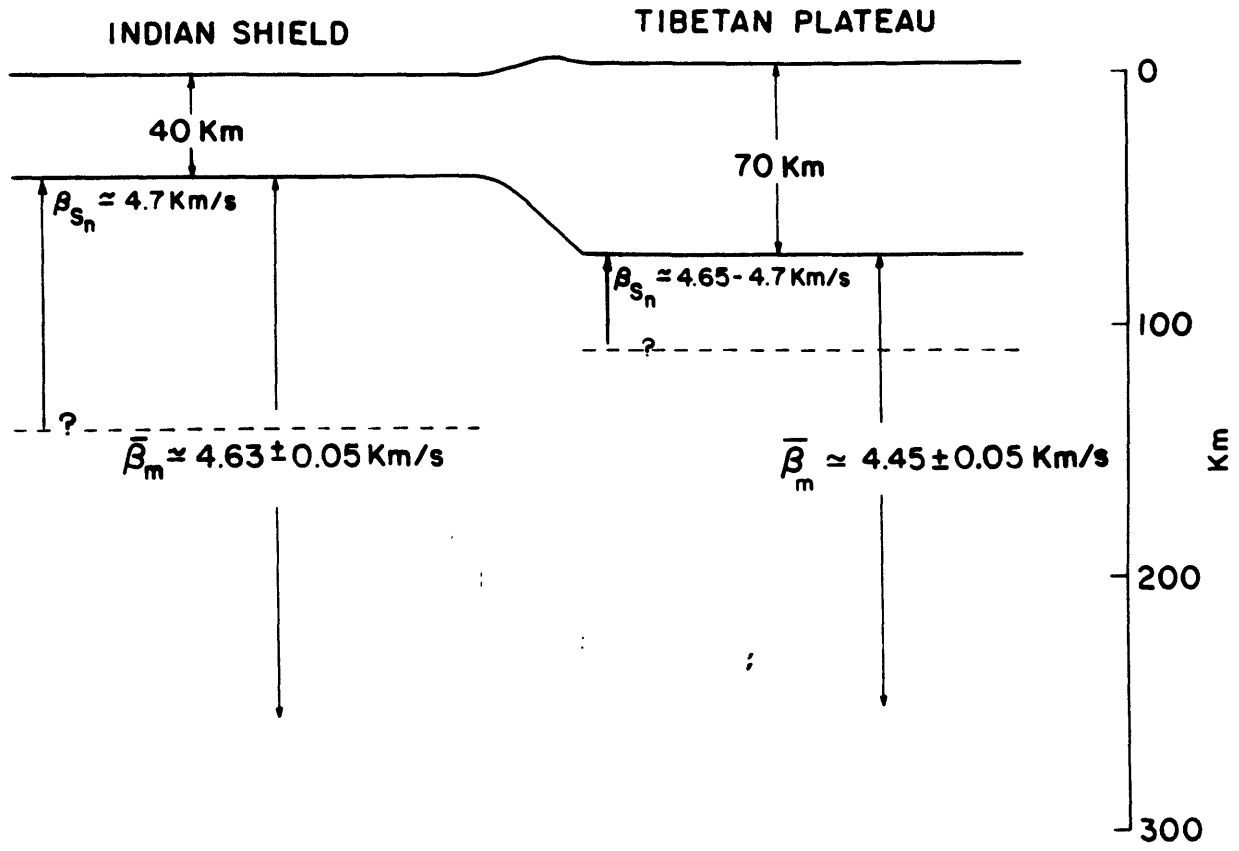

NO DIFFERENCE

Figure 12